
Doctoral Dissertations

Student Theses and Dissertations

Fall 2007

Development of a geographic information system-based virtual geotechnical database and assessment of liquefaction potential for the St. Louis Metropolitan area

Jae-Won Chung

Follow this and additional works at: https://scholarsmine.mst.edu/doctoral_dissertations



Part of the [Geological Engineering Commons](#)

Department: Geosciences and Geological and Petroleum Engineering

Recommended Citation

Chung, Jae-Won, "Development of a geographic information system-based virtual geotechnical database and assessment of liquefaction potential for the St. Louis Metropolitan area" (2007). *Doctoral Dissertations*. 1982.

https://scholarsmine.mst.edu/doctoral_dissertations/1982

This thesis is brought to you by Scholars' Mine, a service of the Missouri S&T Library and Learning Resources. This work is protected by U. S. Copyright Law. Unauthorized use including reproduction for redistribution requires the permission of the copyright holder. For more information, please contact scholarsmine@mst.edu.

DEVELOPMENT OF A GEOGRAPHIC INFORMATION SYSTEM-BASED
VIRTUAL GEOTECHNICAL DATABASE AND ASSESSMENT OF
LIQUEFACTION POTENTIAL FOR THE ST. LOUIS METROPOLITAN AREA

by

JAE-WON CHUNG

A DISSERTATION

Presented to the Faculty of the Graduate School of the

UNIVERSITY OF MISSOURI-ROLLA

In Partial Fulfillment of the Requirements for the Degree

DOCTOR OF PHILOSOPHY

in

GEOLOGICAL ENGINEERING

2007

J. David Rogers, Advisor

Jeffrey D. Cawfield

Neil L. Anderson

Norbert H. Maerz

Donald C. Wunsch

ABSTRACT

The St. Louis Metropolitan area is the focus the U.S. Geological Survey's Earthquake Hazard Program's plan for assessing and reducing the likely risks of an earthquake likely emanating from New Madrid Seismic Zone (NMSZ), which is the most active seismic zone in the Midwestern United States. The St. Louis Metropolitan area consists of three counties in Missouri and four in Illinois, which are divided by the state boundary along the Mississippi River. Both of the state's respective geological surveys have produced their own geologic maps and datasets, employing dissimilar geodata information and systems, with differing map units, map scales, and storage formats, with data stored in hard copy (analog) or digital formats. This combined dissimilar geodata from both states and integrate them into a single Virtual Geotechnical Database (VGDB) in an accepted Geographic Information System (ArcGIS), which can be used to retrieve subsurface data and perform an array of spatial analyses. The VGDB will be made available to the general public and other researchers, and is intended to promote more standardization of geologic interpretations between Missouri and Illinois. The existing body of data was manipulated to extract useful information on the surficial geology, loess thickness, bedrock geology, and well locations in the St. Louis Metro area, which were integrated into a GIS 'information layer.' Measured values of shear wave velocity (V_s) were gathered to assess soil amplification based on NEHRP site classes. Groundwater elevations and depths-to-bedrock basement underling the study area were interpolated using geostatistical methods of kriging and cokriging. The liquefaction potential was also assessed for the study area, estimating the liquefaction potential index (LPI), which is derived from the correlation between LPI values and the depths to groundwater.

ACKNOWLEDGMENTS

Sincere appreciation is expressed to the author's committee members for their guidance. The author would like to especially thank the author's advisor, Dr. J. David Rogers for his insight, guidance, encourage, and financial support in preparation of dissertation. The author is grateful to Dr. Jeffrey D. Cawlfeld, Dr. Neil L. Anderson, Dr. Norbert Maerz, and Dr. Donald C. Wunsch, who served as the committee and offered valuable assistance throughout this dissertation and their classes.

The author wishes to thank Mr. David Shaver at USGS-Rolla for his instruction in GIS technique, Dr. David Grimley at ISGS for providing the geology maps and advising on depth to bedrock mapping, Mr. Bob Bauer and Dr. Andrew Phillips at ISGS for discussing surficial geology and offering ISGS boring data in Illinois, Dr. Buddy Schweig at USGS for kindly paying for ISGS electronic format data, Dr. Richard Harrison at USGS for providing his bedrock geology map and Schultz's work, Mr. David Hoffman at UMR and Mr. Rob Williams at USGS for offering shear wave velocity measurements, Mr. James Palmer at MoDNR for providing the St. Louis geotechnical data, Dr. Ronaldo Luna at UMR for his help in interpreting liquefaction potential, and Deniz Karadeniz for his assistance in doing this research.

The graduate students of Dr. Rogers, who are Conor Watkins, Maung Myat, Ece Karadeniz, and Katy Onstad, provided friendship and were also helpful in many ways. Katherine Mattison and Paula Cochran are acknowledged for their official assistance. Acknowledgements are extended to the members of the St. Louis Area Hazard Mapping Project Technical Working Group for their comments and to the USGS-National Earthquake Hazard Reduction Program and University of Missouri-Rolla for financial support.

Finally, the author is thankful to his father, mother, wife, daughter, and sister/her family who provided support, encouragement, and patience during the completion of this dissertation.

TABLE OF CONTENTS

	Page
ABSTRACT.....	iii
ACKNOWLEDGMENTS	iv
LIST OF ILLUSTRATIONS.....	ix
LIST OF TABLES.....	xiii
1. INTRODUCTION.....	1
1.1. STATEMENT OF PROBLEM.....	1
1.2. OBJECTIVES OF THE STUDY	4
1.3. EXPECTED RESULTS AND SIGNIFICANCE	5
1.4. STUDY AREA	5
1.5. GEOGRAPHIC INFORMATION SYSTEMS (GIS).....	7
1.5.1. Data Input.....	7
1.5.2. Functions	8
1.5.3. Applications.....	11
1.6. OVERVIEW OF VGDB DATA SETS	11
2. COMPILATION OF GEODATA	14
2.1. SURFICIAL GEOLOGIC MAP.....	14
2.1.1. Quaternary Geology.....	14
2.1.1.1 Pre-Illinois (Kansan) and Yarmouth (Interglacial) Episodes.....	14
2.1.1.2 Illinois and Sangamon (Interglacial) Episodes.....	15
2.1.1.3 Wisconsin Episode.....	15
2.1.1.4 Postglacial Deposits.....	16
2.1.2. Compilation.....	17
2.1.3. Discussion.....	21
2.2. LOESS THICKNESS MAP.....	22
2.2.1. Introduction.....	22
2.2.2. Loess Deposits.....	24
2.2.2.1 Loveland Loess.....	24
2.2.2.2 Wisconsinan Loess.....	24

2.2.3. Loess Thickness.	25
2.2.4. Map Compilation.	25
2.3. BEDROCK GEOLOGY	27
2.3.1. Stratigraphy and Geologic Structure.	27
2.3.2. Compilation.	28
2.4. BOREHOLE INFORMATION	38
2.4.1. Data Source	39
2.4.2. Compilation.	39
3. SHEAR WAVE VELOCITY AND SITE AMPLIFICATION	43
3.1. INTRODUCTION	43
3.2. NEHRP SOIL CLASSIFICATION	44
3.3. STUDY AREA	46
3.4. SHEAR WAVE VELOCITY (V_s) DATA ACQUISITION	47
3.5. RESULTS	48
3.5.1. NEHRP Soil Site Classification in STL	49
3.5.2. Characteristic Profiles of Shear Wave Velocity	53
3.5.2.1 Procedure.	54
3.5.2.2 Results.	55
3.5.2.3 Uncertainty	55
4. ESTIMATION OF THE DEPTH TO GROUNDWATER TABLE	63
4.1. INTRODUCTION	63
4.1.1. Previous Studies.	65
4.1.2. Purpose of this Study	66
4.2. STUDY AREA	66
4.3. METHOD	67
4.3.1. Data Set.	67
4.3.2. The Least Squares Approach.	68
4.3.3. Geostatistical Methods.	69
4.3.3.1 Semivariogram.	69
4.3.3.2 Ordinary Kriging.	72
4.3.3.3 Cokriging.	74

4.3.3.4 Error of Estimate.....	76
4.3.3.5 Cross-Validation.	76
4.4. RESULTS OF THE PREDICTIVE MODELS.....	77
4.4.1. Power Regression Map.....	77
4.4.2. Ordinary Kriging Map.	79
4.4.3. Cokriging Map.	81
4.4.4. Cross-Validation Result.	81
4.5. DISCUSSION.....	84
5. ESTIMATION OF DEPTHS TO BEDROCK SURFACE.....	86
5.1. INTRODUCTION	86
5.1.1. Problem.	86
5.1.2. Previous Studies.	87
5.1.3. Purpose of this Study.	88
5.2. STUDY AREA	89
5.2.1. The St. Louis Metropolitan Area (STL).	89
5.2.2. Review of Published Maps.....	89
5.3. DATA	90
5.3.1. Sources of Data.	90
5.3.2. Bedrock Surface Data.....	91
5.4. METHODS EMPLOYED TO INTERPOLATE DEPTH-TO-BEDROCK.....	93
5.4.1. Kriging Map of Depth to Bedrock.	93
5.4.2. Cokriging Map of Bedrock Elevation.	98
5.5. RESULTS	101
6. MAPPING LIQUEFACTION POTENTIAL USING GIS-DATABASES	103
6.1. INTRODUCTION	103
6.1.1. Previous Studies of Regional Liquefaction Potential Mapping.	104
6.1.2. Statement of Problems.....	106
6.1.3. Purpose of this Study.....	107
6.2. BACKGROUND	107
6.2.1. Liquefaction Potential Index (LPI).....	107
6.2.2. Liquefaction Potential Based on Corrected SPT (N_1) ₆₀ Values.	108

6.2.2.1 CSR (Cyclic Stress Ratio).....	108
6.2.2.2 CRR (Cyclic Resistance Ratio).....	109
6.2.2.3 Advantage of the LPI Method.....	110
6.3. STUDY AREA	110
6.3.1. The St. Louis Metropolitan Area (STL).....	110
6.3.2. New Madrid and Wabash Valley Seismic Zones.	111
6.3.3. Liquefaction Features in STL.....	112
6.3.4. Previous Liquefaction Potential Mapping in the STL.....	113
6.4. DATA	113
6.4.1. Geotechnical Boring Data.	114
6.4.2. Quaternary Geologic Map	115
6.4.3. Depth to Groundwater.....	116
6.5. RESULTS	117
6.5.1. Factor of Safety Calculations.	117
6.5.2. Unit Weight of Soil.	118
6.5.3. Estimated Earthquake Magnitude and PGA.....	119
6.5.4. LPI Computation.	119
6.6. DISCUSSION	120
6.6.1. Resultant Map of Liquefaction Potential.....	130
6.6.2. Uncertainty.	133
7. CONCLUSIONS	134
APPENDIX A. SHEAR WAVE VELOCITY	137
APPENDIX B. AVERAGE SOIL UNIT WEIGHTS.....	143
BIBLIOGRAPHY	145
VITA	156

LIST OF ILLUSTRATIONS

Figure	Page
1.1. The St. Louis Metropolitan area, Missouri and Illinois, as defined for this study, consists of 29 USGS quadrangles, which are georeferenced to Universal Transverse Mercator (UTM) Zones 15 and 16. The southern St. Louis Metro area is approximately 200 to 300 km north of the New Madrid Seismic Zone (NMSZ). ...	2
1.2. Four major rivers, geomorphic provinces of alluvial floodplains and uplands, and paleoliquefaction features in the St. Louis metropolitan area. Some of liquefactions are interpreted as having formed by 1811 and 1812 earthquakes emanating from New Madrid Seismic Zone (NMSZ).	6
1.3. Raster data and vector data commonly input into a GIS. The raster data (A) represent the area of continuous interest as a matrix of square cells, while the vector data (B) is composed of points, polylines, and polygons to represent feature shapes.	8
1.4. Common functions of GIS: A) manipulating geospatial data, B) querying stored data, and, C) analyzing spatial problems.	9
2.1. Data sources utilized to construct a seamless Surficial Geologic Map of the St. Louis Metropolitan Area.	17
2.2. Compiled Surficial Geologic Map of the St. Louis Metropolitan Area in a GIS vector format. Note unmapped area in Jefferson County, MO.	18
2.3. Map illustrating the spatial distribution of data sources used to compile the Loess Thickness Map of the St. Louis Metropolitan Area in a GIS vector format.	26
2.4. Isopach map showing the combined thickness of loess deposits of varying age in the St. Louis Metropolitan Area. Loess deposits are locally absent in the floodplains, thickest along the river bluffs bordering the Missouri and Mississippi rivers, and thin rapidly with increasing distance from the main river valleys.	27
2.5. Map showing the areal distribution of the five data sources used to compile a seamless Bedrock Geologic Map of the St. Louis Metropolitan Area.	29
2.6. Map scale matching problems encountered in this study. A) Joining problems at map boundaries resulting from different map scales. B) Before edge-mismatching area of 1:100,000 and 1:24,000 scale maps. C) After edge-matching, by editing the mismatching boundary with another 1:24,000 scale map instead of the 1:100,000 scale map.	31

2.7. Compiled Bedrock Geologic Map of the St. Louis Metropolitan Area in a seamless GIS vector format.	38
2.8. Borehole locations and types in the St. Louis Metropolitan area, Missouri and Illinois in a seamless GIS vector format.	42
3.1. Locations and measuring agencies of shear wave velocity (V_s) measurements.	47
3.2. Estimated average shear wave velocity (V_s^{30}) in the upper 30m and corresponding NEHRP soil site classes plotted on Map of Surficial Materials, at the respective test locations.....	49
3.3. Preliminary NEHRP Soil Site Classification Map.	53
3.4. The reference shear wave velocity (V_s) profiles derived from adjacent boreholes...	57
4.1. General aspects of the permanent groundwater table in humid climates (not including areas underlain by karst, where losing stream might exist).	64
4.2. Comparative profiles illustrating predictions of the depth-to-groundwater with and without considering surface topography (after Hoeksema et al., 1989). Estimates that include consideration of the undulating ground surface using cokriging yield more reasonable predictions because the groundwater table tends to be influenced by the shape and slope of the land surface.	66
4.3. Locations of data points used in the predictions of water table elevation and depth-to-groundwater.	68
4.4. Diagram showing typical semivariogram parameters (nugget, range, and sill).	70
4.5. Spherical, exponential, and Gaussian semivariogram models with the parameters range (a) and sill (C_0).	72
4.6. Relationship between ground surface elevation and groundwater elevations recorded in well logs. This graph suggests a reasonably high correlation between the ground surface and groundwater table elevations. This suggests that cokriging could be employed to estimate the elevation of the groundwater table as a primary variable based on the elevation of ground surface as a secondary variable. The solid line is the best-fit correlation used for the power regression model.	78
4.7. Map showing Predicted Elevation of the Groundwater Table in the St. Louis Metro area, derived from a power regression model. The groundwater table elevations were estimated by substituting 10m DEMs over the study area using a power regression equation.....	79

4.8. (A) Map showing predicted groundwater elevations based on Kriging, and, (B) corresponding standard error map. Note that greatest error is predicted in areas with the least amount of data.	80
4.9. (A) Map showing predicted groundwater elevations based on Cokriging, and (B) the corresponding standard error map.....	82
4.10. Cross-validation data comparing measured versus estimated groundwater elevations and corresponding correlation coefficients, using kriging (A), and cokriging (B).	84
5.1. Example of an erroneous interpolation, which underestimates the bedrock surface because it is pervaded by paleovalley features which were not penetrated by subsurface boreholes.	87
5.2. A) Graph showing the distribution between depth-to-bedrock and ground surface elevation in flood plains and uplands. The bedrock interface lies well beneath the land surface. B) The lower graph illustrates the relationships between bedrock elevation and ground surface elevation in flood plains and uplands. In the uplands, bedrock elevation appears to be more or less proportional to ground surface elevation.....	92
5.3. Schematic diagrams illustrating the proposed technique for estimating the surficial material thickness, employing kriging. A) Approximating the bedrock surface using borings that piercing the bedrock interface. B) Approximating the minimum bedrock surface, using all borings, including those that do not pierce the bedrock interface. C) Of these two approximations, the model then selects the deeper of the two predicted bedrock surfaces. This deeper surface appears to be a more accurate.	95
5.4. Depth-to-bedrock maps predicted by kriging and corresponding standard error maps, showing sample distributions. A) The interpolated bedrock surface using borings piercing the bedrock interface. B) The kriged bedrock surface using all borings, including those that do not pierce the bedrock interface. C) Proposed model then selects the deeper of the two predicted bedrock surfaces. D) Map of kriging standard error. E) Corresponding bedrock elevations, generated by subtracting the kriged final depth-to-bedrock map from ground surface elevations taken from 10m DEMs.	96
5.5. Cokriging maps of A) bedrock interface elevations, and B) Standard error. (C) Corresponding depths-to-bedrock, determined by subtracting the cokriged bedrock elevations from 10m DEMs.	100
6.1. Locations of geotechnical borings used to calculate the liquefaction potential index (LPI).	114

- 6.2. Map illustrating predicted depths to groundwater in the St. Louis Metro area. The depths were estimated by subtracting the cokriged groundwater elevations from the 10m DEM surface elevations. 117
- 6.3. The distribution of depths to groundwater in mapped surficial geologic units. 122
- 6.4. Fundamental relationships derived from the equations for factor of safety (FS) against liquefaction and liquefaction potential index (LPI). A) Data plotted on the upper graph suggests that FS is proportional to groundwater depth. B) LPI data plotted on the lower graph suggests that $(LPI)^{1/2}$ is inversely proportional to the depth of the groundwater table. These relationships are useful in predicting the LPI in unsampled locations within the same mapped surficial geologic units. 125
- 6.6. Liquefaction potential maps inferred from LPI. A) Liquefaction potential for earthquake scenario for a moment magnitude (M)7.5 with 0.10 peak ground acceleration (PGA). B) Liquefaction potential for earthquake scenario for a M7.5 with 0.20 PGA. C) Liquefaction potential for earthquake scenario for a M7.5 with 0.30 PGA..... 131
- 6.7. Map illustrating the standard error of liquefaction potential, based on cokriged depth to groundwater table. The region with the larger error value of cokriging produces less reliable values for liquefaction potential because the regional LPIs were computed based on the cokriged depth to groundwater map. 133

LIST OF TABLES

Table	Page
1.1. Input data sets for the geodata layers compiled in this study.	13
2.1. Correlation of recognized surficial geologic units and map symbols used in the St. Louis Metropolitan area, Missouri and Illinois.	19
2.2. Descriptions of surficial geologic units in the St. Louis Metropolitan area, Missouri and Illinois.	20
2.3. Stratigraphic correlations between recognized bedrock geologic units and corresponding map symbols used in the St. Louis Metropolitan area, Missouri and Illinois.	32
2.4. Descriptions of bedrock geologic units recognized in the St. Louis Metropolitan area, Missouri and Illinois.	34
2.5 Borehole purpose and information contained on logs used for the St. Louis Metropolitan area study, Missouri and Illinois.	41
3.1. NEHRP (National Earthquake Hazards Reduction Program) site classification.	46
3.2. Mean shear wave velocity (V_s^{30}) in the upper 30m grouped by mapped surficial geologic units and corresponding NEHRP soil site classes.	52
4.1. Cross-validation results for ordinary kriging and cokring models.	83
5.1. Input data for depth-to-bedrock interpolations (surficial material thickness).	91
6.1. Historic liquefaction severity assessed from the liquefaction potential index (LPI; Iwasaki et al., 1982).	109
6.2. Surficial geologic units and map symbols used in this study.	116
6.3. Liquefaction Potential Index (LPI) values and corresponding depths to groundwater within mapped surficial geologic units.	121
6.4. Regression of liquefaction potential index (LPI) versus depth to groundwater (DTW) of mapped surficial geologic units.	129

1. INTRODUCTION

1.1. STATEMENT OF PROBLEM

The St Louis Metropolitan area (referred in this study as *STL*) consists of St. Charles, St. Louis, and Jefferson Counties in Missouri and portions of Jersey, Madison, St. Clair, and Monroe Counties in Illinois, which are split by the Mississippi River. In 2004 the St Louis Metropolitan area was identified by the U.S. Geological Survey (USGS) Earthquake Hazard Program's (EHP) plan as one of three urban areas slated for detailed study in the Central and Eastern United States (CEUS) for the next decade. This project represents the initial program of external research funded by the USGS-National Earthquake Hazard Reduction Plan in FY 2005 and 2006. It's intended purpose was to: 1) develop an internet-accessible database for use by scientists, engineers, insurance industry, government agencies, as well as the public; 2) produce natural hazards maps for seismically-induced ground movement hazards, such as lateral spread and liquefaction; and, 3) reduce the risks of hazards posed by earthquakes likely to emanate from the New Madrid Seismic Zone (NMSZ) in the Upper Mississippi Embayment, which is the most active seismic zone in Midwestern United States (Figure 1.1).

Over the past century the Missouri and Illinois states geological surveys have carried out various investigations in the STL area, without any coordination of effort. They have also collected geological information from other agencies in their respective states, and have produced their own geological maps and datasets. Though unintended, both state surveys employ dissimilar geodata information systems, and they employed contrasting mapping criteria (depositional environment versus map units), disparate mapping scales, and dissimilar hardcopy data storage systems. There has never been any over-arching geodatabase or protocol established to conjoin existing geologic, hydrologic, or geotechnical records in the STL area, even though the USGS attempted to compile consistent geologic maps across the state boundary during the 1990s (Harrison, 1997) and surficial geologic maps (Schultz, 1993) of the St Louis 30' × 60' quadrangle at 1:100,000 scale, based on the existing data sources. The St Louis 30' × 60' quadrangle partially covers the STL study area, which consists of 29 7.5-minute quadrangles (described later).

The Missouri Department of Natural Resources, Division of Geology and Land Survey (MoDNR-DGLS) has prepared a CD-ROM titled *Missouri Environmental Geology Atlas (MEGA)* in 2006 and continues to update this, as funds allow. The MEGA contains GIS data layers for the entire state of Missouri. These GIS data layers include bedrock geology, surficial geology, alluvial deposits, well collar locations, known sinkholes, designated wetlands, and contour lines of Paleozoic age bedrock basement rocks, and static groundwater levels. MoDNR-DGLS has also collected and edited geotechnical boring logs from the Missouri Department of Transportation (MODOT) in STL. These subsurface data we used to compile a surficial materials map of the STL area funded by the USGS-National Earthquake Hazard Reduction Program (NEHRP) funded

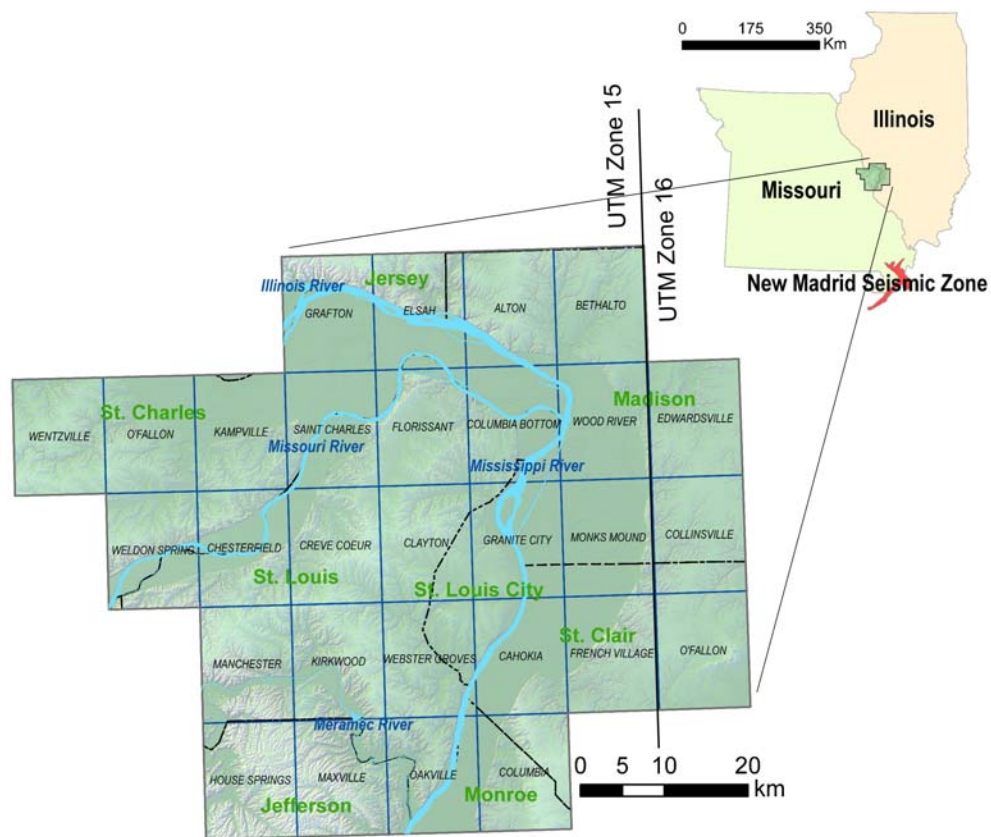


Figure 1.1. The St. Louis Metropolitan area, Missouri and Illinois, as defined for this study, consists of 29 USGS quadrangles, which are georeferenced to Universal Transverse Mercator (UTM) Zones 15 and 16. The southern St. Louis Metro area is approximately 200 to 300 km north of the New Madrid Seismic Zone (NMSZ).

in FY's 2001 and 2002. As part of this USGS-EHP STL study, MoDNR-DGLS also recently completed a map showing the surficial geology of the Wentzville Quadrangle in 2006. Separate USGS-NEHRP grants were given to the University of Missouri-Rolla (UMR) in FY06 to develop a protocol for assessing earthquake hazards on three quadrangles near downtown St. Louis (Columbia Bottom, Granite City, and Monks Mound quadrangles). Several smaller grants have been awarded to MoDNR-DGLS in FY06 and 07 to complete mapping of surficial materials and bedrock geology on the Missouri side of the Granite City and Columbia Bottoms quadrangles, for input into this study. However, most of the 7.5 minute quadrangles on the Missouri side of the STL remain unmapped, while those that have been mapped, remain in analog (hardcopy) formats.

The Illinois State Geological Survey (ISGS) has compiled the logs of almost 17,000 borings in the four counties adjoining St. Louis (Jersey, Madison, St. Clair, and Monroe Counties). These boring logs have been collected through regulatory programs of the state and the ISGS maintains them in a digital database (Oracle) available to the public for a retrieval and copy fee. During the past decade the ISGS has undertaken a project to compile reliable surficial geologic maps at a scale of 1:24,000 (1" = 2,000 feet) along with companion bedrock geologic maps at the same scale. These maps have employed the latest geologic information using state-of-the art technology, using ArcGIS. These STATEMAP 1:24,000 scale quadrangles cover the STL area east of the Mississippi River, in Illinois. The surficial geology map series for STL are also available in GIS formats from ISGS. Additionally, the elevations of the Paleozoic bedrock basement and the thickness of glacial drift statewide scale have been digitized and are also available in GIS formats. For this study we were obliged to combine these dissimilar geodata from the Missouri and Illinois geological surveys and integrate them into a single GIS layer, which were constructed to be seamless. Most of the analog data had to be entered into the VGDB by hand and then converted to a GIS database. The GIS format allows almost endless possibilities for spatial analysis and data mining, and is already accessible to all of those associated with the USGS-EHP multi-year program. The collection of geodata into a single VGDB is intended to encourage scientists and engineers to standardize geologic interpretations and use the database to construct

earthquake hazard maps, using the protocol being established in the pilot study by Karadeniz (2007), under the review of the St. Louis Area Earthquake Hazard Mapping Project-Technical Working Group (SLAEHMP-TWG).

1.2. OBJECTIVES OF THE STUDY

The objectives of this research were to develop a Virtual Geotechnical Database (VGDB) for the St. Louis Metro area in a widely-accepted GIS format, such as ArcGIS, and manipulate this VGDB to make a series of products using for assessing seismic site response and making preliminary evaluations of liquefaction potential in the study area which are based on the probable geologic conditions underlying the area. The stated objectives of this research were as follows:

- 1) collect and digitally input existing geodata into an ArcGIS v.9.1, the most widely accepted GIS format. The existing geodata included geologic, geophysical, and geotechnical information from data compiled by the state geological surveys of Missouri and Illinois, and data released to us by public agencies and private sectors companies. These data were compiled from disparate data sources into a single layer, creating four geodata themes in ArcGIS format: 1) surficial geology, 2) loess thickness, 3) bedrock geology, and, 4) well collar locations (described in Chapter 2),
- 2) gathered the measured values and locations of shear wave velocity (V_s) tests on surficial materials in the STL area, and assessing soil amplification based on established NEHRP Soil Profile Types (sometimes referred to as ‘site classes’) (described in Chapter 3),
- 3) interpolate groundwater elevations (Chapter 4) and depths-to-bedrock basement formations (Chapter 5) between measured data points using geostatistical techniques, and
- 4) as an application of the new VGDB, develop and construct a Liquefaction Potential Map based on three earthquake scenarios of Moment Magnitude (M) 7.5 with 0.10g to 0.30 peak ground acceleration (PGA) (described in Chapter 6).

1.3. EXPECTED RESULTS AND SIGNIFICANCE

The goal of establishing a GIS-based VGDB is to share existing georeferenced information with other groups and individuals interested in assessing subsurface information for an unlimited array of applications, such as engineering design, hazard planning, risk assessments for insurance, geohydrology studies, etc. The compiled VGDB will also aid researchers in assessing potential seismic site response, preparing seismic hazards maps, applying the seismic design tenants of the 2003 International Building Code (adopted by St. Louis and St. Charles Counties in 2006), and influencing planning products for the STL. These products should allow regional planning agencies, such as St. Louis Gateway, to avoid duplicative efforts and costs in years to come.

This research also sought to establish geostatistical interpolation of depths-to-bedrock and probable elevations of the groundwater table across the STL area, and to established an accepted protocol for mapping liquefaction potential in those areas where the physical properties of sediments are more-or-less understood, but where the measured depths-to-groundwater vary, using water well and surface water elevation data in the STL area VGDB.

The accurate locations of water wells and geotechnical borings are crucial metadata for assessing hazards because the physical spacing between these data points influences the uncertainty of predicted positions, between the borings or wells. For example, there is the paucity of reliable subsurface data in the undeveloped portion of eastern St. Charles County, in the lowland flood plain bordering the confluence of the Missouri and Mississippi Rivers. The baseline geodata layers in the VGDB have enabled researchers to assign increased levels of uncertainty in the ‘data gaps’ and allow the SLAEHMP-TWG to establish priorities for subsurface exploration and geophysical evaluations during the balance of the multi-year EHP.

1.4. STUDY AREA

The study area encompasses 29 USGS 7.5-minute quadrangles in the greater St. Louis Metropolitan area of Missouri and Illinois, encompassing a land area of 4,432 km² (Figure 1.1). The topographic elevations in the study area range between 116m to 288m

above mean sea level (1989 NGVD). The St. Louis Metropolitan area includes the confluences of the Missouri, Illinois, and Meramec Rivers with the Mississippi River, and it includes low-lying alluvial floodplains developed along these four major rivers, which are bounded by loess covered uplands, which are locally dissected (Figure 1.2). The floodplains are generally flat with a slope of less than 2%, while slopes of more than 5% are common across the southwestern STL (in the Ozark Uplands) and along the bluffs of the major river valleys (Lutzen and Rockaway, 1987).

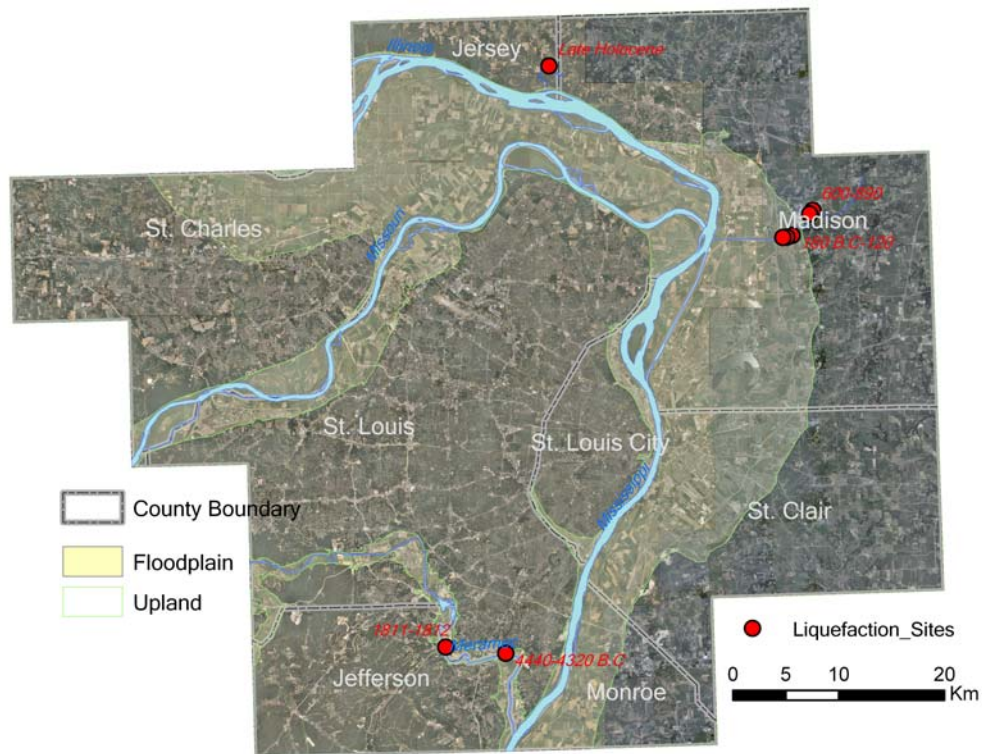


Figure 1.2. Four major rivers, geomorphic provinces of alluvial floodplains and uplands, and paleoliquefaction features in the St. Louis metropolitan area. Some of liquefactions are interpreted as having formed by 1811 and 1812 earthquakes emanating from New Madrid Seismic Zone (NMSZ).

The most likely source of high-amplitude ground motions are earthquakes emanating from the seismically active New Madrid Seismic Zone (NMSZ), located 200 to 380 km south of the STL Metro area. The NMSZ produces about 300 recorded earthquakes each year (since records began in 1974) and it is credited with producing four surface magnitude 8.0+ earthquakes between December 1811 and February 1812. Paleoliquefaction features have been documented along the riverbanks in the STL area (Figure 1.2; Tuttle, 2005; Tuttle et al., 1999), and some of those have been interpreted and/or dated by ^{14}C methods as having formed around the time of the 1811-12 quakes.

1.5. GEOGRAPHIC INFORMATION SYSTEMS (GIS)

A Geographical Information Systems (GIS) is a set of computer programs capable of collecting, storing, transforming, analyzing, and displaying any kind of geographical information which is georeferenced, making it possible to link and combine all kinds of interdisciplinary information that is difficult to associate through other methods (Lo and Yeung, 2002; Rhind, 1989; USGS, 1997). Spatial data are georeferenced in coordinate systems of the Earth. The coordinate systems are usually expressed one of two forms: 1) geographic coordinates (latitude/longitude) given in units of degrees, minutes, and seconds; or, 2) Universal Transverse Mercator (UTM) grid coordinates, a 13 letter-number series, measured in meters.

1.5.1. Data Input. The two most commonly employed spatial data sets are raster and vector data. Either of these can represent a spatial object in GIS, as shown schematically, in Figure 1.3. Raster data represents the area of continuous interest as a matrix of square cells. Each raster cell defines the spatial resolution of the data and contains an attribute value quantifying the feature pertaining to the cell. The vector data is composed of points, polylines, and polygons to represent feature shapes, as defined by x and y coordinates in space. The vector data sets in a spatial database are commonly referred to as layers, themes, or coverages. Raster images to vector graphics or vector to raster conversion can be performed in GIS; however, multiple conversions may introduce the data loss and cumulative error in the process.

As the nations premier map data source, the U.S Geological Survey (USGS) produces and distributes raster and vector geographic data sets. These include: 1) Digital

Raster Graphic (DRG) which is the scanned and georeferenced image of 1:24K USGS topographic maps in order to provide the coordinates of the object of interest, 2) Digital Elevation Models (DEM) with latitude/longitude as well as elevation for each point, allowing a GIS user to create 3-D abstraction of topography, and, 3) Digital Line Graphic (DLG), which represents cartographic data, such as land boundaries, roads, wetlands, shorelines, drainage, and innumerable man-made features.

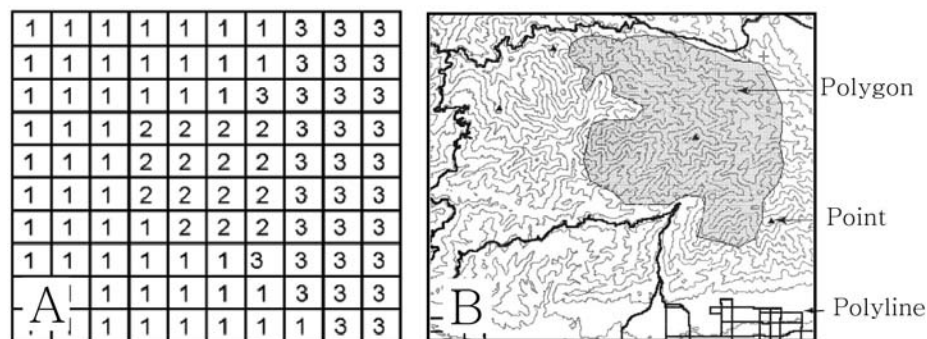


Figure 1.3. Raster data and vector data commonly input into a GIS. The raster data (A) represent the area of continuous interest as a matrix of square cells, while the vector data (B) is composed of points, polylines, and polygons to represent feature shapes.

1.5.2. Functions. An essential feature of GIS is its ability to present a 2- or 3-dimensional perspective view of the world. Over the past few decades, the rapid technologic development of computer processors, digitized data, scanners, and remote sensing systems has enabled GIS to contain and handle enormous quantities of geospatial data, and to integrate that stored data. This type of data commonly includes paper maps, aerial photos, physical data recorded in the field, and remote sensed images of an area of interest (i.e. digital multispectral images, orthorectified digital photos, Light Detection and Ranging [LiDAR] sensed images, Synthetic Aperture Radar (SAR), and Interferometric Synthetic Aperture Radar (InSAR) sensed images).

The functions of GIS (Figure 1.4) include: 1) manipulation (coordinates transformation, edge-matching, and windowing), 2) querying data (classification and retrieval), and, 3) analyzing spatial data (overlay of data layers, calculation of specific attributes, displaying buffering, and networks). Some of the functions and advantages of GIS are the ability to evaluate an almost endless of variables in a very short time, and allowing potential end products to be previewed and adjusted prior to final output (Holdstock, 1998; Parson and Frost, 2000).

(A)

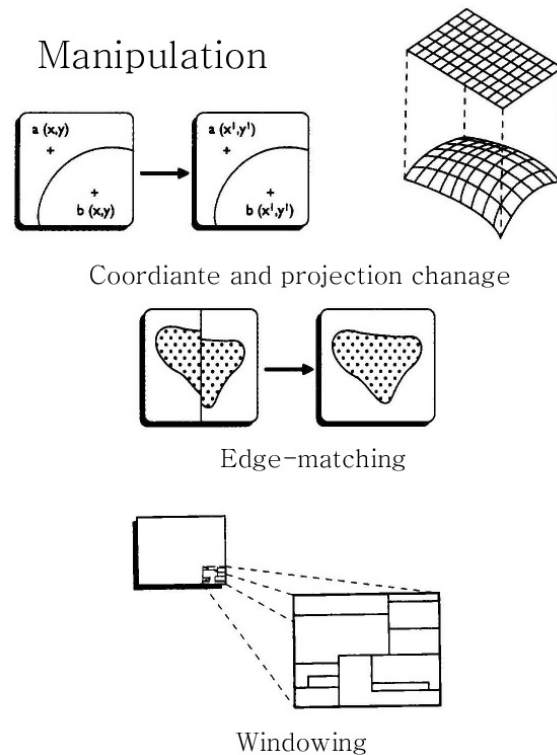
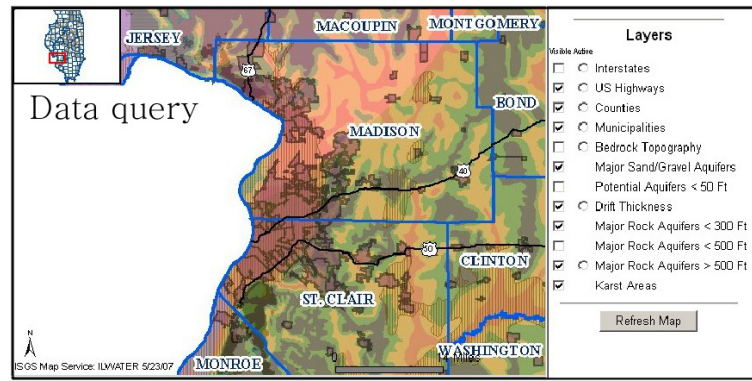


Figure 1.4. Common functions of GIS: A) manipulating geospatial data, B) querying stored data, and, C) analyzing spatial problems.

(B)



(C)

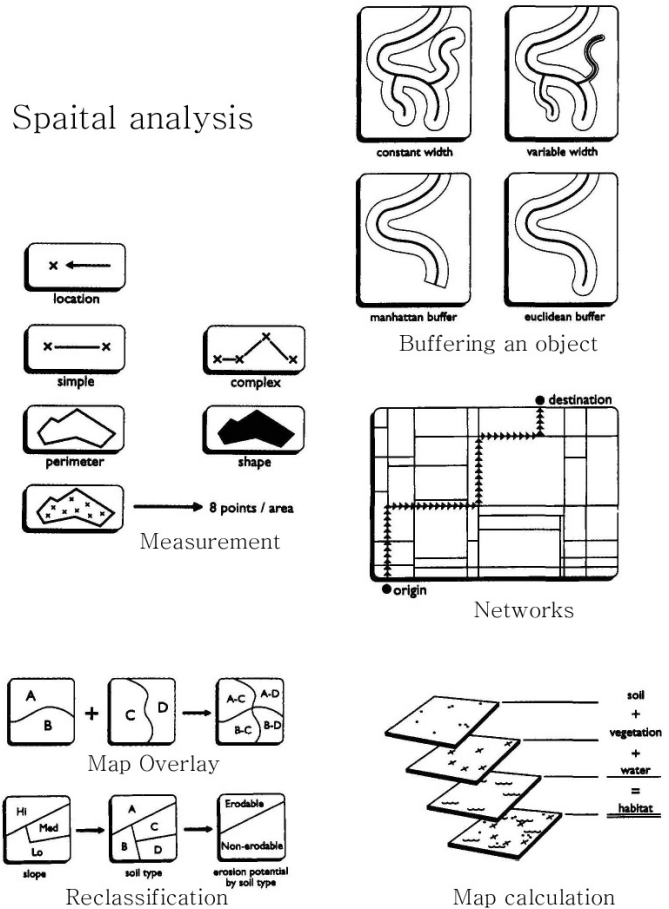


Figure 1.4. Continued

In addition, interpolation techniques in GIS can easily estimate unknown values or quantities in an area bereft of data by expanding the values of adjacent 'data neighborhoods.' Some examples of these statistical techniques are: trend surface analysis, inverse distance weighting, and kriging. Spatial interpolation tools in a GIS have been applied in the fields of air and soil pollution modeling, groundwater movement prediction, and exploration of mineral deposits.

1.5.3. Applications. A GIS provides scientists, engineers, and planners with the capability to collect georeferenced data for local geotechnical, geologic, and hydrologic conditions related to natural hazard impacts and predict corresponding damages. As a result, GIS has quickly emerged as the predominant tool for geological hazard analysis and risk mitigation, and has become widely applied in earthquake hazard assessment (Doyle and Rogers, 2005; Hitchcock, et al., 1999; Luna and Frost, 1998; Mansoor et al., 2004; Sonmez and Gokceoglu; 2005) and fire-rainfall induced landslide hazard assessment (Cannon et al., 2004; Carrara, 1995; Dai and Lee, 2002; Donati and Turrini, 2002).

A GIS database is the collection of geospatial data that are stored in a computer system. Geoscientists and engineers can access a GIS database online or via other carriers and share geologic information compiled in GIS databases. Increasing public access to georeferenced data will gradually reduce duplication of effort and costs, and allow research to be performed in short amount of time (Rogers and Luna, 2004). Local and regional public agencies have been quick to collect existing information, store data in standardized formats, and create GIS databases for public use. These databases are just beginning to contain geodata, and they will likely serve as foundational databases for 1) damage assessments from natural hazards, such as earthquake, landslides, floods, fires, and tornados, and 2) provide guidance for planning decisions and post-disaster emergency response planning.

1.6. OVERVIEW OF VGDB DATA SETS

The GIS-based VGDB is composed of several thematic data sets defined according to the type of information. The existing data used in this study are: 1) geologic

maps from U.S Geological Survey (USGS), Missouri DNR, Division of Geology and Land Survey (MoDNR-DGLS), and the Illinois State Geological Survey (ISGS); 2) geotechnical boreholes and water well logs from MoDNR-DGLS, ISGS, and URS Corporation; 3) shear wave velocity (V_s) data measured by the USGS, ISGS and the UMR; 4) digital raster graphics (DRGs) of 29 USGS topographic quadrangles, covering 7.5' latitude and longitude; and 4) 10m×10m grid digital elevations models (DEM) corresponding to the 7.5' quadrangles, from the USGS.

The DRGs were georeferenced for use in determining the map coordinates of the objects at a scale of 1:24,000. The 29 quadrangles were electronically stitched together, so as to be seamless. The stitched DEMs were used to obtain ground surface elevations for interpolating the depth-to-groundwater and constructing liquefaction potential maps.

Table 1.1. Input data sets for the geodata layers compiled in this study.

Layers	Input Data in Attribute Table	Feature type
Surficial Geology	geologic symbols, unit, and description	Vector (polygons)
Loess Thickness	major contour lines in feet	Vector (polylines)
Bedrock Geology	geologic symbols, unit, description, geologic structures	Vector (polygons, polylines)
Borehole Information	boring location and records	Vector (points)
Vs Values and Locations	Vs values and locations	Vector (points)
Groundwater Table	measured / estimated depth in meter	Vector (points) / Raster (cell)
Depth to Bedrock	measured / estimated depth in meter	Vector (points) / Raster (cell)
Additional USGS sources		
Ground Elevations	Digital elevation model (DEM) 10m resolution	Raster (cell)
Topographic Map	7.5 minute USGS quadrangle	Raster (cell)

The data sources used to create the geodata layers were collected as vector shape files or, directly, from the analog hard copies. Hard copy maps were scanned, rectified into a raster format, and manually digitized into a vector format. Data descriptions and values for individual spatial objects in the vector layers were input into attribute tables. The creation and application of geodata layers were performed using ArcGIS version 9.1 from Environmental System Research Institute (ESRI). The input data sets for presenting each layer in this study are summarized in Table 1.1.

Whenever possible, this study used the Universal Transverse Mercator (UTM) grid coordinates, which are expressed as distance in meters to the east and north. UTM Zone 15 covers Missouri and western Illinois within the STL, whereas eastern Illinois lies within UTM Zone 16. Figure 1.1 shows UTM grid Zones 15 and 16, referencing the 29 USGS 7.5' quadrangles within the STL metro study area.

2. COMPILATION OF GEODATA

2.1. SURFICIAL GEOLOGIC MAP

The surficial geology map is intended to characterize the unconsolidated sediments capping the Paleozoic age bedrock basement. These materials are collectively referred to as the “soil cap” by many engineering seismologists and they can exert a profound influence on seismic site response because of impedance contrasts at the interface between the bedrock and the unconsolidated cover. Information on unconsolidated surficial materials is useful for 1) understanding past depositional environment, 2) estimating engineering characteristics of those units exposed at the ground surface, upon which most structures are founded, and 3) determining those areas capable of magnifying incoming seismic energy, which can damage man-made infrastructure and trigger widespread ground failure, through liquefaction and lateral spreading. This chapter describes the methods used to compile information on surficial geologic materials in the St. Louis Metropolitan area (STL) into a coherent GIS format.

2.1.1. Quaternary Geology. The Quaternary sediments overlying the bedrock basement were deposited during at least three episodes of glaciation: 1) the pre-Illinois, Illinois, and Wisconsin Episodes, 2) intervening interglacial episodes (Yarmouth and Sangamon Episodes), and, 3) a post-glacial episode (Allen and Ward, 1977; Goodfield, 1965; Grimley et al, 2001). The geomorphic provinces exposed in the study area have been divided into floodplains and uplands. The surficial geology in STL varies considerably, including: 1) thick deposits of post-Wisconsin alluvium in the major river valleys, 2) exposed Paleozoic bedrock (dominated by Mississippian carbonates and/or Pennsylvanian shales), and residuum exposed along river-cut bluffs, and, 3) extensive Wisconsin age loess and underlying Illinoian age glacial till, mantling the elevated uplands.

2.1.1.1 Pre-Illinois (Kansan) and Yarmouth (Interglacial) Episodes. At least two sequences of Pre-Illinoian glaciation reshaped the landscape and left diamicton deposits (glacial till), typified by their heterogeneous mix of rock, sand, and silt lying on an eroded bedrock surface. Yarmouthian sediments include alluvium and silty clay of lacustrine origin. These interglacial deposits form the Yarmouth Geosol which overlies

older bedrock or residuum across much of western Illinois. Pre-Illinoian till and interglacial deposits are found locally in the City of St. Louis, and were named the Mill Creek Till by Goodfield (1965). In western St. Charles County a thin layer of Wisconsin stage loess overlies these deposits (Allen and Ward, 1977).

2.1.1.2 Illinois and Sangamon (Interglacial) Episodes. Most of the East St. Louis Metro area was glaciated during the Illinois Interglacial Episode. Materials deposited during that interval include till, outwash deposits (Pearl Formation), and loess (Loveland Loess). These glacial deposits tend to be more extensive than the underlying Quaternary deposits because the Illinoian interglacial episode was the last occasion whereupon continental glaciers actually advanced into what is now the St. Louis area (Grimley et al., 2001).

Sediment accumulated during the Illinoian till/ice margin advance are common throughout the East St. Louis vicinity and have been mapped as the Glasford Formation in Illinois and as the Columbia Bottom Till in Missouri. On the Bethalto Quadrangle in Illinois the Glasford Formation is usually covered with a thin veneer of loess towards the northeast (Grimley, 2005). The Columbia Bottom Till is intermittently exposed in northeastern St. Louis County and is generally more coarse than the lower Mill Creek Till (Goodfield, 1965).

The Sangamon Geosol is an interglacial sediment exposed in the western St. Louis Metro area and forms an important marker horizon for differentiating between the Illinoian Loveland Loess and the younger Wisconsin loess (Goodfield, 1965).

2.1.1.3 Wisconsin Episode. During the Wisconsin Episode, continental glaciation did not reach as far south as the St. Louis Metro area, stopping approximately 130 km northeast of the Edwardsville Quadrangle in Illinois (Phillips, 2003). The Wisconsin glaciation produced a large volume of glacial meltwater and sediments that impacted the Mississippi River drainage basin. Wisconsinan deposits include outwash deposits preserved in terraces, lake sediments, and loess.

Outwash deposits known as the Henry Formation were deposited in the Illinois and Mississippi River valleys during this episode. Slackwater-lake sediments (Equality Formation) were likely deposited in meltwater-flooded lakes and are preserved in the valleys tributary to the Mississippi and Illinois Rivers.

The Wisconsin Episode produced extensive deposits of loess in the elevated uplands adjacent to the major river valleys. The source of the Aeolian loess was periodic winds that swept this silt size material from outwash sediments that had accumulated in the Mississippi and Missouri River Valleys. The loess blankets nearly all of the uplands and reaches its greatest thickness along the bluffs of the Missouri and Mississippi Rivers (up to 30m along the Mississippi River), but thins exponentially, away from the bluffs (Allen and Ward, 1977; Fehrenbacher et al., 1986; Goodfield, 1965; Grimley et al., 2001). These loess deposits consist of Peoria Silt (yellowish brown to gray, low in kaolinite/chlorite in contrast to the Roxana Silt) and the Roxana Silt (pinkish brown to gray). In Illinois, the upper unit is referred to as the Peoria Silt, and it is approximately 30% to 100% thicker than the underlying Roxana Silt in uneroded areas (Fehrenbacher et al., 1986). It is difficult to differentiate the two units in the field if the color break is not distinct; so the entire section of undifferentiated loess is often lumped together and termed the Peoria loess (Goodfield, 1965). This is the most common description noted on most geotechnical boring logs.

2.1.1.4 Postglacial Deposits. Postglacial deposits include alluvial deposits in the floodplains of major rivers and upland streams flowing into the major rivers and deposits of colluvium in bedrock hollows. The alluvial deposits in Illinois are named the Cahokia Formation. In the American Bottoms Quadrangle the ISGS has divided the Cahokia Formation filling the Mississippi River valley into three map units: 1) sandy, 2) clayey, and 3) fan facies. The sandy facies are preserved on former point bars or river channel deposits where the floodplain is slightly higher. The clayey facies is interpreted as abandoned meander channel fills or overbank deposits. The upper unit is alluvial fan deposits that were derived from reworked loess, local mudflows, and local rock talus. These are commonly observed near the mouths of streams that drain from the elevated uplands, cutting through the Mississippi River bluffs (Grimley and McKay, 2004). Colluvial deposits (known Peyton Formation in Illinois) occur along steep side slopes and ravines. This unit is only mapped in the Grafton and Elsayh Quadrangles in Illinois (Grimley, 2002; Grimley and McKay, 1999).

2.1.2. Compilation. Surficial geologic maps were compiled from the publications of the Missouri Department of Natural Resources, Division of Geological and Land Surveys (MoDNR-DGLS), the Illinois State Geological Survey (ISGS), and the U. S. Geological Survey (USGS).

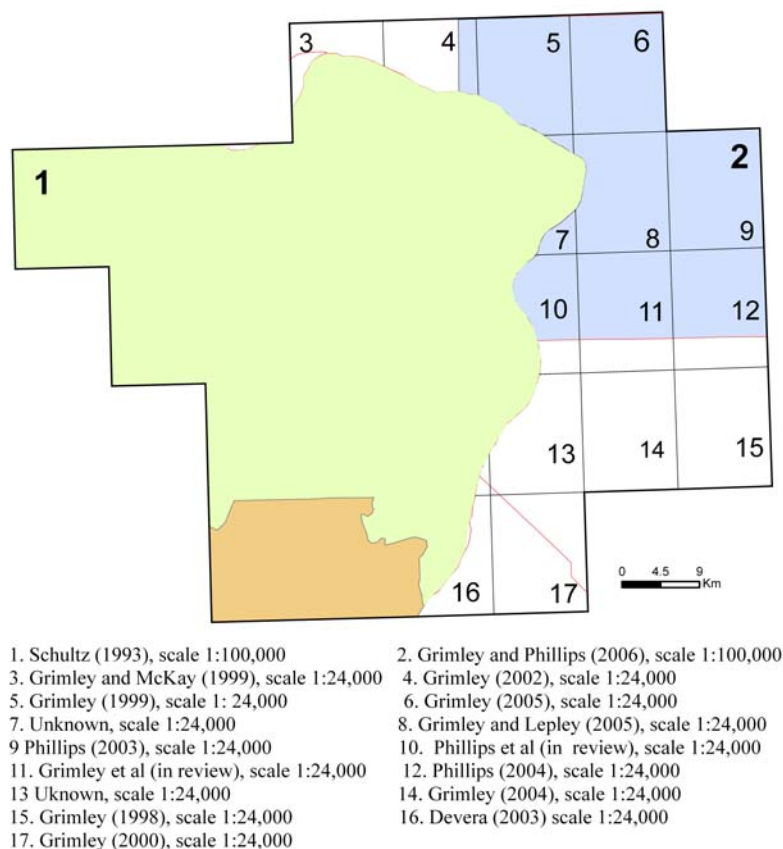


Figure 2.1. Data sources utilized to construct a seamless Surficial Geologic Map of the St. Louis Metropolitan Area.

Schultz (1993) compiled existing data from: 1) the City of St. Louis and St. Louis County (Goodfield, 1965), 2) St. Charles County (Allen and Ward, 1977), and 3) eastern St. Louis, on the Illinois side (Lineback, 1979). He produced an unpublished Open File Geologic Map of St. Louis 30'×60' quadrangle (1:100,000 scale). Schultz provided a copy of his unpublished hand-drawn map and the Missouri portion of the map was

manually digitized and the descriptions of geologic units were input into attribute tables in a GIS format. The Illinois portion of the study area was mapped at 1:24,000 to 1:100,000 scale by the ISGS and the corresponding GIS format was provided by Grimley (2007, personal commun.). The GIS shapefiles of both Missouri and Illinois portions were combined into one GIS geodata set. However, the surficial geology of Jefferson County, Missouri, has not been mapped at a useful scale (<1:100,000) and, thus remains unmapped in this project. 17 data sources (Figure 2.1) were used in compiling the Surficial Geologic Map of the St. Louis Metropolitan Area, presented in Figure 2.2, respectively. A stratigraphic unit and correlation, recognized in Missouri and Illinois, and description by Schultz (1997) and ISGS, are presented in Tables 2.1 and 2.2.

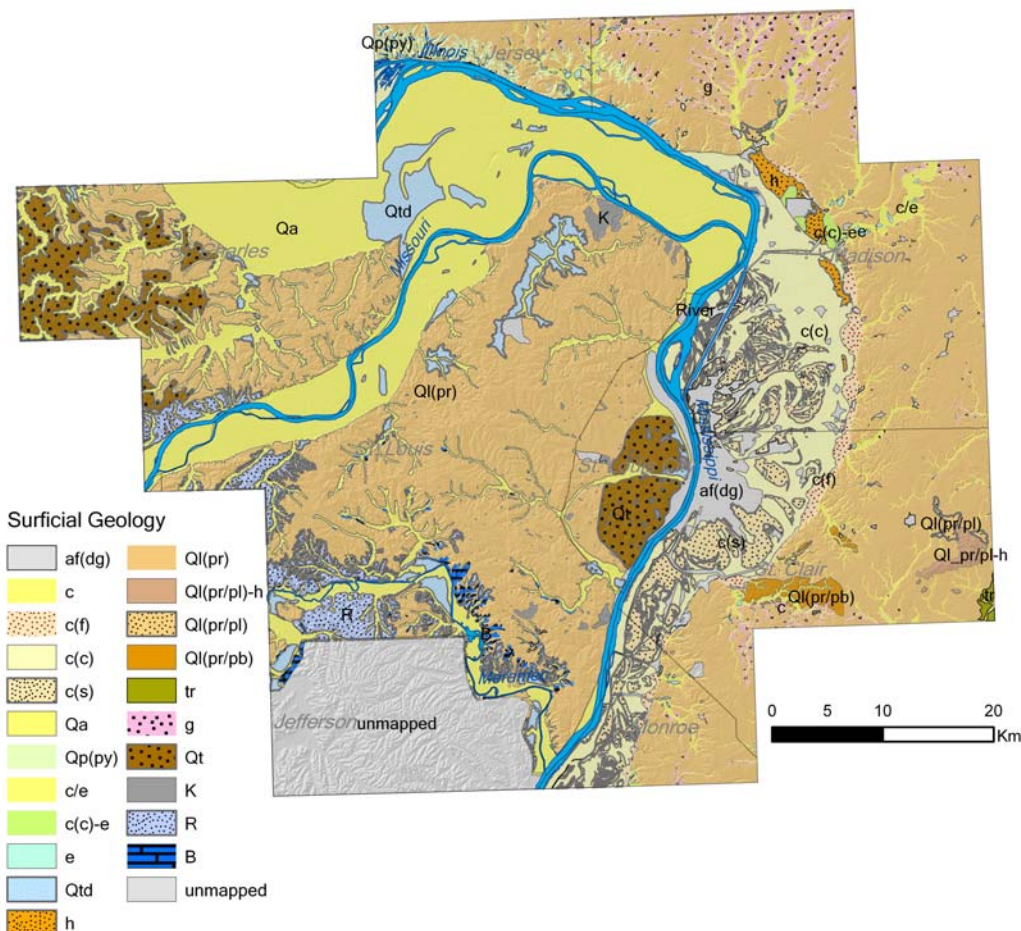


Figure 2.2. Compiled Surficial Geologic Map of the St. Louis Metropolitan Area in a GIS vector format. Note unmapped area in Jefferson County, MO.

Table 2.1. Correlation of recognized surficial geologic units and map symbols used in the St. Louis Metropolitan area, Missouri and Illinois.

Time Scale	Interpretation	This study	Missouri (Schultz, 1993)		Illinois (ISGS publications)	
		Symbol	Symbol	Unit	Symbol	Unit
Holocene (post-glacial)	Man-made fill or cut	af(dg)	af	Artificial fill	dg	Disturbed Ground
	Residuum	R	R	Residuum		
	Alluvium	Qa or c	Qa	Alluvium	c	Cahokia Fm
	Alluvial or colluvial fans	c(f)	Qa	Alluvium	c(f)	Cahokia-Fan
	Alluvium (backswamp, channel-fill or overbank)	c(c)	Qa	Alluvium	c(c)	Cahokia-Clayey
	Alluvium (point bar or channel)	c(s)	Qa	Alluvium	c(s)	Cahokia-Sandy
	Colluvium	Qp(py)	Qp	Peyton	py	Peyton Fm
Holocene over Pleistocene	Alluvium over lake deposits	c/e			c/e	Cahokia Fm over Equality Fm
	Alluvium (clayey) or lake deposits	c(c)-e			c(c)-e	Cahokia-Clayey or Equality Fm
Pleistocene (Wisconsinan)	Lake sediment (slackwater)	Qtd or e	Qtd	Terrace deposits	e	Equality Fm
	Outwash	h			h	Henry Fm
	Loess	Ql(pr)	Ql	Loess	pr	Peoria and Roxana Silts (pr)
Pleistocene (Wisconsinan over Illinoian)	Loess over ice-contact drift	Ql(pr/pl-h)			pr/pl-h	(pr) over Pearl Fm-Hagarstown M
	Loess over outwash	Ql(pr/pl)			pr/pl	(pr) over Pearl Fm
	Loess over till over lake sediment	Ql(pr/pb)			pr/pb	(pr) over Glasford Fm-Petersburg Silt
Pleistocene (Illinoian)	Lake sediment	Qtd or tr	Qtd	Terrace deposits	tr	Teneriffe Silt
	Till and ice marginal sediment	Qt or g			g	Glasford Fm
Pre-Illinoian (Kansan)	Till	Qt	Qt	Till		
		K	K	Karst		
Paleozoic	Bedrock	B	B	Bedrock	R	

Table 2.2. Descriptions of surficial geologic units in the St. Louis Metropolitan area, Missouri and Illinois.

Episode (years B.P.)	Formation	Interpretation	Occurrence	Materials
Hudson (12,000~ present)	Artificial fill	Artificial fill	Areas of man-made cuts or fills	Various soil or rock types
	Cahokia	Alluvium	Stream valley	Silt loam
	Cahokia-Fan	Alluvium	Tributary streams along the Mississippi River	Silt loam
	Cahokia-Clayey	Alluvium	Abandoned channel, swale fill, backswamp	Silty to silty clay loam
	Cahokia-Sandy	Alluvium	Point bar, channel	Very fine to medium sand
	Peyton	Colluvium	Slope bottoms	Silt loam, pebbly silt or pebbly clay
	Cahokia or Equality	Overbank alluvium or lake deposits	On or near the Wood River terrace	Silty clay to fine sand
Wisconsin (75,000 ~ 12,000)	Equality	Lake sediment of slackwater	Terrace	Silt loam to silty clay loam with fine sand
	Henry	Outwash	Wood River terrace and valley floors	Medium to coarse sand
	Peoria and Roxana Silts	Loess (windblown silt)	Blankets all uplands	Silt to silt loam
<i>Sangamon Geosol</i>				
Illinois (200,000 ~ 130,000)	Teneriffe Silt	Lake sediment or loess	Thinnest in upland, thicker as valley fill, contained within Sangamon Geosol	Silty clay loam
	Hagarstown Member of Pearl Fm	Ice-contact sediment	Ice-marginal, glacial channel	Mixture of loam, gravel, and diamicton
	Pearl	Outwash	Terrace	Sand with some gravel
	Columbia Bottom till	Till	Sparsely mapped in the bluff to the west of Columbia Bottom (Goodfield, 1965)	Clayey sandy silt, boulders. Materials are generally coarser than Mill Creek till
	Glasford	Till and ice marginal deposits	Underlying bedrock and overlain by Wisconsinan loess. Crop out along slopes in Bethalto quad.	Mixture of clay, silt, sand, and gravel (diamicton)
	Petersburg Silt	Lake sediment	Slackwater or ice margin	Silt loam to silty clay loam

Table 2.2. (Continued)

<i>Yarmouth Geosol</i>				
Pre-Illinois (500,000 to 200,000)	Mill Creek till	Till	Mapped in St. Louis City (Goodfield, 1965)	Clay, gravel, rock fragment. Smaller content of illinite than Colombia Bottom till
	Banner	Till, alluvium, and lake deposits	Preserved in bedrock valley	Pebbly loam diamicton

2.1.3. Discussion. A vexing aspect of generating a Surficial Geologic Map of the St. Louis Metropolitan area by compiling data of such disparate age, scales, and origins was the disparity between mapped units and scales in Missouri and Illinois. The State of Missouri has traditionally employed depositional environment mapping at scales above 1:62,500 to compile their geologic maps. Palmer and Siemens (2006) have recently mapped Wentzville 7.5' quadrangle at 1:24,000 scale where much of the area is presently being graded for development.

The State of Illinois has utilized formational mapping of recognized map units by correlating stratigraphy, as well as by interpreting depositional environments. The ISGS Metro-East Mapping Project was funded by the USGS STATEMAP program. ISGS recently completed their mapping of all the 1:24,000 scale USGS quadrangles in the Eastern St. Louis Metro area. These new maps include geologic cross sections through the Mississippi River flood plain as well as detailed descriptions of the map units, including tables showing wells and borehole information that aided their interpretations, and information gleaned from pre-existing reports.

The Mississippi River Valley contains numerous oxbows, abandoned channels, point bars, and backswamps, many of which have been filled with silt and sandy clay fill to enable development. As mentioned previously, the ISGS has subdivided the Cahokia Formation into three mapable facies (sandy, clayey, and fan) and mapped the man-placed artificial fill according to grain size and depositional environment. In some of the elevated uplands east of the flood plain in Illinois, the ISGS was able to distinguish

between the Peoria and Roxana Silts (loess) and occasionally identify some of the underlying units (e.g., loess over Pearl Formation, loess over Glasford Formation, etc.).

The Missouri DGLS has not undertaken the same level of detail in mapping their side of the metro area, although it also appears to be much less complicated and less deeply incised than the exposures on the Illinois side, which were more affected by past glaciations. Nevertheless, there exist considerably more uncertainties in the stratigraphy of the recognized surficial materials on the Missouri side, where many 'data gaps' presently exist. A long-term goal of the USGS-EHP for the SLA will be to gradually close as many of these gaps as possible, especially in the more densely populated areas.

In their NEHRP funded study of liquefaction potential in five 1:24,000 scale USGS quadrangles in the St. Louis area, Pearce and Baldwin (2005) noticed that the Quaternary geologic classification used for mapping deposits differs across the state boundaries and that the map units had to be correlated for consistency during their liquefaction susceptibility analysis. They correlated stratigraphic units between Missouri and Illinois on the basis of similar-interpreted depositional environments of each map unit by mapping new Quaternary geology for the Missouri portion and using ISGS publications for the Illinois portion. In order to unify and/or simplify distinctions between dissimilar stratigraphic units in the STL study area, this study proposed correlations of stratigraphic units mapped in Missouri and Illinois based on similarly-interpreted depositional environments of each map unit (described in Chapter 6).

2.2. LOESS THICKNESS MAP

2.2.1. Introduction. It has been recognized that loess thickness affects soil development and productivity, as well as soil management for engineering and other uses (Fehrenbacher et al., 1986). Late Wisconsin loess in the Central United States extends from the Rocky Mountains in Colorado eastward to the Appalachian Mountains in Pennsylvania, and from Minnesota southward to Louisiana (Ruhe, 1983). Soil studies note that late Wisconsin loess forms the major parent material of Midwestern soils and that the thinner loess makes it possible to sharply differentiate soil horizons. Soil development with the thinning of loess from a source has been explained by three possible mechanisms (Fehrenbacher et al., 1986). These include: 1) the process of the

wind carrying loess produces an exponential change in particle size with the distance from the source (the amount of coarser fractions of loess decrease while finer fractions increase), 2) carbonate leaching produces leached loess in the areas of thin loess deposits, whereas this process maintains calcareous loess in the areas of thick loess deposits, and 3) acid retention in the low permeability Sangamon Paleosol underlying thinner loess caps yields a higher water table and, thereby, tends to accelerate the soil development (weathering) process.

The physical properties of loess can cause numerous engineering challenges, due to its unconsolidated nature and uniform silt-size grains. The loess has relatively low bulk density and low-to-moderate compressibility, but dried loess also possesses a moderate shear strength and bearing capacity. Some of the more common engineering problems associated with loess in the St. Louis Metro area have included: 1) slumping and slope failures in river bluffs, steep railroad and highway cuts, after the material becomes saturated, 2) foundation failures where the loess becomes saturated, usually, because of poor drainage, and 3) subsurface erosion and piping of fine-grained particles, which have little apparent cohesion (Su, 2001).

When grains of loess are weakly cemented the loess maintains shear strength without being saturated. Loess covered uplands along Mississippi River valley are generally acceptable material for structural foundations and can often support near vertical cuts because they are generally uniform in composition and have very low swell potential (Rahn, 1996; Smith and Smith, 1984). Pearce and Baldwin (2005) assessed loess deposits in St. Louis as having a very low susceptibility to liquefaction because of their high fines content (> 95% passing the No. 200 sieve) and low groundwater table (because they tend to be self-draining).

The dissected uplands bounding the major alluvial filled river valleys in the St. Louis Metro area are covered with extensive deposits of loess, deposited during the last Quaternary glaciation (Wisconsin Episode). For this study all of the existing geodata describing the loess, its extent and reported thicknesses, was gathered and reviewed for consistency. Much of this information was generated over the years by various publications. After review, the loess data believed to be most reliable was digitized and

contoured to compile a generalized Maps of Loess Thickness in the St. Louis Metropolitan Area.

2.2.2. Loess Deposits. The loess in STL generally overlies interglacial Sangamon Geosol or Illinoian till or lacustrine sediments, although in some areas it lies directly upon residuum or Paleozoic bedrock (Grimley et al., 2001; Schultz, 1993). The Peoria silt and the underlying Roxanna silt form the two major loess deposits, both of which are interpreted as windblown deposits of Wisconsinan age. They were initially identified and described by Frye and Willman (1960). A much older sequence of loess was deposited during the Illinoian Episode, called the Loveland Loess. It is found lying beneath the Roxana loess in a few isolated areas in the eastern STL study area (Fehrenbacher et al., 1986; Goodfield, 1965).

2.2.2.1 Loveland Loess. The Loveland Loess (reddish brown) lies beneath the interglacial Sangamon Geosol. This unit is rarely exposed, possibly due to non-deposition, erosion, or similarity with the younger loess deposits that overlie it where the Sangamon Geosol marker bed is missing. Because it is seldom noted in the STL and does not influence present-day surficial soils, the Loveland Loess is considered to be of minor importance in the St. Louis area (Goodfield, 1965).

2.2.2.2 Wisconsinan Loess. The Roxana Silt is distinguished by its distinctive color, commonly observed as a pinkish brown to pinkish gray silt loam. This unit was deposited during the mid-Wisconsinan, between about 55,000 and 28,000 ^{14}C years before present (B.P.). The younger Peoria Silt consists of a yellow-brown to gray silt loam, which is usually 30% to 100% thicker than the Roxana Silt. The Peoria Silt was deposited during the late Wisconsinan, between about 25,000 and 12,000 ^{14}C year B.P. (McKay, 1977, 1979; Grimley et al., 1998).

X-Ray Diffraction (XRD) patterns present in Wisconsinan loess are characterized by large amounts of montmorillonite and illite, the former usually in excess of the latter. The Peoria Silt exhibits a much lower kaolinite/chlorite level as compared to the Roxana Silt. The grain size distributions of the two loess units indicate that the Peoria Silt consists of approximately 25% clay, 70% silt, and 5% sand. The Peoria Silt has somewhat lower clay content than the Roxana Silt (Goodfield, 1965; McKay, 1977).

Where the Roxana Silt is absent or eroded, or where the color break between Peoria and Roxana units is subtle, can make the two units undifferentiable. Therefore, the entire loessal sequence, including the Roxana Silt, and even the older Loveland Loess, are often lumped together as Peoria Loess and the loessal age is not distinguished (Fehrenbacher et al., 1986; Goodfield, 1965).

2.2.3. Loess Thickness. The STL study area includes four major rivers (Illinois, Mississippi, Missouri, and Meramec) and the loess deposits mantling the elevated uplands originated from the adjoining river valleys during the Wisconsin glacialiation and somewhat earlier. Local variation in the physical properties of the loess (such as grain size and composition) appear to be influenced by paleovalley width, paleovalley orientation, and paleowind direction. The grain size distribution appears to be more complicated in the uplands adjacent to the confluence of Mississippi, Missouri, and Illinois rivers because the loess-forming grains in this area were probably provided by three distinct depositional sources, whereas the St. Charles and St. Louis areas along the lower Missouri River valley are attributed to a single source (Goodfield, 1965; Grimley et al., 2001).

The loess is thickest along the bluffs bordering the modern Missouri and Mississippi valleys and thins rapidly away from these bluffs (Allen and Ward, 1977; Fehrenbacher et al., 1986; Goodfield, 1965; Grimley et al., 2001). The further removed the loess is from the major river valleys, the more fine-grained its grains become. In Illinois various studies have been undertaken using several kinds of mathematical expressions to demonstrate the thinning of loess from a discrete source. An exponential model is commonly considered to best explain the observed decrease in loess thickness away from the major river valleys (Fehrenbacher et al., 1986).

2.2.4. Map Compilation. The isopach maps of loess thickness in the St. Louis Metro area were digitally compiled into a GIS format. The sources of this data included Goodfield's (1965) dissertation covering St. Louis County, Thorp and Smith (1952) for St. Charles and Jefferson counties, and the Illinois State Geological Survey (ISGS) for the three counties in Illinois. The Missouri portion mapped by Goodfield (1965) and Thorp and Smith (1952) were manually digitized and the values of loess thickness (in feet) were input into an attribute table in ArcGIS. The Illinois portion was mapped by the

ISGS and the corresponding GIS shapefile was provided by Grimley (2007, personal commun.). The GIS shapefiles of both Missouri and Illinois portions were then combined into a single GIS shapefile. The five data sources (Figure 2.3) and the compiled map illustrating the total reported thickness of loess (combination of Peoria loess and Roxana

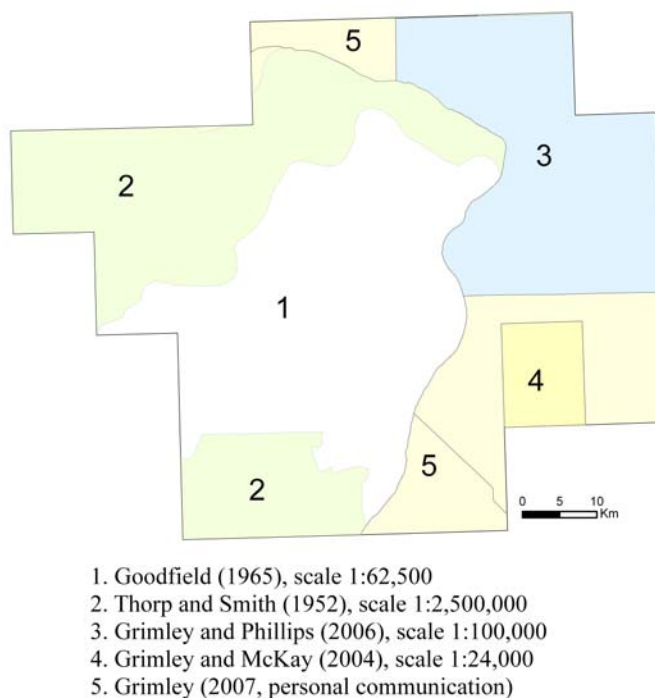


Figure 2.3. Map illustrating the spatial distribution of data sources used to compile the Loess Thickness Map of the St. Louis Metropolitan Area in a GIS vector format.

units in feet) are presented in Figure 2.4. The Illinois portion was mapped at scales between 1:24,000 and 1:100,000; the City and County of St. Louis was mapped at a scale of approximately 1:62,500, while St. Charles and Jefferson Counties, MO were mapped at the considerably smaller scale of 1:2,500,000 (by Thorp and Smith, 1952). Therefore, there exists a much greater level of uncertainty in the loess data for St. Charles and Jefferson Counties as compared with the rest of the study area mapped by others.

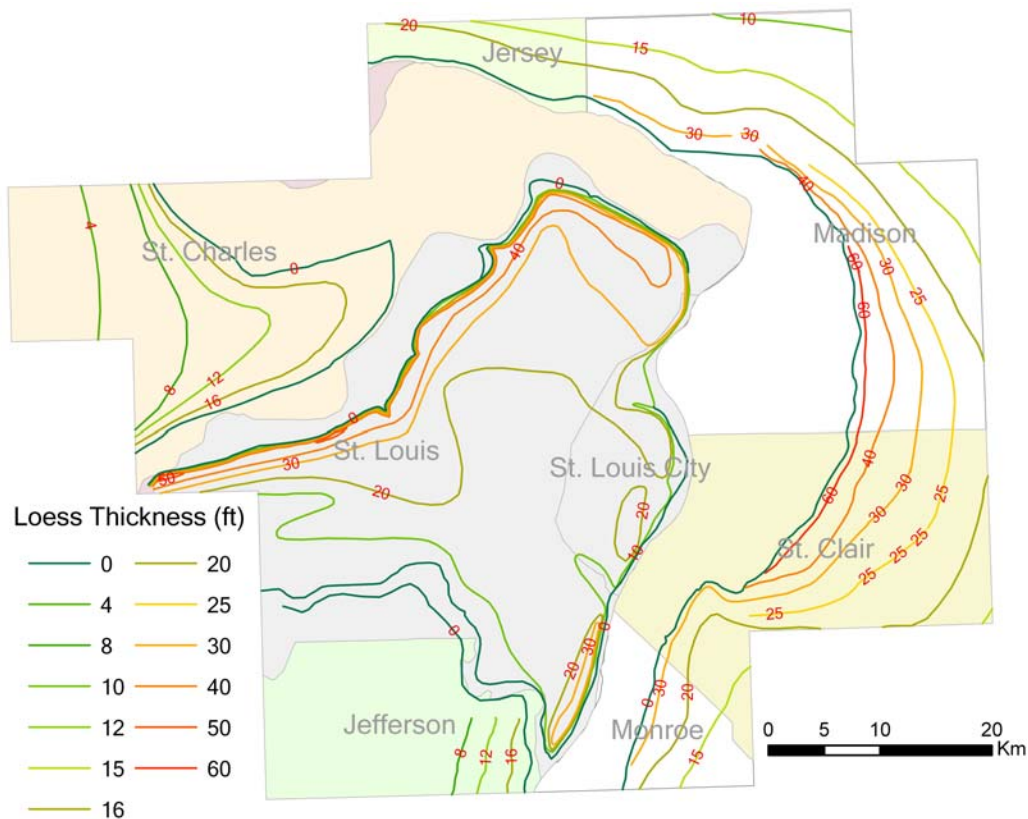


Figure 2.4. Isopach map showing the combined thickness of loess deposits of varying age in the St. Louis Metropolitan Area. Loess deposits are locally absent in the floodplains, thickest along the river bluffs bordering the Missouri and Mississippi rivers, and thin rapidly with increasing distance from the main river valleys.

2.3. BEDROCK GEOLOGY

Paleozoic age bedrock basement rocks, dominated by Mississippian age carbonates and Pennsylvanian age shales, influence the fundamental shape of the land surface in the St. Louis Metro area. Bedrock geologic maps provide information on 1) the host rock and geologic structure, including economic mineral deposits such as coal and petroleum, and 2) the stability of structure foundations and road cuts (Devera, 2004; Devera and Denny, 2003; Satterfield, 1977).

2.3.1. Stratigraphy and Geologic Structure. The St. Louis metropolitan area is located between the Ozark Uplift to the southwest and Illinois Basin to the north and east. Bedrock exposures are limited in the STL area due to the thick cover of Quaternary loess,

glacial till, residuum, and/or alluvial deposits. Most of the bedrock outcrops are exposed in river cut bluffs and man-made exposures for road cuts and rock quarries. Subsurface data, such as water well and geotechnical boring logs, and geophysical surveys, have been used to unravel the geologic structure of the STL region (Denny and Devera, 2001a, 2001b; Devera, 2003; Devera, 2004; Devera and Denny, 2001; Harrison, 1997; Satterfield, 1977).

The oldest exposed rock in the STL area is an Ordovician formation found in Jefferson County. The youngest sediment is the Quaternary alluvial deposits infilling the modern flood plains along major water courses. The Paleozoic bedrock units underlying the Mississippi River flood plain are not defined on the Missouri side, but are on Illinois side.

The regional orientation of the older Paleozoic strata is more or less near-horizontal; although beds mainly strike north to northwest or northeast and dip gently (2 to 3 degrees) toward the east (Denny and Devera, 2001a, 2001b; Devera and Denny, 2001, 2003; Devera, 2000; Harrison, 1997; Satterfield, 1977). The geologic structures in the study area were plotted on the basis of existing maps in hardcopy form (Devera, 2000, and Harrison, 1997) and GIS digital format in the Missouri Environmental Geology Atlas (MoDNR-DGLS, 2006). These geologic structures include asymmetric folds, such as the Waterloo-Dupo anticline, and related faults, such as the St. Louis fault zone. The major geologic structures are described in detail by Harrison (1997), Denny (2003), and Devera (2000, 2004).

2.3.2. Compilation. The purpose of this chapter is to compile pre-existing bedrock geologic maps of the St. Louis metropolitan area into a GIS format. Geologic maps were compiled from the publications of the Missouri Department of Natural Resources, Division of Geology and Land Survey (MoDNR-DGLS), the Illinois State Geological Survey (ISGS), and the U. S. Geological Survey (USGS). The maps (1:24,000 scale) of the House, Maxville, and Oakville quadrangles in Missouri were manually digitized and the descriptions of geologic units were input into attribute tables. The bedrock geology of St. Louis 30'×60' quadrangle (1:100,000 scale) was compiled by Harrison (1997) and the corresponding GIS shapefiles were kindly provided by Harrison (2006, personal commun.). This map was used for the Missouri portion. The statewide

map (1:500,000 scale) of Illinois was prepared by Kolata (2005) and the Illinois portion of the study area was provided by the ISGS as a series of GIS shapefiles (Kolata, 2007, personal commun.).

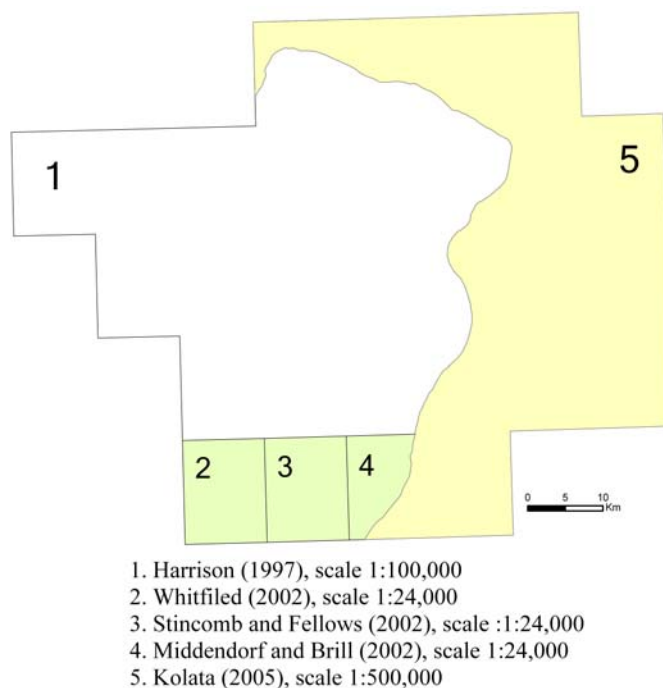


Figure 2.5. Map showing the areal distribution of the five data sources used to compile a seamless Bedrock Geologic Map of the St. Louis Metropolitan Area.

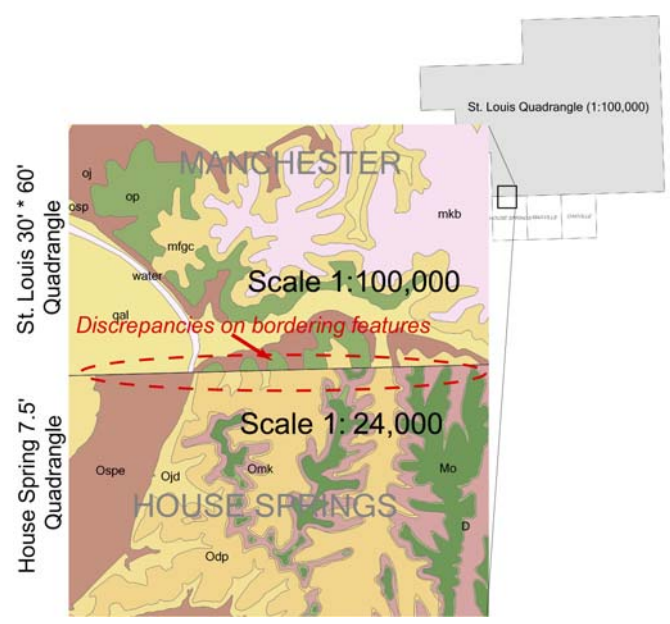
The five digitized maps included three 7.5-minute quadrangles in Missouri, Shultz's (1997) open file map, and Kolata's (2005) statewide map. These maps were combined and integrated to produce the first seamless map of the Bedrock Geology of the St. Louis Metropolitan Area in one GIS shapefile. Figure 2.5 presents the index map showing the respective areas covered by the five data sources for compiled bedrock geology map.

A challenging problem in stitching the bedrock geologic maps was the disparity of scale between three 1:24,000 scale quadrangles in southern St. Louis Metro area and

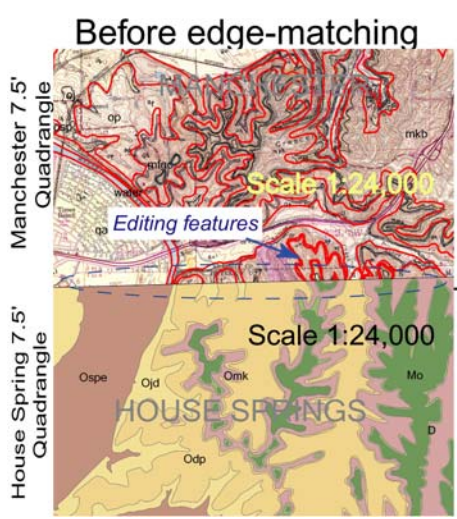
the 1:100,000 scale St. Louis Quadrangle near the St. Louis – Jefferson County boundary. The disparity of the different scales created a very obvious joining problem at the map boundaries. In order to solve this problem, the boundaries of the 1:100,000 scale map were edited with the 1:24:000 scale bedrock geologic maps (sources 2, 3, and 4 in Figure 2.5), instead of 1:100,000 scale map, using ArcGIS software. After the mismatching edges were edited, these GIS formatted maps were conjoined, as shown in Figures 2.6A, B, and C.

The map symbol and unit correlation are shown in Table 2.3. The description and thickness of each unit are presented in Table 2.4. The compiled seamless Bedrock Geologic Map of St. Louis Metropolitan Area is shown in Figure 2.7.

(A)



(B)



(C)



Figure 2.6. Map scale matching problems encountered in this study. A) Joining problems at map boundaries resulting from different map scales. B) Before edge-mismatching area of 1:100,000 and 1:24:000 scale maps. C) After edge-matching, by editing the mismatching boundary with another 1:24,000 scale map instead of the 1:100,000 scale map.

Table 2.3. Stratigraphic correlations between recognized bedrock geologic units and corresponding map symbols used in the St. Louis Metropolitan area, Missouri and Illinois.

ERA	SYSTEM	SERIES	FORMATION	SYMBOL	
CENOZOIC	Quaternary	Holocene	Alluvium	Qal	
		Pleistocene	Terrace Deposit	Qt	
			Unconformity		
MESOZOIC	Tertiary	Pliocene	Grover Gravel	Tg	
		Miocene			
			Unconformity		
PALEOZOIC	Pennsylvanian	Missourian	Pleasanton Group	Pp	
		Desmoneisian	Modesto Formation/McLeansboro Group	Pmo	P
			Shelburn-Patoka	Psp	
			Carbondale	Pcar	
			Marmaton Group	Pm	
			Cherokee Group	Pc	
		Atokan	Tradewater	Pt	
			Unconformity		
	Mississippian	Chesterian	Yankeetown Sandstone	Myra	
			Renault Limestone		
			Aux Vases Sandstone		
			Ste. Genevieve Limestone		Msg
			Lower Pope Group		Mpl
			Unconformity		
Meramerician		St. Louis Limestone	Msl		
		Salem	Ms	Mws	
		Warsaw	Mw		
Osagean		Keokuk-Burling Limestone	Mkb	Mkbf	
Kinderhookain	Fern Glen and Bachelor	Mfgc			
	Chouteau Limestone	Mc			
		Unconformity			
Devonian	Upper Devonian	Bushberg Sandstone and Glen Park Limestone	Db		
Silurian			Su		
			Unconformity		

Table 2.3. (Continued)

Ordovician	Cincinnati/ Champlainian/Mohawkian	MaQuoketa Shale	Om	Omk
		Cape Limestone/Kimmswick Limestone	Ok	
	Champlainian/Mohawkian	Decorah		Okd
		Plattin Limestone	Op	Odp
	Mohawkian	Joachim Dolomite	Oj	
		St. Peter Sandstone	Osp	

Table 2.4. Descriptions of bedrock geologic units recognized in the St. Louis Metropolitan area, Missouri and Illinois.

SYSTEM	FORMATION	DESCRIPTION	THICKNESS (m)
Quaternary	Alluvium	Gravel, sand, clay, and silt on floodplains of major rivers and smaller streams. Gravel is subrounded to angular. Alluvium is intermixed and interbedded	0.3 to 65
	Terrace Deposit	Sand, gravel, clay, and silt. This deposit includes colluvium. Sand derived from local rock, colluvium, and residuum. Rounded to subangular gravel from local rock and cherty residuum. Clay and silt from loess and colluvium.	0 to 6
	Unconformity		
Tertiary	Grover Gravel	Gravel, sand, and clay. This unit consists of rounded, light-brown chert pebbles, and lesser quantities of red (hematitic) chert, purple quartzite, and white to pink quartz pebble. Oolitic chert or pebbles are also common. Matrix is red to tan sand and clay with sparse zircon and tourmaline.	0.3 to 10
	Unconformity		
Pennsylvanian	Pleasanton Group	(undivided) Shale and sandstone. Mapped only in Missouri	up to 30
	Modesto Formation / McLeansboro Group	Limestone, shale, sandstone, and thin coal layer. Mapped only in Missouri	up to 23
	Shelburn-Patoka	Shale (gray to red), limestone (gray), and siltstone. The basal limestone is a dark gray, argillaceous, fossiliferous wackestone. Its nodular bedding is locally replaced by fossiliferous shale. Mapped only in Illinois	0 to 25
	Carbondale	(undivided) Shale (gray carbonaceous and pyritic). Limestone, sandstone, and coal are also found. The base is marked by a rooted coal bed (0.5m). Mapped only in Illinois between Illinois and Mississippi rivers	33
	Marmaton Group	(undivided) Intercalated shale, limestone, clay, and coal. Mapped only in Missouri	25
	Cherokee Group	(undivided) Cycles of sandstone (massive), siltstone, shale, clay, and coal. Mapped only in Missouri	33
	Tradewater	Sandstone and shale (dark). Shales are interbedded with sandstone beds. Siltstone, fire clay, coal, and limestone are minor. Mapped only in Illinois. Sandstone occurs in channels, as sheet-like bodies, and in a basal bed that is locally conglomeratic and crossbedded	10 to 25
	Unconformity		
	Yankeetown Sandstone	Calcareous sandstone, variegated shale, and chert.	>14

Table 2.4. (Continued)

Mississippian	Renault Limestone	Limestone, and lesser variegated shale, fine-grained sandstone, sandy limestone, and conglomerate near the base. Pure limestone is found in Illinois	10 to 30
	Aux Vases Sandstone	Sandstone, siltstone, shale (minor), and local lens of dolomite and limestone. Sandstone is gray, hematitic in places and very fine to fine grained. Tourmaline is found. Large scale trough cross or massive bedding are common. Interfingers with various facies of the underlying Ste. Genevieve Limestone	up to 20
	Ste. Genevieve Limestone	Limestone (white, massive, clastic). Oolitic beds dominate in the upper part and crossbeds and ripple marks are prominent in the lower part. Gray chert is common and local black or red chert is found. In the upper part of the formation, fine-grained calcareous sandstone beds are interbedded within shale or limestone. This unit in St. Louis area has a conglomeratic base and rests unconformably on an eroded top of the St. Louis Limestone	45
	Lower Pope Group	(undivided) Limestone: Mostly light-colored crinoidal and oolitic grainstones and packstones. Minor wackestones, lime mudstone, and dolomites are found. This rock resembles the Ste. Genevieve Limestone. Exposures are found along the Mississippi River. This group is described by Devera (2006) and Nelson (1998)	20 to 25
	Unconformity		
	St. Louis Limestone	Limestone (dark-gray, finely crystalline, thin to massive) and the thin beds of shale (bluish-gray). Intraformational breccia with shale matrix occurs in the lower part. Brecciation is believed to cause karstification of gypsum and anhydrite. This unit is typically found in St. Louis downtown area	30 to 75
	Salem	Limestone: Fossiliferous calcarenite of fossil set or fragment in a matrix ranging from micrite and sparite. Banded overgrowths around fossils are common. Minor fine-grained limestone, sandstone, chert, and evaporites. Chert zone ("cannon ball or bulls-eye") occurs in the upper of this formation in the St. Louis. The foraminifera, <i>Globoedothyra baileyi</i> is an index fossil	20 to 55
	Warsaw	Shale (dark, fissile) and intercalated dolomite or dolomitic limestone (argillaceous and silty) in the upper half. Shaly to argillaceous, cherty very fossiliferous, finely crystalline, dolomitic limestone in the lower half.	20 to 30
	Keokuk-Burling Limestone	(undivided) Two units are difficult to differentiate. Keokuk: Limestone (medium crystalline). Crinoidal fossil horizons are common. Light-gray, nodular chert occurs in the lowermost and upper most thirds. Similar to Burlington Limestone, however, Keokuk contains a greater heterogeneity of fossil, with more abundant bryozoans, corals, and brachiopods. Burlington: Limestone (medium to coarsely crystalline). Large crinoid stems are common. Beds are commonly cross stratified. Up to 3m thick chert occur erratically. The lower unit of 5.5~9m thick and 50% chert in the St. Louis is called the "Lower Burling Limestone) 50% chert	53 to 60

Table 2.4. (Continued)

	Fern Glen and Bachelor	Fern Glen: Calcareous shale (red and green), shaley limestone, and a basal bed of massive, dolomitic limestone. This formation thickens away from the Illinois basin. Quartz sand layer from Bachelor-Bushberg formation occurs in the base. Bachelor: Sandstone (pale-green, calcareous, quartzose) containing conphosphatic nodules at its base	9 to 18
	Chouteau Limestone	Argillaceous (gray) limestone in irregular beds(< 0.3m thick). Bedding planes are typically wavy and have shale partings. Most beds are fossiliferous and crinoids are dominant It thickens westward out of the Illinois basin	1 to 21
Unconformity			
Devonian	Bushberg Sandstone / Glen Park Limestone	Bushberg Sandstone: Discontinuous, massive sandstone (yellow to light brown, fine- to coarse-grained, friable quartz). Glen Park Limestone: Limestone (gray, oolitic, fossiliferous). Limestone in the south Glen Park is 0.3m thick or less and contains phosphatic pebbles.	0 to 7.5
	Cedar Valley Limestone / Joliet / Kanakee / Edgewood Limestone	Cedar Valley: Limestone and sandstone. The base is a (brown to gray)sandstone overlain by fossiliferous and argillaceous limestone. Joliet: Dolomite and minor shale; yellowish brown to gray. The surface in Dagett Hollow contains polygonal mud cracks. Chert nodules sporadically occur. <i>Sthenarocalymene celebra</i> (trilobite) is found in the quarries, east Grafton. Kanakee: Dolomite (yellowish brown to buff gray) and shale (greenish gray tint). This unit contains glauconite and fossils (brachiopod, straight cephalopods, and trilobites). Edgewood Limestone: Dolomite (brown to buff gray) and shales (greenish gray tint). Chert nodules, glauconite, or fossils sporadically occur	30 to 40
Unconformity			
Ordovician	MaQuoketa Shale	Shale: massive platy mudstone to fissile claystone or shale containing basal argillaceous dolomite/calcareous mudstone. This unit occurs in the southwestern third of the St. Louis quadrangle, where it was cut out along a regional unconformity at the base of Upper Devonian rocks. Outcrop of 1m shale is found at the top of the Webber Quarry (House Springs Quadrangle)	up to 45m
	Cape Limestone / Kimmswick Limestone	Limestone (coarsely crystalline, medium-bedded to massive fossiliferous). Weathered outcrops are pitted or honeycombed. Minor chert occurs in the lower part of the formation. <i>Receptaculites</i> (sunflower coral) is a index fossil. Outcrops are scattered and usually covered by Fern Glen colluvium or slump blocks. Enlarged solution joints are common and are filled with Pennsylvanian clay and sand.	18 to 36
	Decorah	(undivided) Limestone and shale. Light brownish to greenish limestone or lime mudstone interbedded with organic-rich reddish brown shales. The chert is dark gray. Strophominid brachiopods are the dominant fossils. Metabentonite (white, 5~15cm thick) occurs near the base of this unit. Outcrop is covered by chert colluvium and boulders from Kimmswick and Fern-Glen formations	12

Table 2.4. (Continued)

Plattin Limestone	(undivided) Limestone. Gray mudstone interbedded with thin, laminated to cross-laminated grain stone. Thin shale beds occur in upper part; shale forms partings in the middle and lower parts. Burrow markings are a distinctive feature. Its base in Missouri is placed at a prominent, oolitic limestone-conglomerate bed (1~2m thick). This unit thickens eastward	25 to 90
Joachim Dolomite	Dolomite (silty, argillaceous, fine crystalline, yellowish-brown to gray). This unit is thin- to massive-bedded and contains interbedded dolomitic limestone and thin shale. Beds just above the underlying St. Peter Sandstone are locally sandy.	25 to 40
St. Peter Sandstone	Sandstone (well-sorted, medium- to fine-grained quartzite). Basal (1~2m; Kress Member) consists of weathered and reworked green shale, sandstone, and chert detritus. The base is one of regional unconformities in the Midcontinent. This unit is a major regional aquifer. That of pure silica is extensively quarried. Thickness toward the northeast	6 to 15

2.4.1. Data Source. The Missouri Department of Natural Resources, Division of Geology and Land Survey (MoDNR-DGLS) collected and edited geotechnical boring records for the Missouri side of the St. Louis Metropolitan area in order to create a database of surficial materials for the St. Louis Area funded by the U.S Geological Survey (USGS)-National Earthquake Hazard Reduction Program (NEHRP) in 2001-02. The boring records were supplied to DGLS by the Missouri Department of Transportation (MoDOT) and a few other public agencies, such as St. Louis Metropolitan Sewer District and Bi-State-Metrolink. Most of the geotechnical borings drilled by MoDOT were drilled for highway and bridge construction. Boring locations in Missouri are contained in Universal Transverse Mercator (UTM; zone 15), North American Datum (NAD) 1983 coordinates. The data source is identified by project and boring number convention for more detailed information (Palmer, 2006). The MoDNR-DGLS database is expected to serve as a compilation of fundamental soil properties for mapping surficial materials and earthquake hazards in the St. Louis area and was made available to the public in CD-ROM in April 2007.

The Illinois State Geological Survey (ISGS) has collected and maintained logs for boreholes drilled in Illinois by the Illinois Department of Transportation and other regulatory programs of the state. The ISGS data contain: 1) all borings and water wells issued by the Illinois Department of Mines and Minerals and by the Illinois Department of Public Health and county health departments, and, 2) some engineering borings submitted by the Illinois Department of Transportation (IDOT) and other private agencies. Each borehole has a unique identifier numbered using an American Petroleum Institute (API) code. The data points in Illinois were originally referenced with the geographic coordinate system (latitude/longitude) and these points were converted to UTM coordinates (zone 15 and 16) for this study.

2.4.2. Compilation. The existing borehole information databases from the Missouri and Illinois geological surveys were provided in Microsoft Access 97 and spread sheet formats, respectively.

The borehole records covered 2,394 sites in Missouri and 4,817 sites in Illinois over a land area of approximately 4,400 km². The borehole databases maintained by Missouri and Illinois generally contain many different kinds of logs. Table 2.5 shows a

tabulation of boring type (originally classified by MoDNR-DGLS and ISGS) and the respective number of borehole records used in the subject study. The GIS map (Figure 2.8) presents boring locations and types of the St. Louis Metro area, plotted in UTM coordinates (Zones 15 and 16).

Table 2.5 Borehole purpose and information contained on logs used for the St. Louis Metropolitan area study, Missouri and Illinois.

State	Borehole purpose	# of records	Information noted on logs
Missouri	Bedrock	2338	Depth to bedrock, Bedrock type Core recovery (%), Rock Quality Designation (RQD)
	Core log	729	
	Grain Size	93	Grain size analysis of soil
	Material	2330	Description of soil material
	Physical Property	1906	Standard Penetration Test (SPT) N-value, Cone Penetration Test (CPT), ASTM class, Unit weight (water content,%), Liquid limits, and Plastic index
	Water Observation	961	Depth to groundwater
	Site	2394	
Illinois	Highway Log	857	Description of soil material
	Highway Engineering	496	Standard Penetration Test (SPT) N-value
	Highway Head	2226	Description of geotechnical boring
	Log	3636	Description of soil material
	Water Well	4728	Description of water well
		Site	4817

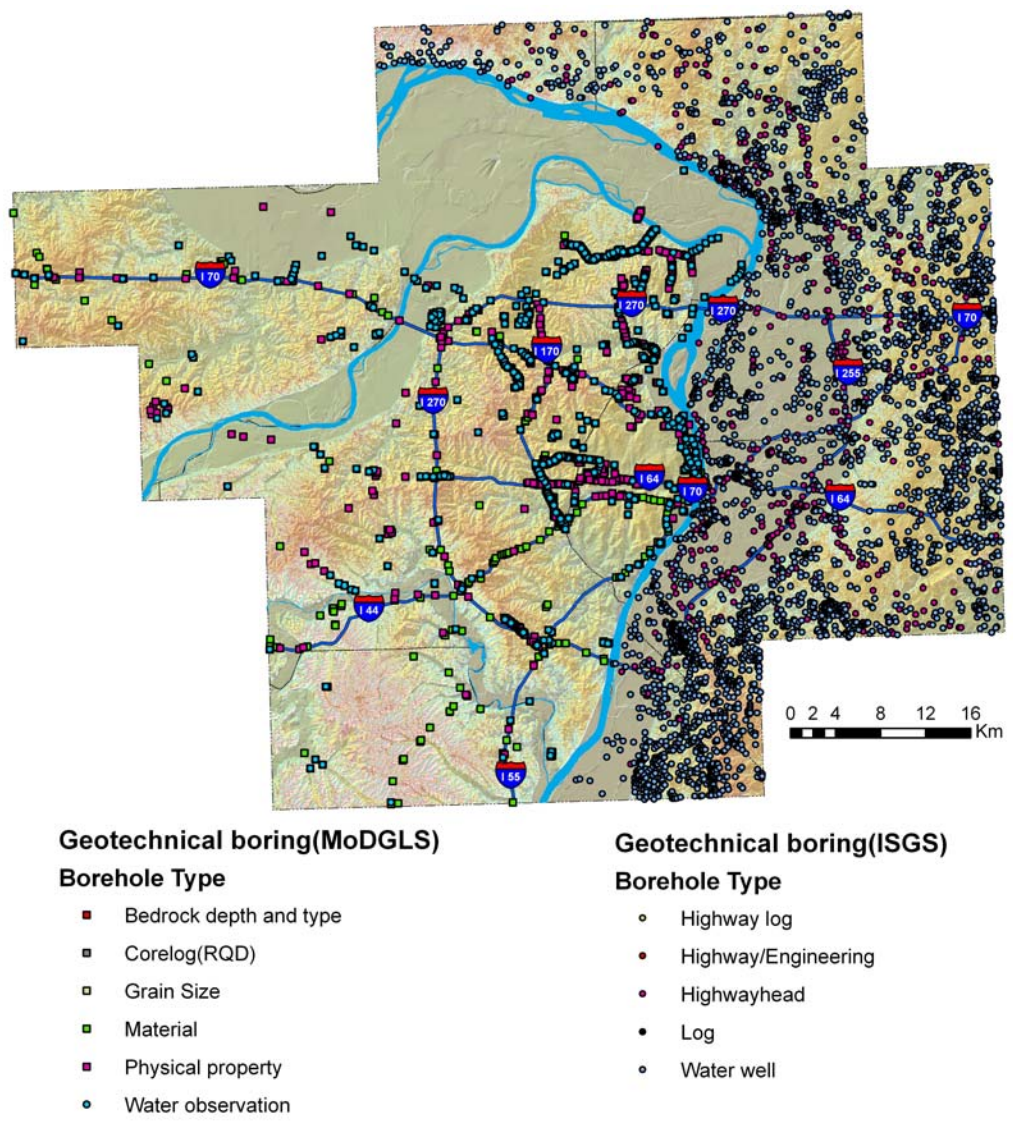


Figure 2.8. Borehole locations and types in the St. Louis Metropolitan area, Missouri and Illinois in a seamless GIS vector format.

3. SHEAR WAVE VELOCITY AND SITE AMPLIFICATION

3.1. INTRODUCTION

In the earthquake damages observed after the 1906 San Francisco and the 1989 Loma Prieta earthquakes in California, structures founded on filled ground or soft soils sustained more damage than those situated on stiff soil or rock sites (Kelly, 2006; Kramer, 1996; Borcherdt, et al., 1991). Soft soils, such as unconsolidated sediments in flood plains, are generally more susceptible to ground motion amplification and subsequent ground failures associated with failure mechanisms, such as soil liquefaction and lateral spreads.

The simplest way of accounting for site conditions when estimating potential seismic hazards is to consider the impedance contrast likely to be generated at the bedrock/soil cap interface beneath a site of interest. This estimate is commonly made by comparing the shear wave velocity (V_S) of the shallow subsurface with that of the weathered and less weathered or unweathered rock lying beneath the site. The shear wave velocity (V_S) generally decreases as the void ratio of the soil cap increases. The void ratio is inversely related to the dominant grain-size, sorting, and the packing density of soil particles. Thus, as the grain size of an unconsolidated sediment decreases and the age decreases (becomes younger, and less indurated), V_S is likely to decrease (Fumal and Tinsley, 1985). Seismic shaking tends to increase where sites are underlain by low density (unconsolidated) sediments with low shear wave velocity (V_S). This is in accordance with the conservation of elastic wave energy, which states that the seismic wave amplitude from particle velocity increases in sediments with lower density and slower V_S waves (Kramer, 1996). Therefore, softer soils generally exhibit low shear wave velocities and produce greater ground amplification than stiff soils with higher V_S values.

The fundamental complication in estimating seismic site response is that V_S values are usually measured at discrete points and some method of extrapolation beyond the point of measurement is something of a requisite assumption. A fundamental approach is to correlate surface geology/stratigraphy with these discrete velocity measurements and then extrapolate, based on the stratigraphy (Park and Elrick, 1998; Tinsley and Fumal, 1985). Given the assumption that the V_S values depend on the

physical properties of materials, V_s values can be correlated and characterized with lithologic units and, therefore, V_s profiles generated at particular sites or within recognized stratigraphic units can be: 1) generated from the measured V_s values and then, 2) correlated with these same soil/rock/stratigraphic units (Wills et al., 2000). These V_s reference profiles for specific geologic/stratigraphic units are called “characteristic profiles” by engineering seismologists. They are commonly used in site-response analyses of large areas, extending well beyond the areal limits of a typical project site and intended to assess the effects of underlying geologic deposits (the ‘soil cap’) on ground motion amplification (Gomberg et al., 2003; Romero and Rix, 2001; Wills et al., 2000).

Previous studies have demonstrated that the average V_s in the upper 30m (V_s^{30}) is inversely correlated with the average horizontal spectral amplification of earthquake ground motion (Borcherdt and Gibbs 1976; Borcherdt et al., 1991). Based on the mean observed amplification, intensity increment, and corresponding V_s^{30} values measured in specific geologic units, Borcherdt et al (1991) grouped near surface geologic units into four V_s^{30} classes, and then mapped amplification potential for geologic units in the San Francisco Bay area. Their results indicated that low V_s^{30} values (< 300m/s) imply high amplification capability and, are generally found on unconsolidated Quaternary deposits like artificial fill, Holocene estuarine clays, or Holocene alluvium.

3.2. NEHRP SOIL CLASSIFICATION

To assess the susceptibility to ground amplification, in 1994 the National Earthquake Hazards Reduction Program (NEHRP) defined six soil profile types (S_A , S_B , S_C , S_D , S_E , and S_F) following the study by Borcherdt (1994), which suggested a consistent relationship between site response and V_s^{30} . According to the NEHRP guidelines, the weighted average V_s is obtained using the following equation;

$$V_{S30} = \frac{\sum_{i=1}^n d_i}{\sum_{i=1}^n \frac{d_i}{V_{Si}}}$$

where d_i = the thickness of any layer between 0 and 30m, V_{Si} = the shear wave velocity (m/s), and $\sum_{i=1}^n d_i = 30\text{m}$.

The description of six site classes defined in terms of V_S^{30} in accordance with NEHRP provisions is shown in Table 3.1 (BSSC, 2003).

This study sought to: 1) assign appropriate NEHRP soil site classes for near surface geologic units in the STL area based on corresponding measured V_S^{30} values, 2) prepare a NEHRP soil site classification map, and, 3) create characteristic V_S profiles (0 to 30m) for surficial geologic units in the St. Louis Metropolitan area.

Table 3.1. NEHRP (National Earthquake Hazards Reduction Program) site classification.

Soil Site Class	Avg. V_s (m/s) in the upper 30m	General Description
S_A	$V_s > 1500$	Hard rock
S_B	$760 < V_s \leq 1500$	Rock with moderate fracturing and weathering
S_C	$360 < V_s \leq 760$	Very dense soil, soft rock, highly fractured and weathered rock
S_D	$180 < V_s \leq 360$	Stiff soil
S_E	$V_s \leq 180$	Soft clay soil
S_F		Soils requiring site-specific evaluations

3.3. STUDY AREA

The St. Louis Metropolitan area (*STL*) is located on unconsolidated Quaternary deposits which generally consists of: 1) low-lying alluvial deposits in the flood plains of four major rivers (Mississippi, Missouri, Illinois, and Meramec), and, 2) loess and/or glacial till deposits mantling elevated uplands bounding either side of the flood plains. Information gleaned from the logs of 1,634 geotechnical borings in *STL* suggests that the Quaternary deposits are generally about 22 ± 11 m and 10 ± 6 m (mean \pm standard deviation) thick in the flood plains and on the elevated uplands, respectively. Unconsolidated sediments within the flood plain are generally deeper and more heterogeneous than those mantling the uplands.

Bauer et al. (2001) prepared a map portraying seismic shaking potential for the high-risk area surrounding the New Madrid Seismic Zone at a scale 1:250,000, which included portions of five states. Due to the lack of V_s measurement in the St. Louis Metro area, the V_s values for each geologic unit were assigned based on existing V_s measurements of similar units measured at a few sites in the Midwest and the nationwide average value was estimated based on material characteristics. Each geologic unit was assigned an assumed V_s value and the aggregate soil cap thickness was stacked to create an approximation of the material thickness, an average V_s value was determined for the upper 30m, and a NEHRP site class was assigned for the combined 'soil stack.' The

resulting map provides a rough outline that follows the areal limits of the flood plains along major rivers, which are classified as Soil Site Class F; the eastern STL area in Illinois was classified as Soil Site Class C or D; St. Louis County was classified as Soil Site Class C or D (northern part), and St. Charles County as Soil Site Class C. The City of St. Louis, St. Louis County, and St. Charles County adopted the 2003 International Building Code in 2006, which includes the 2000 NEHRP provisions incorporating soil profile type to estimate ground motion loads for earthquake-resistant building design.

3.4. SHEAR WAVE VELOCITY (V_s) DATA ACQUISITION

117 shear wave velocity (V_s) profiles were measured and provided to our study team by the University of Missouri-Rolla (UMR), the U.S. Geological Survey (USGS), and the Illinois State Geological Survey (ISGS). The locations of these V_s tests and coding for their respective sources were plotted using GIS (Figure 3.1). Each value of V_s in the upper 30m (V_s^{30}), the corresponding surficial geologic unit upon which the tests were performed, and the data source are summarized on APPENDIX A. For the MASW profiles not extending to 30m, the velocity from 20m to 30m was assumed to be constant (Hoffman 2007, personal commun.).

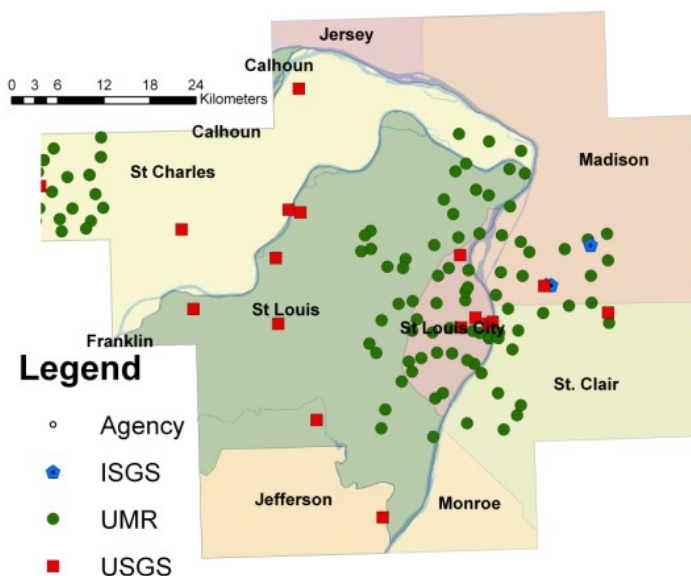


Figure 3.1. Locations and measuring agencies of shear wave velocity (V_s) measurements.

3.5. RESULTS

Due to the variety and uneven distribution of V_s^{30} data collected over the study area, the measured V_s^{30} sites were grouped by the geologic units underlying the respective test sites, which were assumed to have similar ages, physical properties, and landforms. The study area was divided into six major groups, defined by mapped surficial geologic units: 1) artificial fill, 2) alluvium, 3) terrace or lake deposits, 4) loess, 5) till, and 6) karst. Alluvium deposits were then subdivided into seven subgroups, divided by considering the location (along major and minor rivers) or stratigraphic facies (e.g. Cahokia fan, clay, or sands in Illinois). Other deposits, such as loess and till, were distinguished by location (St. Charles County, St. Louis County and/or City, and Illinois area). Figure 3.2 shows the distribution of test sites and values of V_s^{30} at those sites determined for their respective surficial geologic units. The values of V_s^{30} within any mapped stratigraphic unit were found to exhibit noticeable variations. This might be attributed to the varieties of grain size distribution, bulk density, induration, and thickness of the sediment from one location to another (Bauer et al., 2001).

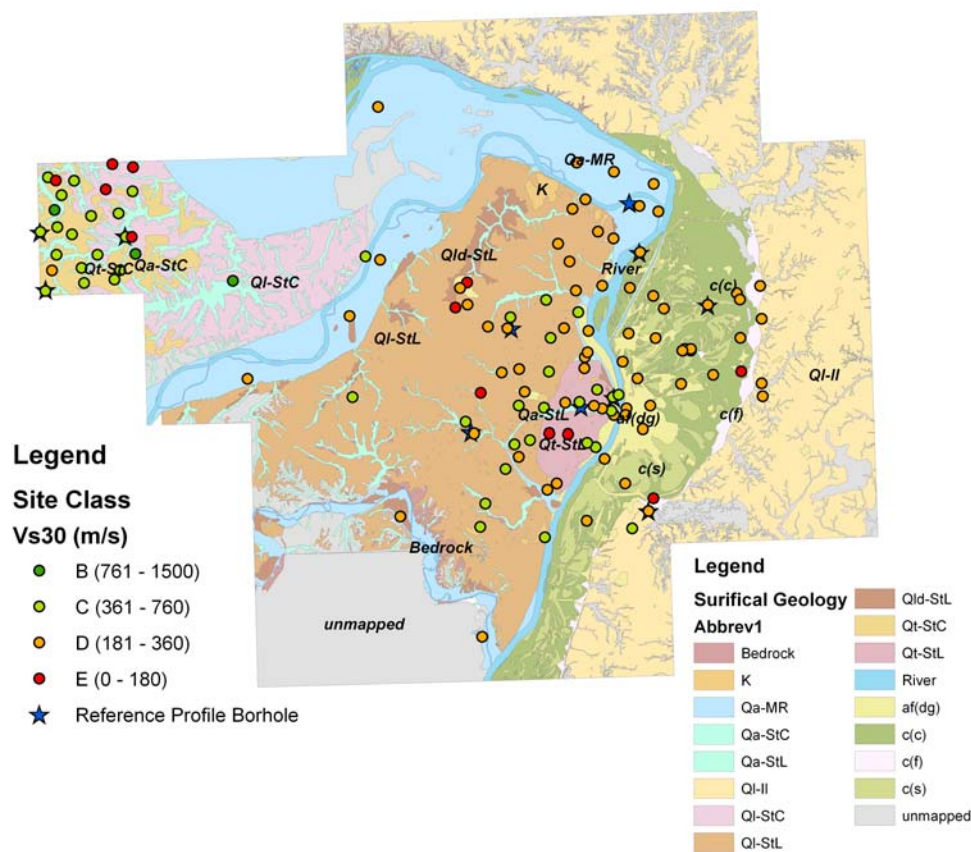


Figure 3.2. Estimated average shear wave velocity (V_s^{30}) in the upper 30m and corresponding NEHRP soil site classes plotted on Map of Surficial Materials, at the respective test locations.

3.5.1. NEHRP Soil Site Classification in STL. The arithmetic mean value of V_s^{30} for a corresponding surficial geologic unit was computed and assigned the each mapped geologic unit according to the NEHRP soil site classification scheme, tabulated in Table 3.2. There was a high degree of variation in the calculated V_s^{30} values and large expanses of the study area that were not tested. Because of these uncertainties, the following criteria were used to assign NEHRP soil site categories to the mapped surficial geologic units:

1) The distribution of V_s^{30} values were found to straddle some of the NEHRP classification boundaries between soil site class categories within the same mapped units (e.g. Cahokia fan, terrace or lake deposits, loess and till in St. Louis County and/or City).

For example, there were only two V_s tests made on Cahokia fan facies and these each fell into different soil site classifications (Bauer et al., 2001). If the arithmetic mean of V_s^{30} in a given unit is close ($< \pm 20\text{m}$) to the established soil site class boundaries (listed in table 3.1), these units were informally assigned to both categories (e.g., S_E to S_D for Cahokia fan, S_C to S_D for terrace or lake deposits, and S_C to S_D for loess and till in St. Louis County and/or City).

2) The percentage of V_s tests falling within the various NEHRP soil site class categories for each mapped surficial geologic unit were computed. For example, of six sampled sites on loess in the St. Charles County, four of the sites could be classified as category S_C , two of the sites as category S_B , and the mean V_s^{30} value (715 m/s) of six sites as category S_C . So, 67% of the tests carried out on this map unit could be considered to be within category S_C .

3) Shear wave velocity data were not measured in a few of the mapped surficial units nor were any tests conducted on the Paleozoic bedrock. In the areas bereft of V_s data, these were designated as “No Data” or “Bedrock”, respectively.

The resultant map of NEHRP soil site classification based on the mapped surficial geologic units and the arithmetic mean V_s^{30} values are shown in Figure 3.3. The alluvial deposits along major rivers typically exhibit lower shear wave velocities than those along the minor stream courses in the dissected loess covered uplands. Most of the surficial units tested in Missouri exhibited greater variability than those in Illinois. This is probably due to the longer period of subaerial exposure and variations in residual soil weathering processes in the upland sites. In these areas weathering rates vary markedly, depending on drainage and pore water chemistry (Goodfield, 1965).

The NEHRP Soil Classification Map (Figure 3.3) estimates the respective soil site classes by the mapped surficial geologic units and by geomorphic province. In St. Charles County (north of the Missouri River) the alluvial, loess, and till deposits are classified as category S_C , while those in St. Louis County and/or the City of St. Louis and Illinois, were classified as S_C to S_D or S_D . This suggests that most of the surficial deposits in St. Charles County exhibit higher V_s^{30} value than those in St. Louis City and County, and Illinois. Given the contrast in recent geomorphic history on either side of the Missouri River, these kinds of differences should be expected.

As stated in the original article by Borchardt et al. (1991), the NEHRP soil site class maps are not intended to predict actual ground motion amplification at individual sites. The maps are intended to highlight general zones for which underlying deposits may be capable of amplifying incoming seismic energy. The statistics listed in Table 3.2 should be useful insofar as they provide the observed range of values in the respective units across a wide array of geomorphic provinces that comprise the STL study area. More precise predictions of site amplification require site-specific assessments, using data generated on the site under evaluation.

Table 3.2. Mean shear wave velocity (V_s^{30}) in the upper 30m grouped by mapped surficial geologic units and corresponding NEHRP soil site classes.

Surficial Geologic Unit			V_s^{30} (m/s)					NEHRP Class	
Material	Location	Symbol	Site count	Range	Median	Mean	Standard deviation	Site Type	% in category
Artificial Fill	along Mississippi River	af(dg)	14	159~620	242	277	113	S_D	77
	along streams in St. Charles County	Qa-StC	3	409~454	437	433	22	S_C	100
	along streams in St. Louis County & City	Qa-StL	6	240~456	314	319	76	S_D	83
Alluvium	along Major Rivers in Missouri side	Qa-MR	10	192~259	230	228	23	S_D	100
	Cahokia fan	c(f)	2	137~254	195	195	83	S_D to S_E	50/50
	Cahokia sandy	c(s)	9	197~264	221	226	24	S_D	100
	Cahokia clayey	c(c)	11	194~304	228	229	31	S_D	100
Terrace or Lake deposits	St. Louis County & City	Qld-StL	5	200~615	347	360	155	S_C to S_D	20/80
	St. Charles County	Ql-StC	6	410~1123	686	715	239	S_C	67
Loess	St. Louis County & City	Ql-StL	24	182~720	341	368	113	S_C to S_D	46/54
	Illinois	Ql-II	5	201~386	249	270	69	S_D	80
Till	St. Charles County	Qt-StC	13	293~840	440	448	141	S_C	92
	City of St. Louis	Qt-StL	6	218~560	292	340	130	S_C to S_D	33/64
Karst	St. Louis County & City	K	5	410~534	506	487	55	S_C	100

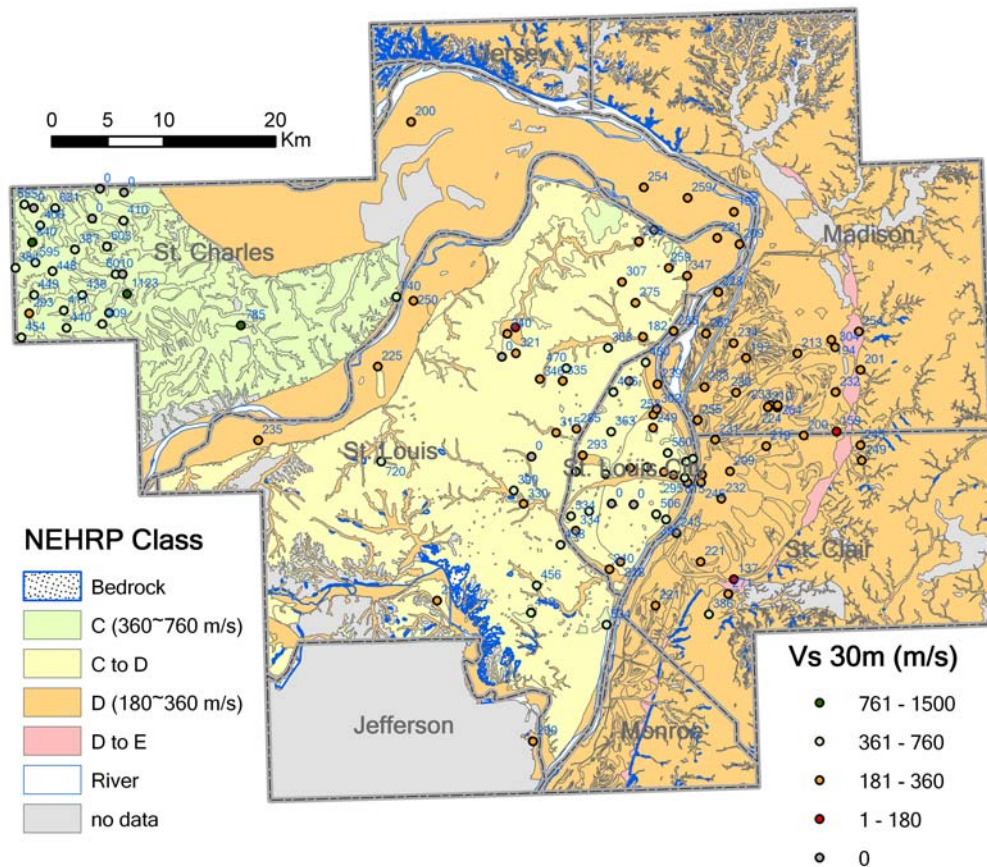


Figure 3.3. Preliminary NEHRP Soil Site Classification Map.

3.5.2. Characteristic Profiles of Shear Wave Velocity. The characteristic profiles of shear wave velocity (V_s) are intended to define those stratigraphic units that exhibit distinctive shear wave velocity properties. These profiles are input into one and two-dimensional site response programs that evaluate seismic site response. The thickness and V_s characteristics of the ‘soil cap’ overlying dense bedrock tends to control site response, by either damping or magnifying the incoming seismic energy. These kinds of assessments are of particular importance to structures with long fundamental periods (>0.8 sec), such as high rise buildings, bridges, towers, or long structures, such as bridges and pipelines. Individual and compiled characteristic V_s profiles for a specific geologic units are also helpful in ascertaining which factors tend to exert the greatest control on site amplification in any given area. For instance, the compilations of V_s data

carried out in this study showed that in the alluvial filled valleys, V_s tends increase simply as a function of depth (confinement), and little else. The characteristic profiles in the St. Louis Metro area will be used in site response analyses to assess the effects of surficial geologic units on ground motions amplification.

In a similar study of the Memphis Metro area, Romero and Rix (2001) characterized V_s profiles in surficial geologic units infilling the Upper Mississippi Embayment (to a depth of ~1000m). Characteristic V_s profiles were inferred and generalized by identifying layers with similar V_s in the upper 70m, with the range of variability (+/- 45m/s) from the mean characteristic profile, and its standard deviation. Based on the characteristic profiles obtained for the greater Memphis area, the Holocene flood plain of the Mississippi River was ascertained to have a fairly uniform V_s profile. This flood plain area was found to be the most vulnerable to ground motion amplification. Pleistocene loess deposits in terraces exhibited more variability and the highest V_s values measured in the Memphis study. These areas were found to be less susceptible to site amplification.

3.5.2.1 Procedure. Characteristic V_s profiles were constructed for each surficial geologic unit to better represent the average V_s values within the upper 30m (when there was sufficient data to that depth). Characteristic profiles are usually based on subsurface boring data collected in the vicinity of V_s measurement sites in order to assist in constraining the V_s model. The characteristic V_s profiles were constructed according to the following procedure:

- 1) V_s profiles were overlain from each V_s test carried on specific mapped surficial geologic units. The thickness of each stratigraphic layer was inferred from the similarity of V_s values and the nearest subsurface information, taken from borehole logs located between < 50m to as much as 1km from the V_s measurement sites.

- 2) The measured V_s values within discrete stratigraphic horizons of each mapped surficial unit were then calculated as the arithmetic mean of the data for that particular horizon, and a characteristic V_s value was assigned to each horizon, as shown in Figure 3.4.

- 3) Several extremely high values of V_s (compared to the other profiles) within loess deposits in St. Charles County and Illinois were considered outliers and were not

used in calculating the arithmetic mean of V_s in the mapped surficial units to which they were assigned. These data were suspected of being in weathered rock and residuum horizons, that were not identified in nearby boring logs because the borings lay at considerable distance from the measurement sites.

4) The depth-to-bedrock and underlying lithology (limestone and dolomite versus shale) varies considerably across the study area. V_s is locally impacted by buried “bedrock knobs,” by uneven weathering surfaces, blocky and/or boulder colluvium, old filled sinkholes, and active karst features, such as vugs, voids, and caverns. All of these irregularities introduce considerable data scatter and uncertainties. A number of the MASW tests collected in the Wentzville quadrangle were particularly problematic, insofar that they predicted much higher V_s values than observed anywhere else in the STL study area. There were insufficient borings in close proximity to one of these test sites, so it was excised from the calculations.

3.5.2.2 Results. The characteristic profiles for the selected surficial geologic units are shown in Figure 3.4. The referenced boring numbers and collar locations are indicated in individual profiles. Where the depth-to-bedrock is not reported in an adjacent borehole near the V_s measurement site, the depth-to-bedrock was modeled employing the (ordinary) kriging method and the uncertainty of depth- to-bedrock at each test site was statistically estimated from the kriged standard error (σ). The magnitudes of uncertainties were generally higher in areas of sparse data. The kriged predictions in the regions that area bereft of borehole data may not adequately represent the estimates and corresponding uncertainties (Dunlap and Spinazola, 1980).

3.5.2.3 Uncertainty. Uncertainties exist in all of the characteristic V_s profiles, due to local variations in stratigraphy, weathering, bulk density, geologic structure, depth-to-bedrock, and instrumental or human error (Gomberg et al., 2003; Romero and Rix, 2001). Gomberg et al. (2003) unraveled the stratigraphy of the upper 500 m of surficial (unconsolidated) materials in the Memphis area and determined the corresponding uncertainties in the predicted depths of the stratigraphic horizons. Gomberg et al. (2003) found that the predictions depended on depth, quality, and spacing between borings piercing those horizons. They employed a moving least-squared algorithm and then correlated these data with their measured shear-wave velocity

profiles. These results were subsequently incorporated into the calculation of site response on a 1 km grid, which was the basis of the seismic hazard maps prepared for the six quadrangles surrounding Memphis, in Shelby County, Tennessee.

The characteristic profiles form a critical component in site response analyses, allowing the effects of surficial geologic deposits amplify or deamplify incoming seismic wave energy, depending on the impedance contrasts at the bedrock-soil cap boundary, the thickness of the soil cap, and the frequency of the ground motion (Borcherdt et al., 1991; Romero and Rix, 2001; Wills et al., 2000). Characteristic profiles are used in the area-wide assessments because each individual V_s measurement is subject to a number of uncertainties (described above). By grouping all of the V_s data for a recognized unit in a given geomorphic province, much of the uncertainty caused by localized perturbations in the soil-rock column at specific test sites is “smoothed out” and a more realistic characterization is thereby created which is better suited to assessing the likely effects of site amplification over a broad area, covering hundreds of square kilometers, or more.

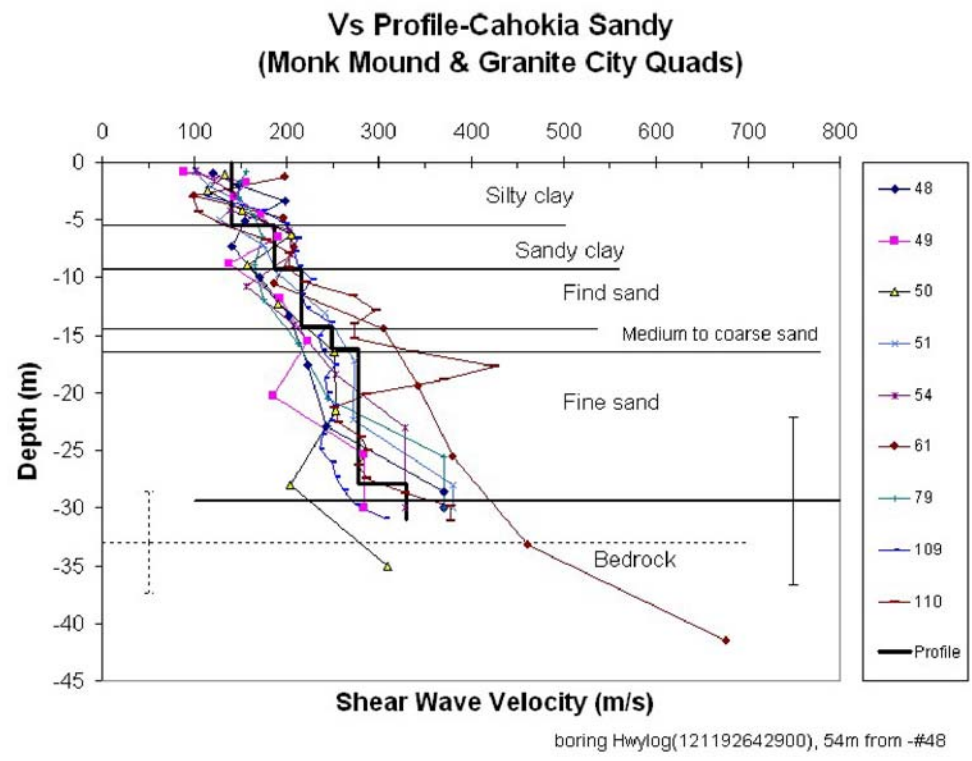
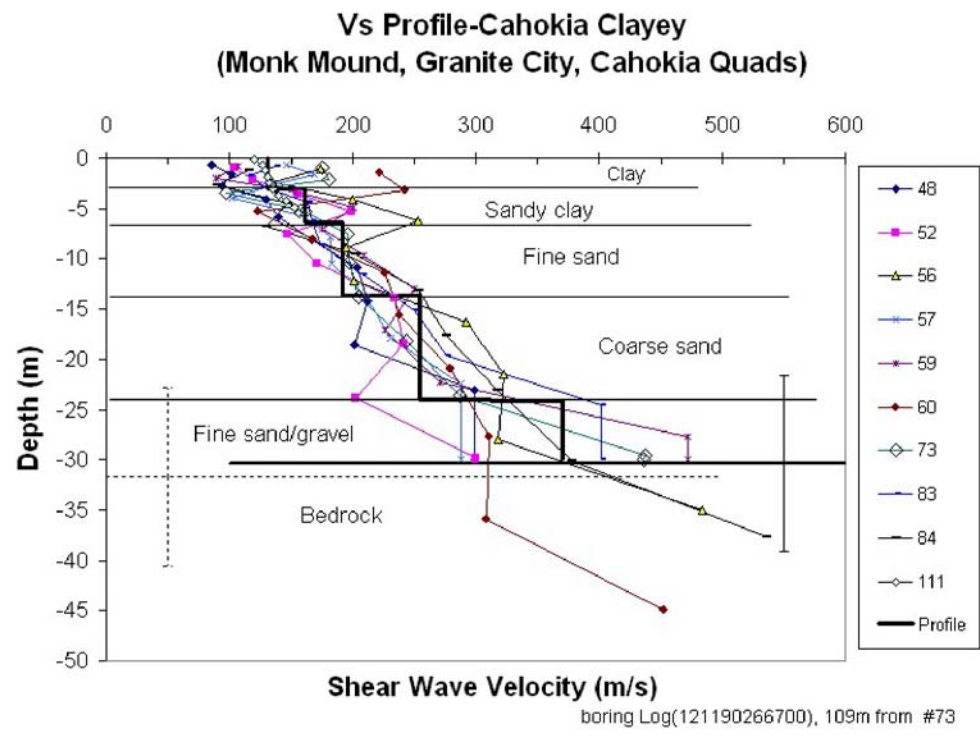
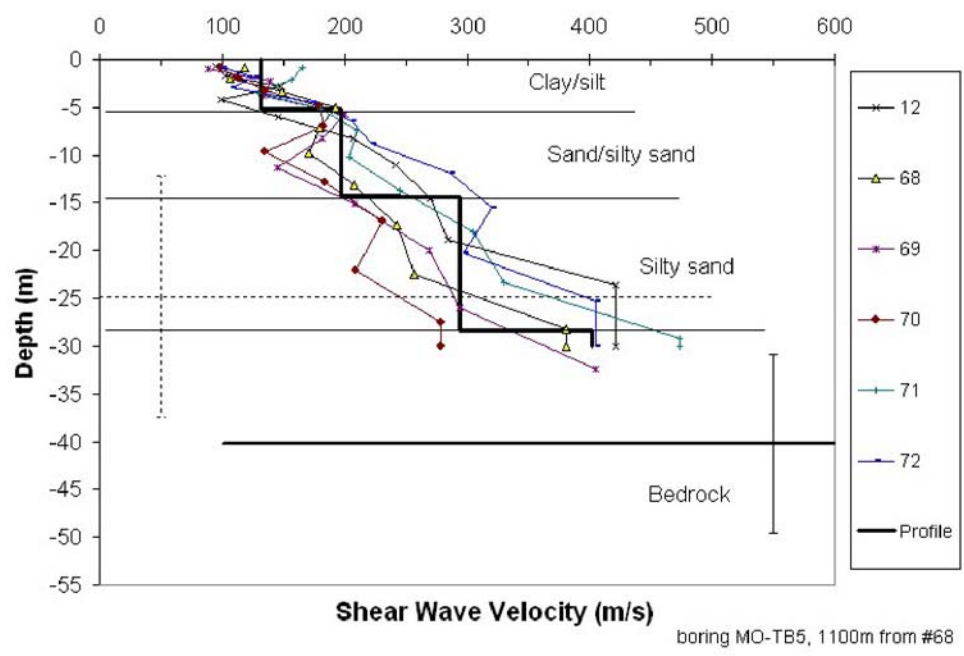


Figure 3.4. The reference shear wave velocity (V_s) profiles derived from adjacent boreholes.

Vs Profile-Alluvium along major rivers in Missouri side



Vs Profile-Alluvium along streams in St. Louis

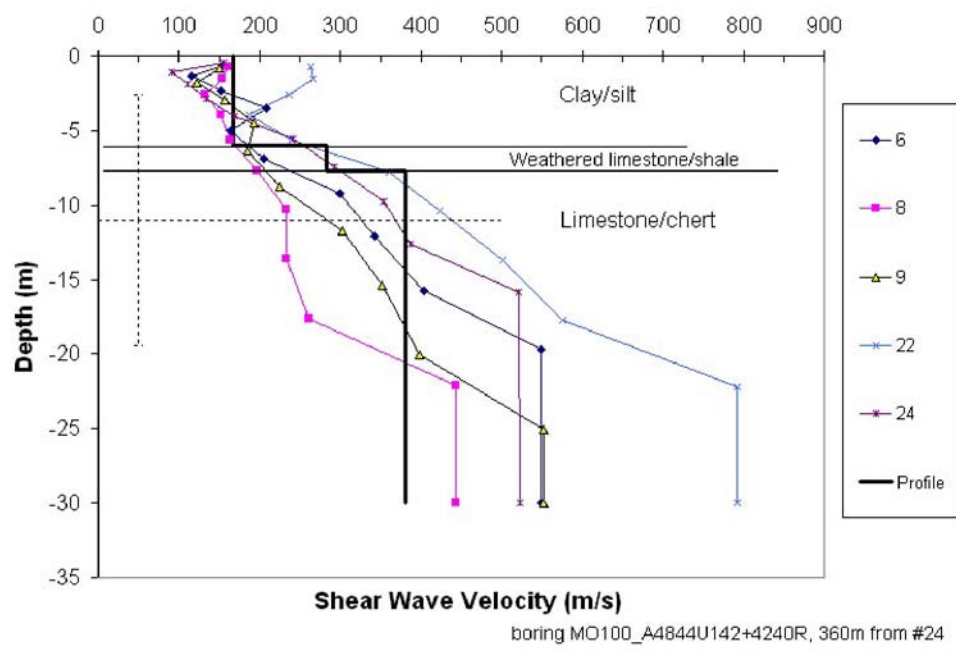


Figure 3.4. Continued

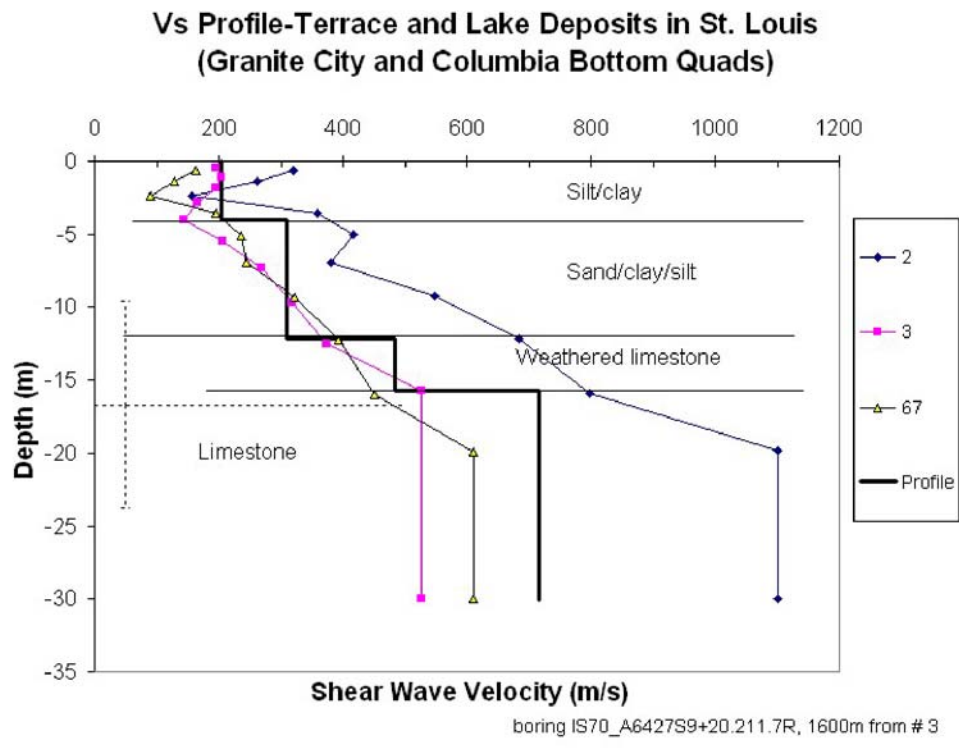
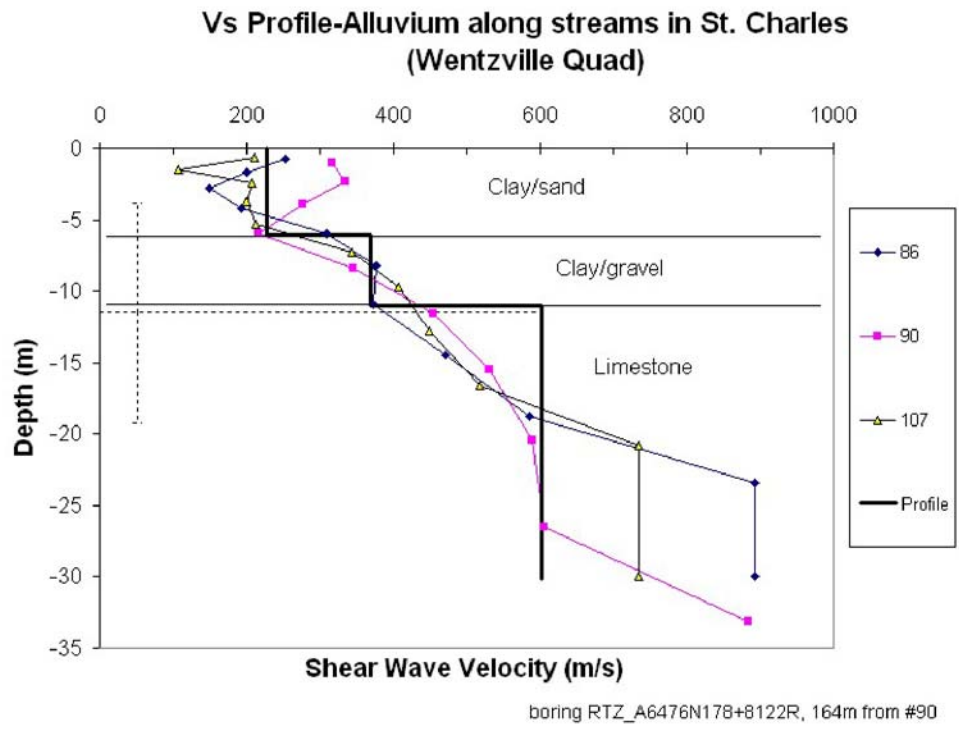
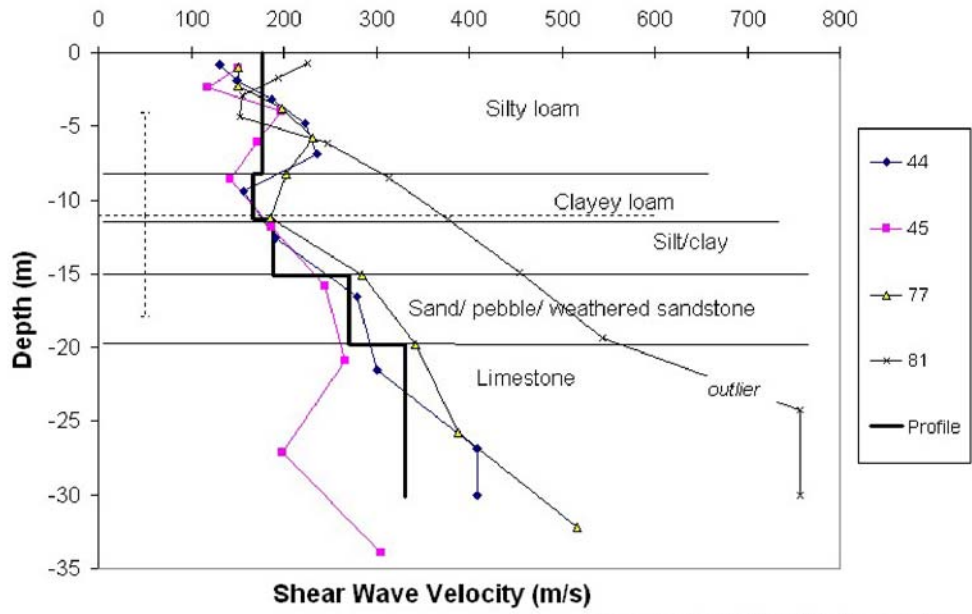


Figure 3.4. Continued

Vs Profile-Loess in Illinois



Vs Profile-Loess in St. Louis

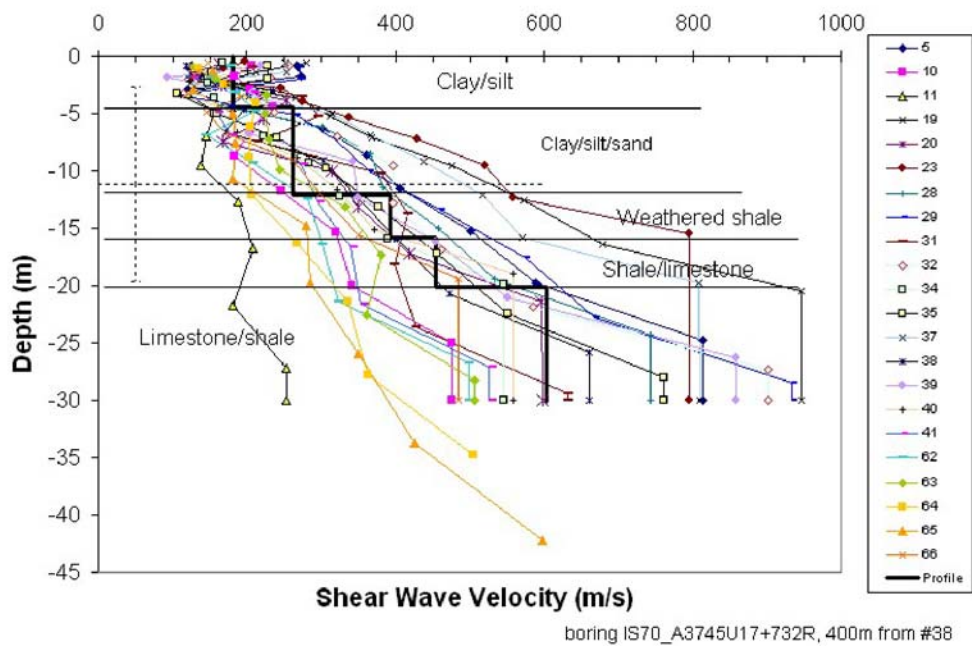
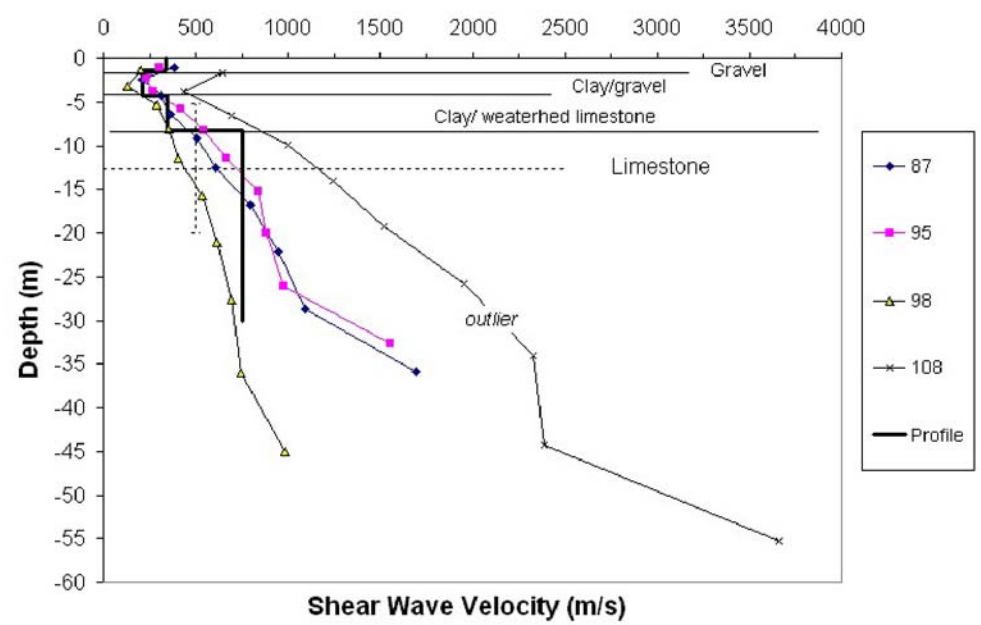


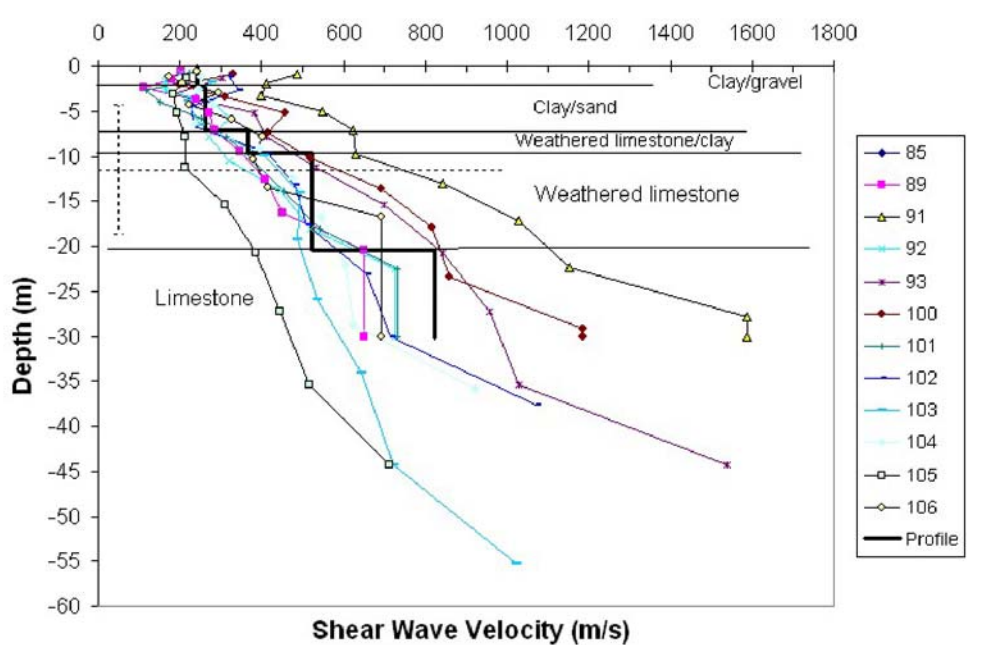
Figure 3.4. Continued

Vs Profile Loess in St. Charles (Wentzville)



boring IS70_A08512U3+9140L, 114m from #87

Vs Profile-Till in St. Charles (Wentzville Quad)



boring IS70_6-624-1U8+67041R, 90m from #89

Figure 3.4. Continued

Vs Profile-Till in City of St. Louis

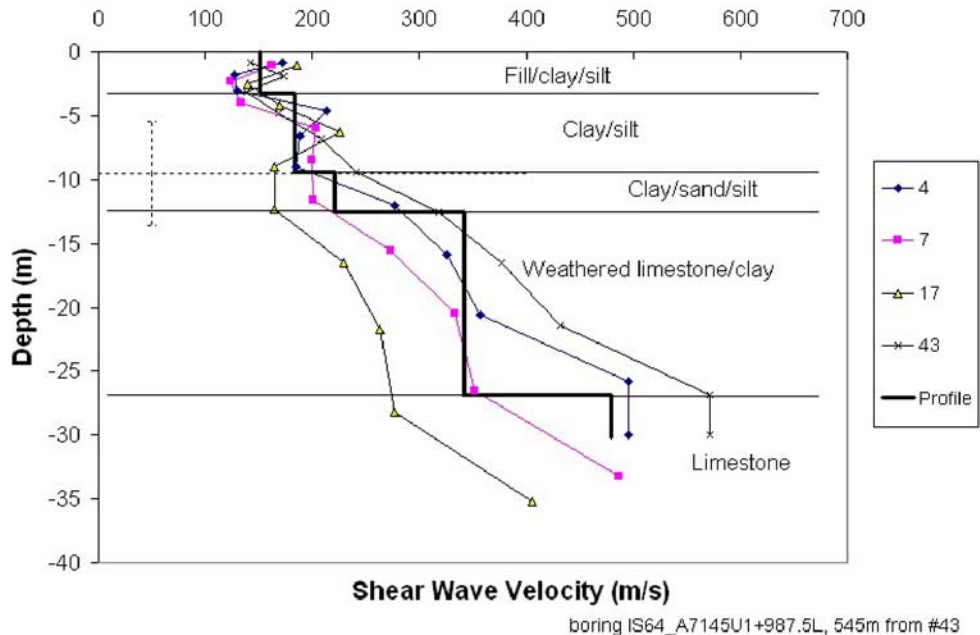


Figure 3.4. Continued

4. ESTIMATION OF THE DEPTH TO GROUNDWATER TABLE

4.1. INTRODUCTION

The elevation of the permanent groundwater table and its relative position with respect to sloping ground surfaces are important factors in geoengineering assessments of geoenvironmental, geotechnical, and hydrogeologic conditions. Water table contouring has long been used to estimate the preferred paths of the groundwater flow, recharge, and loss assessments. Natural hazards such as landslides, shaking-induced liquefaction, and lateral spreading are all driven by pore pressure imbalances, driven by relatively short-term changes in groundwater conditions. These transient conditions are often difficult to predict, absent some sort of site-specific data collected over some meaningful time interval, which would allow changes in the groundwater levels and/or recharge regimen to be noticed.

The elevation of the permanent groundwater table generally meets the following specifications, sketched in Figure 4.1; 1) it tends to be influenced by the slope of the land surface, often mimicking peaks and valleys (King, 1899; Domenico and Schwartz, 1998; Peck and Payne, 2003); 2) the depth to groundwater table is generally observed to be proportional to ground surface elevation in hilly areas in humid climates (Daniels et al., 1984; Peck and Payne, 2003); and 3) the water table level is equal to the land surface elevation in perennial streams, water courses, and lakes (Daniels et al., 1984; Peck and Payne, 2003).

The groundwater table elevation or depth below ground surface is typically measured at point locations in water wells, environmental monitoring wells, or in geotechnical borings. The groundwater table is usually interpolated between these measured data points. Mapping the elevation of the groundwater table mapping requires some obedience to simple hydrologic principles and appropriate techniques that have been developed for any given area, depending on the underlying geology.

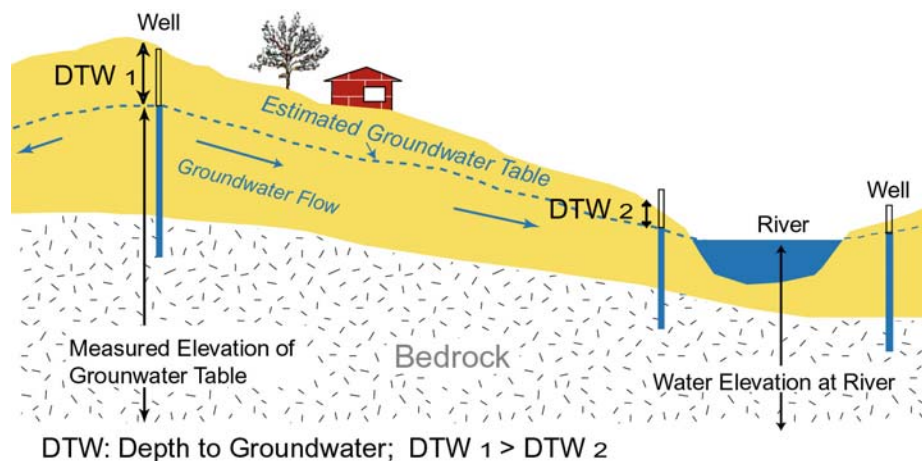


Figure 4.1. General aspects of the permanent groundwater table in humid climates (not including areas underlain by karst, where losing stream might exist).

Mapping groundwater elevations from well data can prove troublesome in alluvial flood plains where the depth to groundwater is low to zero and the land surface elevations and water table levels are not well correlated. In these cases the water table may be so conductive that external pressures, such as those imposed by a rising river level, can cause wells several kilometers away to respond within a matter of a few hours. This situation has been documented along the south side of the lower Missouri River, in limestone quarries more than 1.6 km from the river. In that situation, ground water pressures appear to be transmitted quickly through a series of open fractures or faults developed within an underlying formation.

Groundwater table elevations are usually estimated from observations of well levels (before pumping) and water levels of adjacent rivers, streams, or lakes, which are part of the groundwater system (water levels in active quarries are not reliable indicators if they are being pumped). By connecting at points between water surfaces, the water table levels reflected in these features can be used to approximate the minimum groundwater table elevation (Andres and Martin, 2005; Sepulveda, 2003).

4.1.1. Previous Studies. Computer-assisted approaches may incorporate surface mapping methods, such as trend surface interpolation, geostatistics, and methods of landform classification. Many of these predictive tools are currently wired into off-the-shelf GIS software, such as ArcGIS.

Williams and Williamson (1989) used linear regression between water level data and topographic data in subareas defined by geomorphic province and/or characteristics. With this information, they predicted the depth-to-groundwater, deriving the multiple linear regression related to the 5-mile grided land surface level, considering local topographic deviations. Similarly, O'Hara and Reed (1995) analyzed multiple-regression techniques for predicting elevation head in specific aquifers, and quantified the relation between the variations in the water table elevation beneath undulating outcrops to larger scale variations in the regional and local land surface elevations. They mapped the depth to water table in Mississippi, subtracting the water table elevation from the land surface elevation.

Sepulveda (2003) introduced the minimum water table interpolated between lakes and streams. He developed the method of determining the water table level in Florida by computing the multiple linear regressions among water level measurements as the dependent variable, the minimum water table altitude as the first independent variable, and the depth to the minimum water table as the second independent variable.

Applying Sepulveda's (2003) mapping method, Andres and Martin (2005) generated the minimum water table from a polynomial regression and then, adopted the multiple linear regression method to back out the water table elevations under dry and wet conditions for the Inland Bays Watershed in Delaware.

Dunlap and Spinazola (1980) were among the early workers who employed kriging to predict and contour the water table surface using 1,859 data points in west-central Kansas encompassing a land area of 1350 km². Hoeksema et al. (1989) applied cokriging techniques to estimate groundwater elevations using ground surface elevation as second independent variable. Hoeksema et al (1989) determined that there was a distinct advantage in using cokriging models over conventional kriging. According to their study, cokriging provided more precise estimates of the water level that are

consistent because it included consideration of the impacts of undulating topography on the ground water surface (see profiles in Figure 4.2).

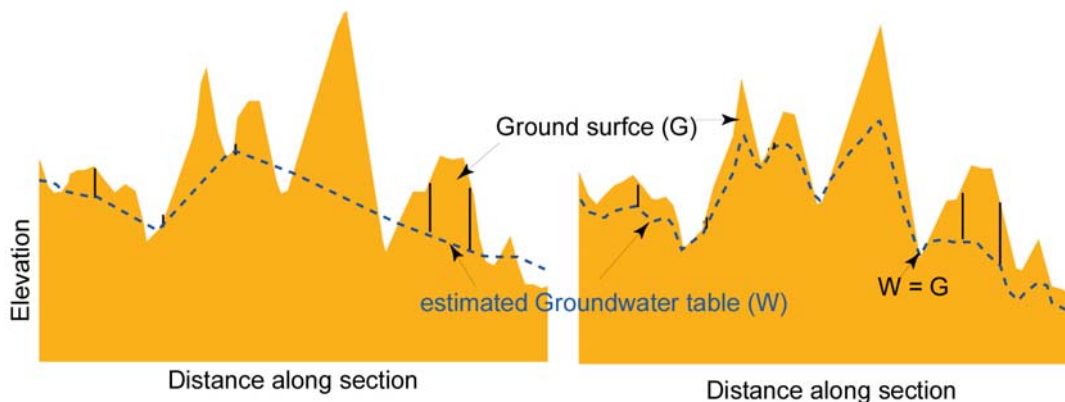


Figure 4.2. Comparative profiles illustrating predictions of the depth-to-groundwater with and without considering surface topography (after Hoeksema et al., 1989). Estimates that include consideration of the undulating ground surface using cokriging yield more reasonable predictions because the groundwater table tends to be influenced by the shape and slope of the land surface.

4.1.2. Purpose of this Study. In this study, the elevation of the permanent groundwater table beneath the St. Louis Metro area was interpolated by employing the least squares approach, as well as geostatistical methods, such as (ordinary) kriging and cokriging; using software packages included in ArcGIS v. 9.1 software. The estimated errors of (ordinary) kriging and cokriging were statistically evaluated, and the advantages and the disadvantages of each model are described.

4.2. STUDY AREA

The study area encompasses 29 7.5-minute USGS quadrangles in the St. Louis metropolitan area of Missouri and Illinois, which encompasses a land area of 4,432 km². This area will be referred to in this study as *STL*. The topographic altitude in *STL* generally ranges from 116m to 288m above sea level. *STL* includes the confluences of four major rivers: the Mississippi-Missouri, Mississippi-Illinois, and Mississippi-

Meramec rivers. The STL Metro area is naturally bounded by low-lying alluvial flood plains developed along these four major rivers. All of the rivers are bordered by elevated loess covered uplands, except the lower 16 km of the Missouri River, which is bounded by the Mississippi River flood plain on its north side. The floodplains are generally flat, with a slope less than 2%, while slopes between 5% and 200% are found along the bluffs of the river valleys and in the elevated uplands (Lutzen and Rockaway, 1987).

4.3. METHOD

4.3.1. Data Set. Groundwater elevation data were collected and analyzed to prepare a contour map illustrating the estimated elevation of the permanent groundwater surface. The input data consisted of the following components: 1) 1,069 well logs obtained from the Missouri and Illinois state geological surveys, recorded between January 1959 to December 2005 (for sites with multiple water level data, the most recent measurements were selected for analysis), 2) 469 elevations (about 1 km apart) along the major river channels interpolated from digital raster graphics (DRGs; scale 1: 24,000), and 3) 2,100 data points along perennial water courses taken from hydrography digital line graphics (DLG) prepared by the USGS. The ground surface elevation of data points of 2) and 3) were extracted from 10m digital elevation models (DEM) of each quadrangle that were stitched together. The water table elevations in perennial channels, lakes, and ponds were assumed equal to the ground surface elevation. These were used to aid in the interpolation of the groundwater table using geostatistical methods. This study assumed that the water levels in the surficial aquifers did not fluctuate appreciably over time, even during periods of prolonged drought. This is a conservative assumption for evaluations of seismic site response and liquefaction potential, but it will overestimate these effects if the water table were lower than assumed when an earthquake occurs. The locations of the well logs and interpolated water table elevations are shown in Figure 4.3.

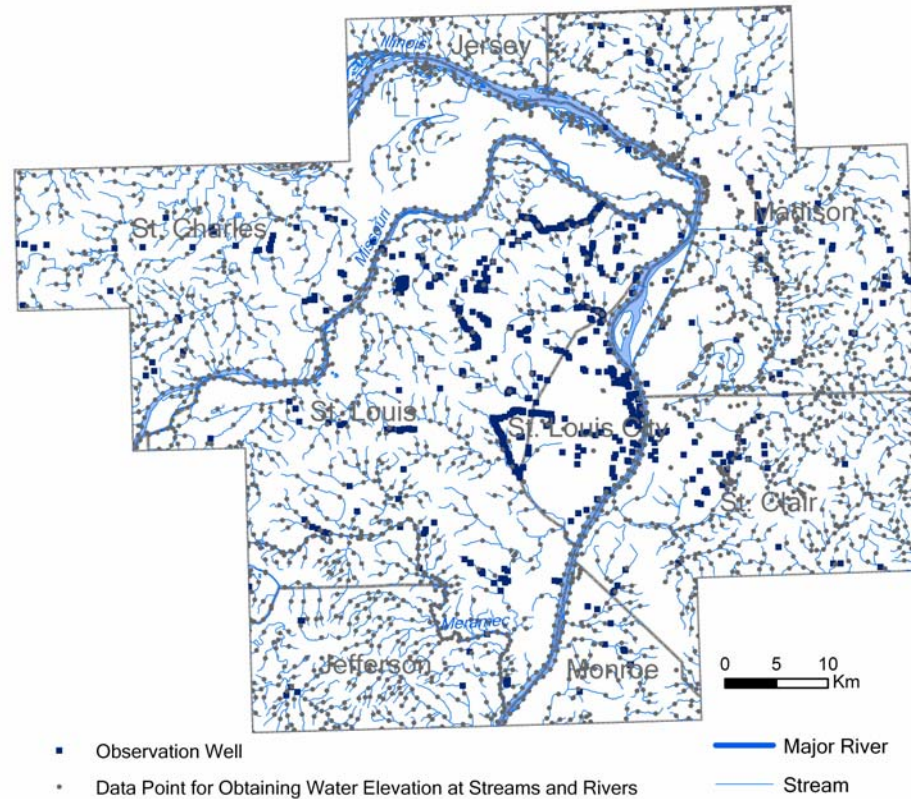


Figure 4.3. Locations of data points used in the predictions of water table elevation and depth-to-groundwater.

4.3.2. The Least Squares Approach. The least squares approach is usually referred to as linear regression. This method provides an approximate estimate derived from the average trend of any true variable. Linear regression estimates are calculated, minimizing the sum of the square deviation of the estimated value from the actual values. It can be stated as follows;

$$\sum_{i=1}^n (Y_i - Y_i^*)^2 = \min \quad (1)$$

where Y_i = the true value and Y_i^* = the estimate of $Y_i = b_0 + b_1(Y_i)$.

The coefficients b_0 and b_1 are determined by the condition that the sum of the square residuals be held as small as possible.

In this study, power regression provided the most realistic predictions as compared to other regression models, such as simple linear or polynomial. This is probably because the simple linear model assumes that the water table lies at a constant depth (determined by statistical analysis) beneath the ground surface. This would mispredict groundwater surfaces wherever the slope of the phreatic surface deviated from the slope of the ground surface. In the higher elevations with steeper topography, the depth-to-groundwater exhibits much greater variability, due to the undulating nature of the overlying landscape. For these reasons simple linear models are unacceptable for constructing spatial distributions of predicted depth-to-groundwater. The polynomial model allows for inflections of a desired surface, but it also violates the basic concept that the groundwater elevation is generally proportional to the ground elevation.

Power regression is based on a function of linear regression, where both axes are scaled logarithmically. The power regression postulates that

$$Y = a \times X^b \quad (2)$$

where Y = the dependent variable, X = independent variable, a = the amplitude, and b = exponent of the fitting function.

4.3.3. Geostatistical Methods. This procedure estimates unsampled values by calculating the weights assigned to the individual neighboring points. These weights depend in the spatial relationship between values and distances between the sampled and unsampled data points. These spatial relationships are quantified using the fundamental theory of geostatistics, used to construct a semivariogram (Isaaks and Srivastava, 1989; Johnston, 2003; Kelkar and Perez, 2002).

4.3.3.1 Semivariogram. Semivariograms are built in the assumption that the spacing between adjacent data points correlates to with measured values. In other words, data pairs that are closer are assumed to exhibit similar values, but those separated by greater distance can be expected to exhibit increasingly dissimilar values. In semivariogram graphs, the lag size is typically plotted on the X-axis. It is the distance

from the center of the cell to the center of the semivariogram surface, and the semivariance on the Y-axis represents dissimilarity. The semivariance increases as distance increases. In a theoretical curve, the Y intercept is known as the ‘nugget.’ A non-zero nugget implies that points infinitesimally close to one another have different values. The lag value and semivariance value, at which the curve flattens out, are called the range and sill, respectively (see Figure 4.4).

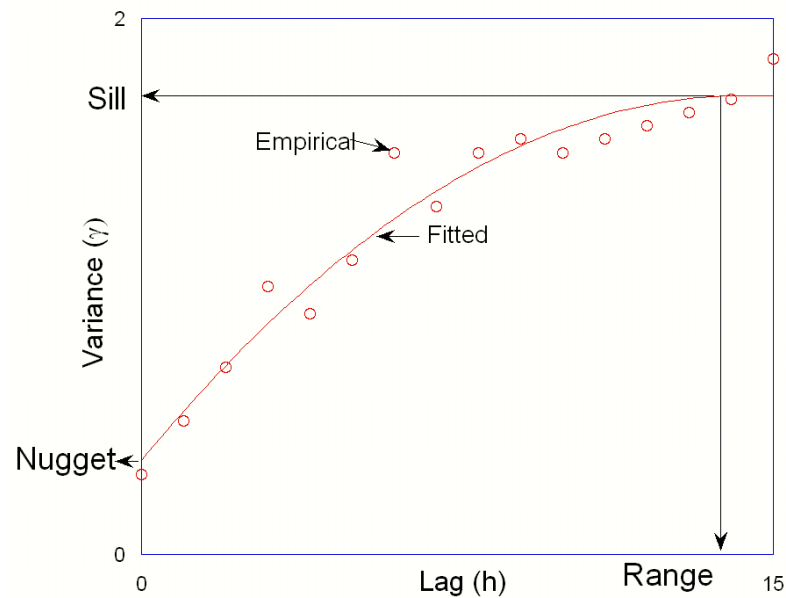


Figure 4.4. Diagram showing typical semivariogram parameters (nugget, range, and sill).

The goal of semivariance modeling is to determine the best fit for a model that will pass through the points in the semivariogram. It is defined as

$$\gamma(h) = \frac{1}{2} \text{Var}[X(u) - X(u+h)] = \frac{1}{2} \left(E\{[X(u) - X(u+h)]^2\} - E\{[X(u) - X(u+h)]\}^2 \right) \quad (3)$$

where $\gamma(h)$ = the semivariance, h = the lag (distance between points), and $E[X(u)]$ = expected value of $X(u)$.

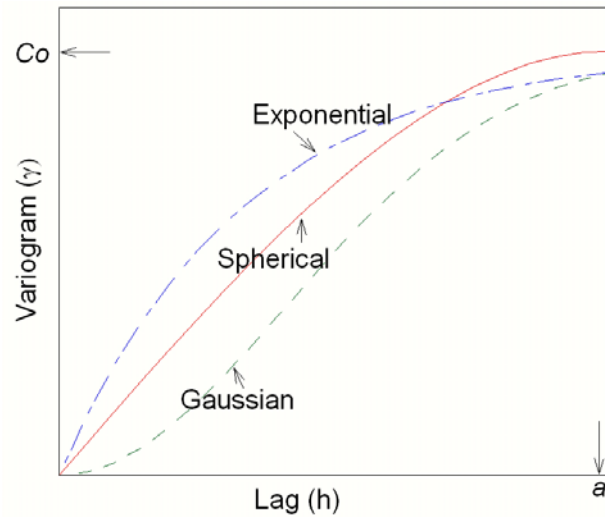


Figure 4.5. Spherical, exponential, and Gaussian semivariogram models with the parameters range (a) and sill (C_0).

4.3.3.2 Ordinary Kriging. Kriging is a geostatistical technique commonly used to estimate values at unsampled locations between known data points, using a linear estimation procedure. The estimated value is unbiased and should result in minimum error variance. Ordinary kriging is routinely employed in the geohydrology and environmental industries for assessing subsurface conditions. Kriging is also flexible, because the mean value(s) do not need to be input into the analysis and it is easily adapted to local variations. Detailed discussions of kriging can be found in Journel and Huijbregts(1978), Isaaks and Srivastava (1989), and Kelkar and Perez (2002).

The estimated value at an unsampled location is obtained by

$$X^*(u_0) = \sum_{i=1}^n \lambda_i X(u_i) + \lambda_0 \quad (7)$$

where $X^*(u_0)$ = estimated value at a location, u_0 , $X^*(u_i)$ = sample value at a location u_i , λ_i = weighting factor, and λ_0 = a constant.

In an unbiased condition, the difference between the predictions and the true values should be zero. This premise is expressed as

$$E[X(u_0) - X^*(u_0)] = 0 \quad (8)$$

Equation 7 can be expressed as

$$E[X(u_0)] = \lambda_0 + \sum_{i=1}^n \lambda_i E[X(u_i)] \quad (9)$$

If we assume that $E[X(u_0)] = E[X(u_i)] = m(u_0)$, where $m(u_0)$ = the local mean.

Because $m(u_0)$ is unknown, we can force λ_0 to be zero. Thus we can write equation 9 as

$$\lambda_0 = m(u_0) \left(1 - \sum_{i=1}^n \lambda_i \right) \text{ and } \sum_{i=1}^n \lambda_i = 1. \quad (10)$$

The equation 7 is simplified as

$$X^*(u_0) = \sum_{i=1}^n \lambda_i X(u_i). \quad (11)$$

Minimizing error variance results in the ordinary kriging system

$$\left\{ \begin{array}{l} \sum_{i=1}^n \lambda_j C(u_i, u_j) + \mu = C(u_i, u_0) \quad i=1, \dots, n \\ \sum_{i=1}^n \lambda_j = 1 \end{array} \right\} \quad (12)$$

or

$$\left\{ \begin{array}{l} \sum_{i=1}^n \lambda_j \gamma(u_i, u_j) - \mu = \gamma(u_i, u_0) \quad i=1, \dots, n \\ \sum_{i=1}^n \lambda_j = 1 \end{array} \right\} \quad (13)$$

where $C(u_i, u_j)$ = the covariance, $\gamma(u_i, u_j)$ = semivariogram between two points u_i and u_j , and μ = Lagrange multiplier.

Here, covariance is defined as

$$C[X(u), X(u+h)] = C(h) = E[X(u), X(u+h)] - E[X(u)] \cdot E[X(u+h)]. \quad (14)$$

Equation 12 can be written in matrix form

$$C \cdot \Lambda = c \quad (15)$$

where C = covariance matrix, c = covariance vector, and Λ = vector of weighting factor.

The weighting factor (λ_i) can be obtained by solving the matrix:

$$\Lambda = C^{-1} \cdot c. \quad (16)$$

Once a weight is calculated, the estimated value $X^*(u_0)$ is obtained using

$$X^*(u_0) = \sum_{i=1}^n \lambda_i X(u_i). \quad (17)$$

The error variance can then be estimated and the relationship between semivariogram and the model covariance developed (Isaaks and Srivastava, 1989).

$$\sigma^2 = C(u_0, u_0) = \sum_{i=1}^n \lambda_i (u_i, u_0) - \mu \quad (18)$$

4.3.3.3 Cokriging. Because the elevation of the groundwater table tends to mimic the ground surface in hilly terrain (King, 1899; Domenico and Schwartz, 1998), kriging without considering ground surface elevation usually leads to erroneous

predictions, which include unrealistic groundwater levels, well above an undulating ground surface (Hoeksema et al., 1989). Cokriging is a multivariate extension of kriging. Cokriging can improve the estimate by considering a bounding ground surface elevation as a second variable. Cokriging presumes that the principal variable of interest (groundwater table) and the covariable (ground surface elevation) are spatially related to each other. The input data must include water table elevations and ground surface elevations measured at the same location (point of spatial reference; Hoeksema et al., 1989).

The equation employed by cokriging to estimate a datum in unsampled locations can be written as

$$X^*(u_0) = \sum_{i=1}^n \lambda_{X_i} X(u_{X_i}) + \sum_{k=1}^m \lambda_{Y_k} Y(u_{Y_k}) \quad (19)$$

where $X^*(u_0)$ = estimated value at location, u_0 , $X(u_{X_i})$ = sample value located at u_{X_i} , $Y(u_{Y_k})$ = covariable value located at u_{Y_k} , λ_{X_i} = weighting factor at $X(u_{X_i})$, and λ_{Y_k} = weighting factor at $Y(u_{Y_k})$.

By applying the unbiased conditions:

$$E[X^*(u_0) - X(u_0)] = m_X \left(1 - \sum_{i=1}^n \lambda_{X_i}\right) - m_Y \sum_{k=1}^m \lambda_{Y_k} = 0 \quad (20)$$

where m_X and m_Y = expected values of X and Y variables, respectively.

Equation 19 results in:

$$\sum_{i=1}^n \lambda_{X_i} = 1 \text{ and } \sum_{k=1}^m \lambda_{Y_k} = 0. \quad (21)$$

Minimizing the variance, the cokriging system is finally obtained:

$$\begin{aligned} \sum_{i=1}^n \lambda_{X_i} C_X(u_{X_i}, u_{X_j}) + \sum_{k=1}^m \lambda_{Y_k} C_C(u_{X_i}, u_{Y_k}) + \mu_X &= C_X(u_0, u_{X_i}) \text{ for } j=1, \dots, n \\ \sum_{i=1}^n \lambda_{X_i} C_C(u_{X_i}, u_{X_j}) + \sum_{k=1}^m \lambda_{Y_k} C_Y(u_{Y_i}, u_{Y_k}) + \mu_Y &= C_C(u_0, u_{Y_k}) \text{ for } k=1, \dots, m \end{aligned} \quad (22)$$

where C_X = the covariance for variable X , C_Y = the covariance for variable Y , C_C = the cross covariance between X and Y , and μ = Lagrange multiplier.

The error variance can be also expressed as

$$\sigma^2 = C_X(u_0, u_0) - \sum_{i=1}^n \lambda_{X_i} C_X(u_0, u_{X_i}) - \sum_{k=1}^m \lambda_{Y_k} C_C(u_0, u_{Y_k}) - \mu_X = 0 \quad (23)$$

The various applications of cokriging have been described by Isaak and Srivastava (1989), Journel and Huijbregts (1978), Kelkar and Perez (2002), and Myers (1982).

4.3.3.4 Error of Estimate. One of the advantages of using statistical approaches is that they allow for simultaneous calculations of statistical measures of uncertainty associated with the predictions. Kriging provides a variance estimate at each interpolated point. These variance estimates are called kriging errors, or ‘errors of estimate.’ The statistic actually calculated is the standard deviation, or square root of the variance. The kriging errors generally increase in areas bereft of data. A contour map of these errors usually highlights the areas of greatest uncertainty, and are often used to aid decisions regarding where additional data points may be required to refine the predictive model, and, thereby, lessen the uncertainty associated with the prediction (Dunlap and Spinazola, 1980).

4.3.3.5 Cross-Validation. Cross-validation is a process by which the sample value at a particular location is temporarily removed from the data set, and another value is estimated, using whatever model is chosen. Then the estimate derived from the predictive model is compared to the actual sample value at the same location. This procedure is repeated for all of the known samples or data points. Each model can be subjected to cross validation and then compared for accuracy by analyzing the estimated

errors. The error between the estimated and measured values is used to calculate the following statistics: mean error (ME), root-mean-square error (RMSE), kriged mean standardized error (MSE), and kriged root-mean-square standardized error (RMSSE).

$$\begin{aligned}
 r_{ui} &= X^*(u_i) - X(u_i) \\
 ME &= \frac{1}{N} \sum_{i=1}^N r_{ui} \cong 0 \\
 RMSE &= \sqrt{\frac{1}{N} \sum_{i=1}^N r_{ui}^2} \text{ Minimum} \\
 MSE &= \frac{1}{N} \sum_{i=1}^N \frac{r_{ui}}{\sigma_{ui}} \cong 0 \\
 RMSSE &= \sqrt{\frac{1}{N} \sum_{i=1}^N \frac{r_{ui}^2}{\sigma_{ui}^2}} \cong 1
 \end{aligned} \tag{24}$$

where $X^*(u_i)$, $X(u_i)$, r_{ui} , and σ_{ui} are the estimated value, the observed value, the error (residual), and the standard deviation of the estimated error, respectively, at point, u_i .

4.4. RESULTS OF THE PREDICTIVE MODELS

4.4.1. Power Regression Map. The power regression equation was used to describe the approximate relation between groundwater and ground surface elevations (Figure. 4.6). The power regression model was constructed using the following assumptions; 1) the groundwater table tends to mimic the geometry of the sloping ground surface; 2) similar ground elevations tend to generate similar depths-to-groundwater; and 3) as the ground surface increases in elevation above an adjacent valley bottom, the depth-to-groundwater can be expected to increase (assuming the depth-to-groundwater is variable over the study area). The power regression equation was employed to calculate the relative elevation of the groundwater table, based on the land surface elevation as the independent variable and the groundwater elevation as the dependent variable.

$$\text{Groundwater table elevation} = 1.1902 \times \text{Land surface elevation}^{0.9586} \quad (R^2 = 0.9332) \tag{25}$$

The power regression model was then incorporated into a spatial function using GIS that computed the groundwater table derived from the regression equation of the land surface elevation. 10m DEMs provided by the USGS were employed for the interpolation. As a consequence, the predicted groundwater elevation map will inherit the same resolution as the 10m DEMs. Figure 4.7 presents a map showing the Predicted Elevation of the Groundwater Table in the St. Louis Metro area, generated by using the power regression equation.

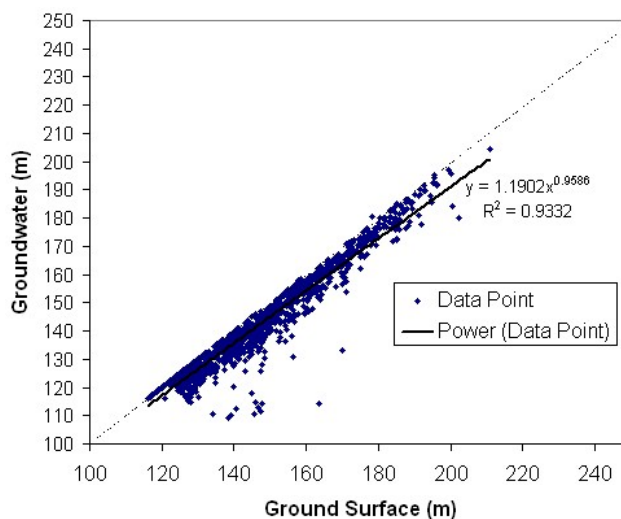


Figure 4.6. Relationship between ground surface elevation and groundwater elevations recorded in well logs. This graph suggests a reasonably high correlation between the ground surface and groundwater table elevations. This suggests that cokriging could be employed to estimate the elevation of the groundwater table as a primary variable based on the elevation of ground surface as a secondary variable. The solid line is the best-fit correlation used for the power regression model.

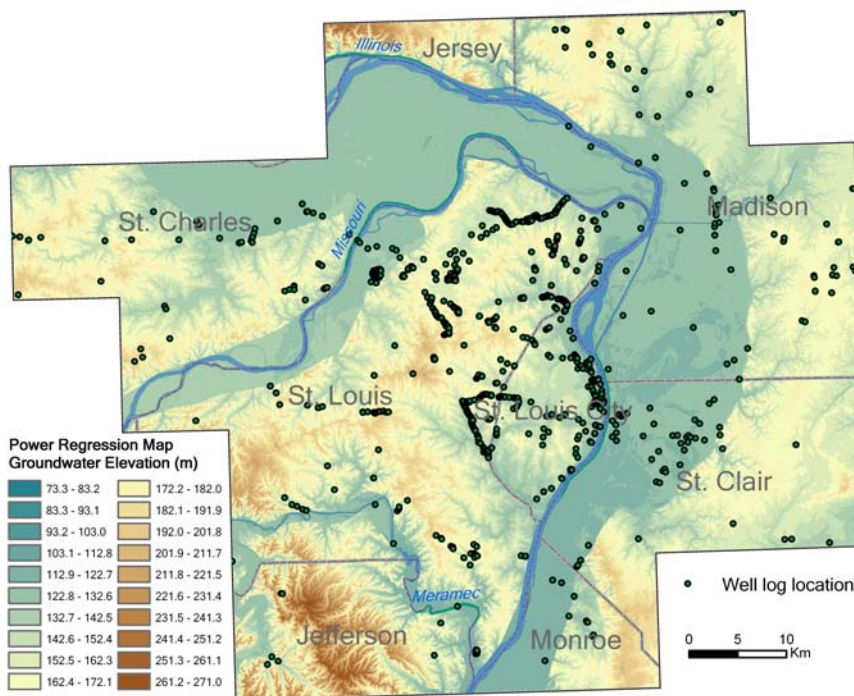
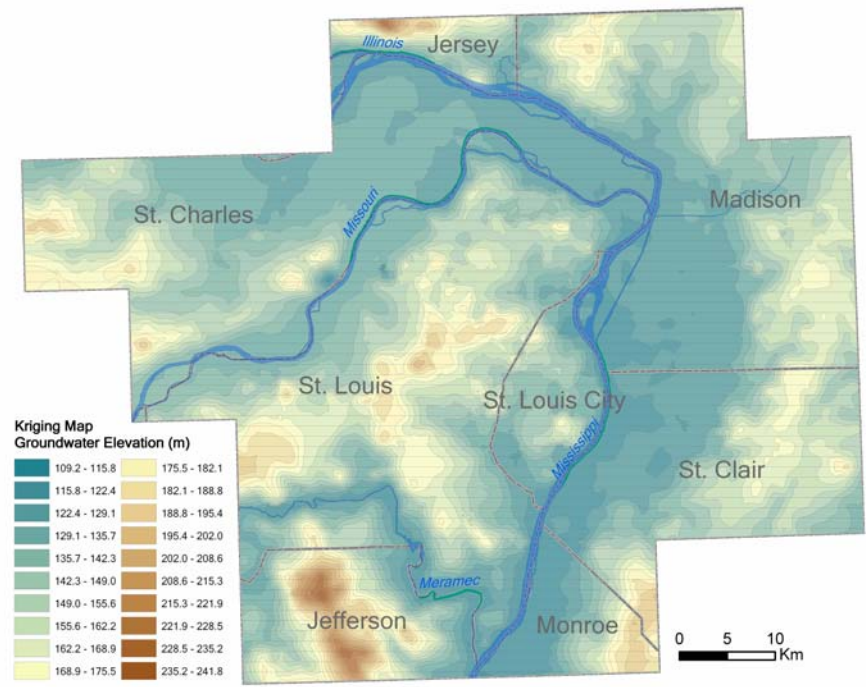


Figure 4.7. Map showing Predicted Elevation of the Groundwater Table in the St. Louis Metro area, derived from a power regression model. The groundwater table elevations were estimated by substituting 10m DEMs over the study area using a power regression equation.

4.4.2. Ordinary Kriging Map. Preliminary analysis of the well data using an experimental semivariogram suggested that no significant anisotropies exist in the input data and that the semivariogram behavior at the origin appeared to be linear. We compared several of the best-fit theoretical models with the well data, and determined that a spherical model with lag numbers of 12 resulted in a kriged root-mean-square standardized error closer to 1.0 than any of the other models, concluding that this was the best-fit model. The final result obtained by (ordinary) kriging is shown in Figure 4.8A and the corresponding estimation error is presented in Figure 4.8B.

(A)



(B)

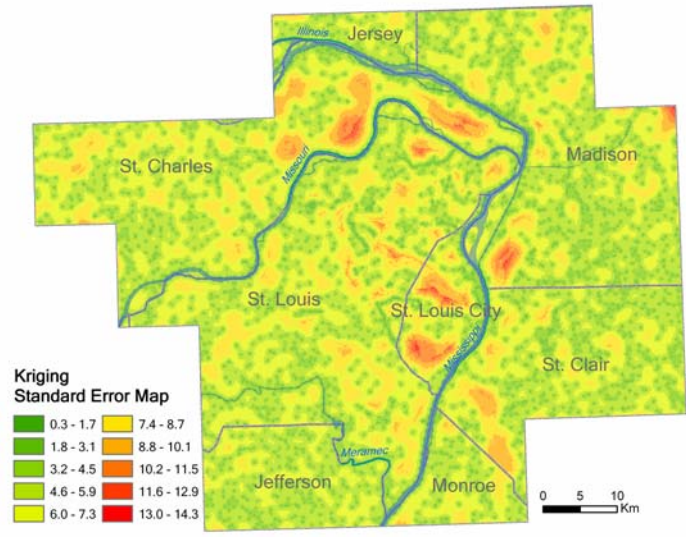
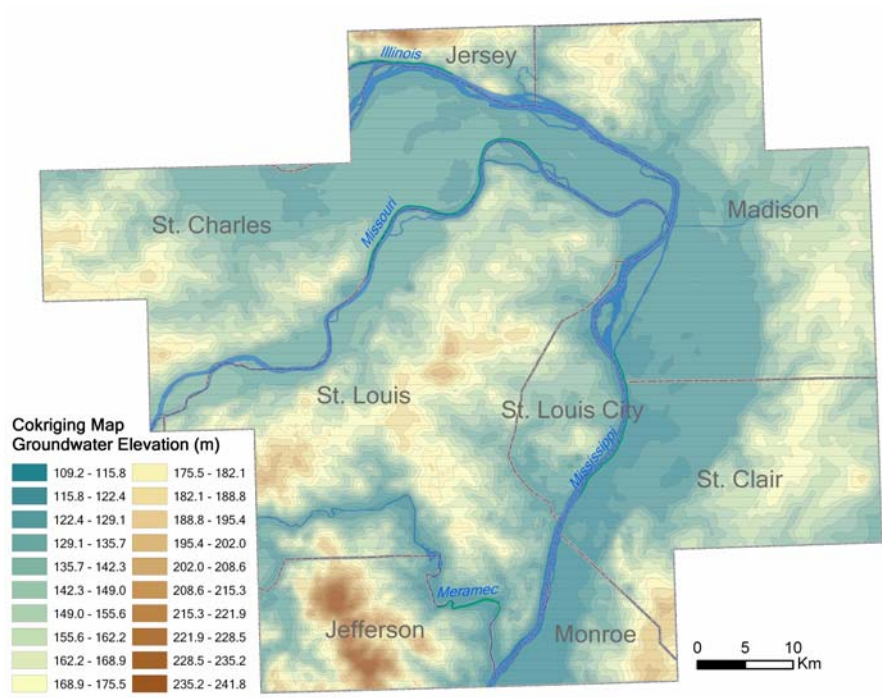


Figure 4.8. (A) Map showing predicted groundwater elevations based on Kriging, and, (B) corresponding standard error map. Note that greatest error is predicted in areas with the least amount of data.

4.4.3. Cokriging Map. Figure 4.6 suggests that the measured water table and ground surface elevations are proportional to each other, based on the 1,069 wells (the correlation coefficient = 0.96). Because of this strong correlation, it was felt that cokriging would be a viable tool to realistically estimate the elevation of the groundwater table across such a large area. 500m × 500m spaced elevation points were extracted from 30m × 30m DEM using MICRODEM software. These ground surface elevation points were employed as second variables for cokriging. The predictive map was prepared by using cokriging with the same input data used in the (ordinary) kriging analyses described previously. Figure 4.9A presents the map of Predicted Groundwater Elevations based on Cokriging and Figure 4.9B shows the corresponding estimation error map.

4.4.4. Cross-Validation Result. The results of cross-validation analyses for the kriging and cokriging methods are summarized in Table 4.1. The results based on ME indicate that the interpolation using kriging yielded values closer to zero than cokriging. The RMSE values indicate that cokriging performed better than the kriging methods. Cokriging generated an RMSE of 4.1020, while kriging generated an RMSE of 5.2750. The Kriging analyses resulted in an MSE of -0.0233, which is closer to zero than that achieved by cokriging. Cokriging resulted in an RMSSE of 1.006, which is closer to 1, compared with the RMSSE calculated for ordinary kriging.

(A)



(B)

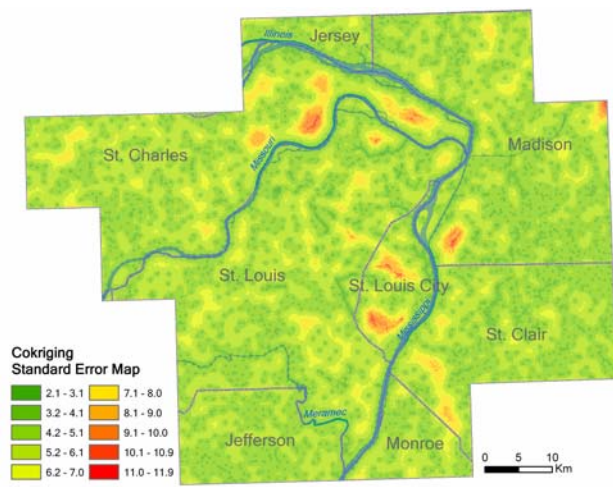


Figure 4.9. (A) Map showing predicted groundwater elevations based on Cokriging, and (B) the corresponding standard error map.

Table 4.1. Cross-validation results for ordinary kriging and cokriging models.

Calculation	Kriging	Cokriging
ME	-0.2375	-0.3730
RMSE	5.2750	4.1020
Kriged MSE	-0.0233	-0.0615
Kriged RMSSE	1.0440	1.0060
Correlation coefficient	0.9270	0.9570

The correlation coefficient between the actual and the predicted values at measured wells is a measure of the overall quality of the predictive model and the estimation procedures thereby employed. The correlation coefficient describes the dispersion around the linear regression line. The ideal value of a correlation coefficient is 1.0. Figure 4.10 presents cross-validation plots that suggest that cokriging produces a slightly higher correlation coefficient (0.957) between the observed and predicted values than that generated by ordinary kriging (0.927).

Table 4.1 summarizes cross validation results generated by kriging and cokriging for the same well data. These comparisons show that including ground elevation data as a second variable in cokriging reduces the estimated variance. Although the kriging produced the more unbiased estimates, being closer to zero, the cokriged interpolation was statistically more accurate; with an RMSSE close to 1.0. This indicates that the cokriging estimation variance was adequately predicted. The correlation coefficient was also nearly 1.0, which suggests that the cokriged elevation estimates are likely closer to the actual values.

Taken together, both validation measures suggest that cokriging produced slightly better estimates with smaller uncertainties in their predicted values at known locations. The addition of ground surface elevations as a second variable improved the model's predictions.

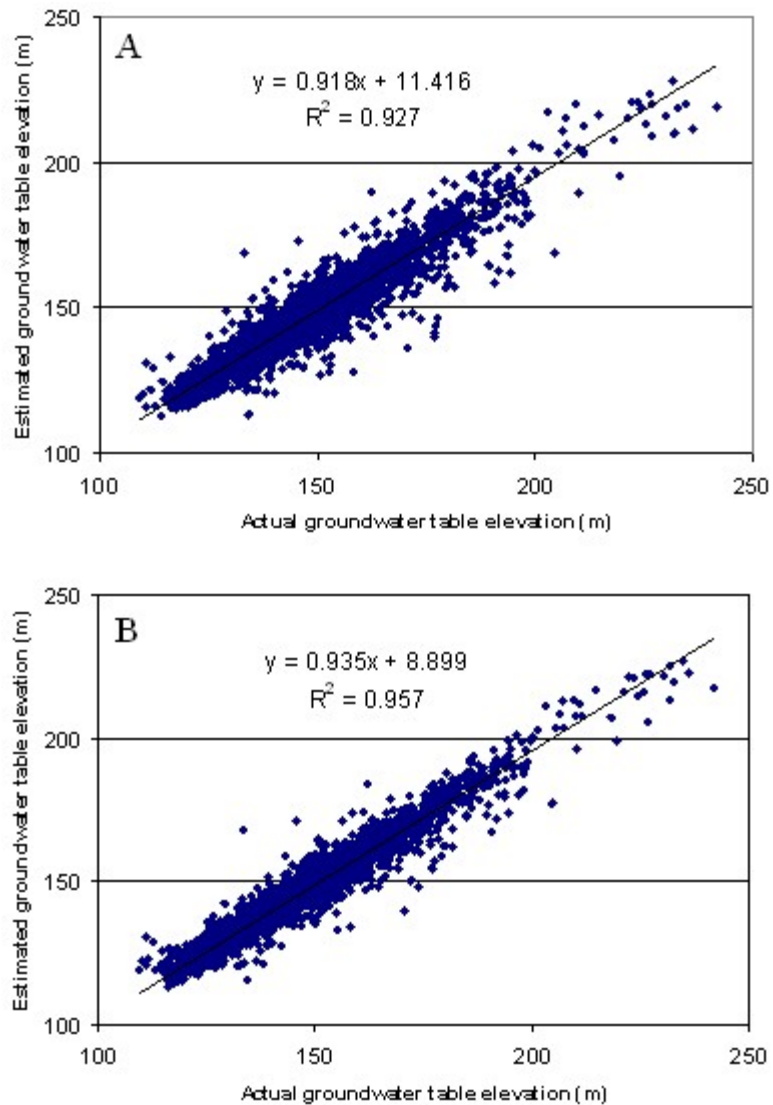


Figure 4.10. Cross-validation data comparing measured versus estimated groundwater elevations and corresponding correlation coefficients, using kriging (A), and cokriging (B).

4.5. DISCUSSION

Estimates of permanent groundwater elevation obtained by the least squares approach were more detailed and accurate, in part, because they were based on a much larger number of regularly-spaced data points (DEM grid accuracy), and, therefore, account for smaller scale variations. However, this technique is not an exact interpolator.

The least squares approach calculates an interpolated value from a mathematical trend derived from the entire data set, instead of limiting the calculations to the closest data points (Gambolati and Volpi, 1979; Dunlap and Spinazola, 1980; Olea, 1999). This method appears to be deficient for modeling local anomalies, such as water well drawdown and other situations where surface elevations and groundwater elevations are not well correlated with one another.

On the other hand, geostatistical models, such as (ordinary) kriging and cokriging are exact interpolators using measured data points. They manipulate and compare data from the nearest adjacent data points to estimate levels in adjacent unsampled areas by incorporating the autocorrelation structure of the data. The primary advantages of kriging over the other methods are its ability to: 1) to interpolate an actual value at measured data points, and, 2) to provide kriged estimates and the corresponding uncertainties at unmeasured sites (Dunlap and Spinazola, 1980).

A disadvantage of geostatistical models is that they fail to consider local topographic variations, or misrepresent them, because ground surface elevations are not included as primary variables. Geostatistical models showed reasonably accurate results in the regions where there was abundant data, but were less accurate in those regions where less data exists. In the elevated highlands, groundwater levels were often overestimated because of the steeply incised terrain, where few wells have been advanced in the valley bottoms. Cokriging appears to produce a slightly better prediction, because it incorporates ground surface elevations as a second variable. This inclusion of a second variable provides a slightly improved prediction of the groundwater elevation. The results of our cross validation analyses also suggest that the inclusion of ground elevation data in cokriging reduces the estimation variance.

5. ESTIMATION OF DEPTHS TO BEDROCK SURFACE

5.1. INTRODUCTION

The bedrock surface is generally recognized as the top of an older lithified rock stratum that underlies unconsolidated Quaternary sediments. This underlying material is also described colloquially as the “bedrock basement” or “basement rock,” which comprise most of the Earth’s crust. The position of the bedrock-soil cap interface is of great import to assessments of seismic site response (Kramer, 1996; Borchardt et al., 1991). Knowledge of the likely elevation of the bedrock-soil cap interface is also crucial to the interpretation of shear wave velocity data recorded at the ground surface, upon unconsolidated materials overlying the bedrock basement. Sites underlain by thick accumulations (>14m) of unconsolidated sediments appear to be more prone to magnification of ground motion than those on shallow bedrock in the St. Louis Metro area (Rogers et al, 2007).

5.1.1. Problem. Contour maps illustrating depth-to-bedrock are commonly constructed by interpolating subsurface data gleaned from geotechnical boring logs. These maps can be prepared using manual contouring (if sufficient data exist) or computationally, using software programs, like SURFER. Most contouring algorithms are programmed to employ smoothing techniques when contouring buried surfaces. This is because deeply weathered surfaces, such as those commonly developed in carbonate rocks (such as karst) can create unsolvable problems because of deeply incised irregularities, such as sinkholes, caves, or pinnacles and cutters, infilled with residual soils. The quality and reliability of most contouring algorithms improves with a greater density of data points.

In rugged terrain, the bedrock surface may present a complex horizon, depending on the severity of weathering. These features include: innumerable hummocks, close depressions, haystacks, and voids (Hasenmueller, 2006). In rugged terrain interpolation techniques may necessitate unrealistically smooth contouring of the bedrock surface because: 1) contouring algorithms often produce smoothed surfaces that overestimate bedrock surface in features such as paleovalley systems, and, 2) a local contouring model

for a single generic landform may lead to erroneous estimates in different geomorphic settings, even if nearby (Hasenmueller, 2006; Nyquist et al., 1996; Figure. 5.1).

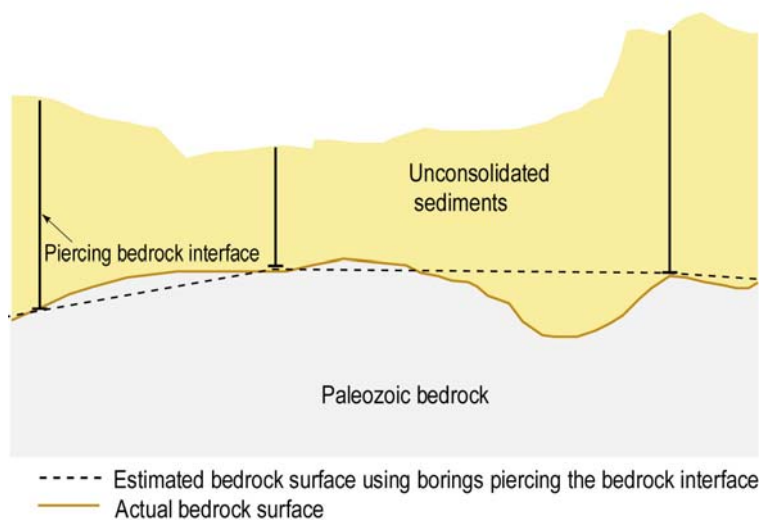


Figure 5.1. Example of an erroneous interpolation, which underestimates the bedrock surface because it is pervaded by paleovalley features which were not penetrated by subsurface boreholes.

5.1.2. Previous Studies. A number of methods have been proposed to overcome problems associated with defining the top of bedrock surface, as described in the previous section. Nyquist et al. (1996) employed cokriging technique using ground surface elevation data to improve the bedrock topography map of Oak Ridge, Tennessee, where bedrock and surface topography are strongly correlated.

Gao et al. (2006) interpolated an initial depth-to-bedrock surface using a kriging technique that employed an array of subsurface data, including data points penetrating the bedrock interface. They refined the depth-to-bedrock elevations by repeating the interpolation using additional data gleaned from water wells that terminated above the

bedrock interface, but extended beyond (deeper) the supposed bedrock surface, as it was initially interpolated.

Similarly, Hasenmueller (2006) proposed a mapping method to subdivide Monroe County, Indiana, using relationships between the bedrock and digital elevation models (DEM). Hasenmueller (2006) mapped the depth-to-bedrock in three subareas with different modeling techniques, which incorporated the following models:

1) An independent bedrock surface model. This model was intended to be used in areas where paleovalleys have been excavated into the bedrock without any physical correlation to the existing ground surface (these features are virtually undetectable without borehole penetrations of high quality geophysical surveys). The bedrock surface is initially approximated using data that pierces the bedrock interface, and then adjusted by considering subsurface data which does not pierce the bedrock interface. This second approximation can be warped downward, depending on the geologic interpretations drawn from adjacent areas, or from local experience.

2) Dependent bedrock surface model. A dependent bedrock surface sub-parallel to the ground surface can be modeled by computing the relationship between the thickness of unconsolidated deposits (soil cap) and the structural trend of the existing ground surface.

3) Bedrock outcrop model. In this technique bedrock exposed at or near the ground surface is assumed to be identical to the ground surface elevation.

5.1.3. Purpose of this Study. In this study, data from subsurface boreholes and a few seismic reflection profiles were used to interpolate a regional map of the depth to the Paleozoic bedrock in the ST. Louis Metro area. The depth-to-bedrock map doubles as a thickness of surficial materials (soil cap) map. These data could also be represented in a top-of-bedrock elevation map for the same area. This study employed ordinary kriging for estimating depth-to-bedrock and cokriging for estimating the bedrock surface topography. The results of the different approaches are compared and discussed below.

5.2. STUDY AREA

5.2.1. The St. Louis Metropolitan Area (STL). The topography of the bedrock surface underlying the St. Louis Metropolitan area appears to have been carved by glacial and fluvial processes during the pre-Illinois, Illinois, and Wisconsin glacial episodes (Allen and Ward, 1977; Goodfield, 1965; Grimley and Phillips, 2006). The two dominant landforms produced by these processes are alluvial filled flood plains with surface elevations between 107m and 203m and elevated loess and till covered uplands with surface elevations between 125m to 288m above sea level. The Quaternary glacial and postglacial sediments unconformably overlie the Paleozoic bedrock strata, mostly Mississippian carbonates and Pennsylvania shales. The most diagnostic features left by the glacial advances are boulder-sized fragments in the glacial diamicton, lying directly upon the underlying bedrock.

5.2.2. Review of Published Maps. The bedrock topography in St. Louis City and County and the unconsolidated material thickness in St. Charles County have been mapped and described by Goodfield (1965) and Allen and Ward (1977), respectively. Bergstrom and Walker (1956) contoured bedrock elevations and sediment thickness in the Mississippi River valley in vicinity of *American Bottoms*. Herzog et al. (1994) prepared a statewide map of bedrock surface elevations for Illinois by compiling data from and revising pre-existing maps. More recently, Grimley and Denny (2004) mapped the bedrock topography of the French Village Quadrangle in Illinois, using 192 subsurface data points using the spline method and tension option.

Blankets of wind blown loess reach thicknesses of approximately 12m to 15m along the bluffs of the Missouri River in the St. Louis uplands. This mantle of loess thins to as little as 1.5m to 3m along ridgetops in southwestern St. Louis (Goodfield, 1965; Lutzen and Rockway, 1987). According to Allen and Ward (1977), the thickness of loess and/or glacial till in the St. Charles uplands ranges from 1 to 19m. Alluvial sediments filling the Mississippi and Missouri River valleys in St. Charles County reach thicknesses in excess of 30m (alluvial fill in the Mississippi River valley reaches greater thicknesses).

Bergstrom and Walker (1956) reported that the elevation of the bedrock surface in Mississippi River valley averages approximately 93m and that the bedrock surface slopes gradually towards the edges of the flood plain, and increases in steepness approaching the

bluffs bounding either side of the flood plain. Bergstrom and Walker (1956) also found that the alluvial fill in the Mississippi River was consistently deeper than 33m, with the deepest part up to 51m, on the Illinois side.

5.3. DATA

5.3.1. Sources of Data. The geotechnical borings used in this study were supplied by the Missouri (MoDGLS) and Illinois (ISGS) geological surveys, The Missouri and Illinois departments of transportation, private and public agencies. MoDGLS supplied 2,637 geotechnical boring records while the ISGS supplied 3,997 boring records in Microsoft Access and Excel spread sheets, respectively. Additional boring logs came from the following sources: 1) 1,540 boring logs in Missouri from the Missouri Environmental Geology Atlas (MEGA; 2007), 2) 311 geotechnical borings in the Columbia Bottom Quadrangle measured and provided by URS Corporation in a hardcopy format, and 3) 58 boring logs along two highway bridge alignments (State Route 364/Page Ave. Extension) archived by MoDOT.

Lithologic descriptions contained in these geotechnical borings were evaluated and reviewed to determine bedrock depth and elevations. The bedrock surface in each borehole was assumed to be that depth wherein continuous rock was encountered (as opposed to rock fragments). Thin partings of shale or limestone interbedded with shale occasionally made it difficult to discern the absolute bedrock surface elevation. Boreholes that did not pierce the bedrock interface were also analyzed to help constrain the minimum depth to the bedrock surface (a valuable piece of information, as described later).

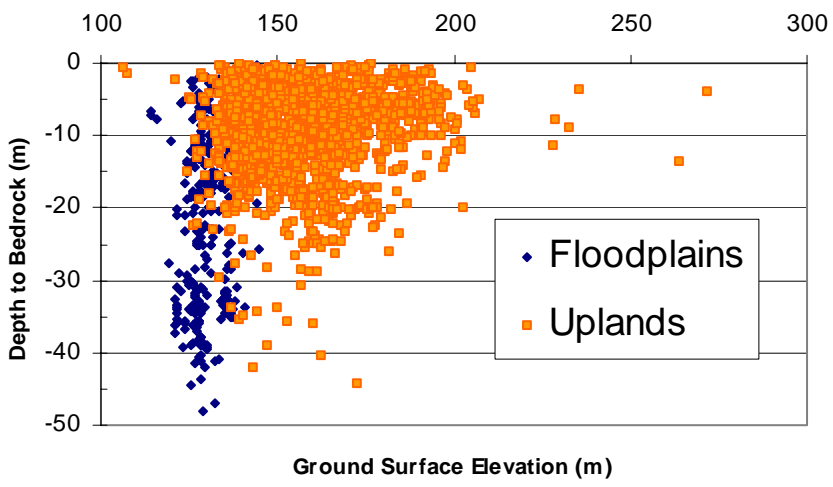
The selected data points for ordinary kriging consisted of 17 seismic reflection profiles measured and interpreted by Williams et al (2007); 5,087 geotechnical borings terminating in the Paleozoic bedrock, and an additional 3,165 borings terminating above the Paleozoic bedrock surface. The cokriging interpolations ignored the 3,165 borings terminated above the bedrock. 5,087 borings pierced the bedrock interface where reliable collar elevations were noted, or these elevations were extracted from the 10m DEM. These borings were included in the cokriging interpolation. These datasets were classified into data type, state, and landform, as summarized in Table 5.1.

Table 5.1. Input data for depth-to-bedrock interpolations (surficial material thickness).

Location		Geotechnical borings to bedrock surface		Seismic reflection
Landform	State	Piercing	Not piercing	
Floodplain	Missouri	450	115	9
	Illinois	348	1060	1
Upland	Missouri	2888	788	6
	Illinois	1401	1193	1
sub-total		5087	3156	17
		Total		8260

5.3.2. Bedrock Surface Data. According to the boring logs and seismic reflection profiles, bedrock elevations in the study area varied between approximately 78m and 174m in the flood plains and between 90m and 269m in the uplands. The thickness of unconsolidated deposits in the flood plains ranged from zero to 48 m, with a statistical averages of 23 ± 12 m (mean \pm standard deviation). The thickest unconsolidated deposit exceeds 45m in the Mississippi River flood plains (American Bottoms; Figure. 5.2A). The thickness of unconsolidated surficial materials in the uplands varied between zero and 48 m, and averaged approximately 12 ± 8 m; the surficial materials mantling uplands in Illinois averaged 13 ± 8 m. These are about the same thickness as similar deposits west of the Mississippi River, in Missouri, which average 12 ± 7 m.

(A)



(B)

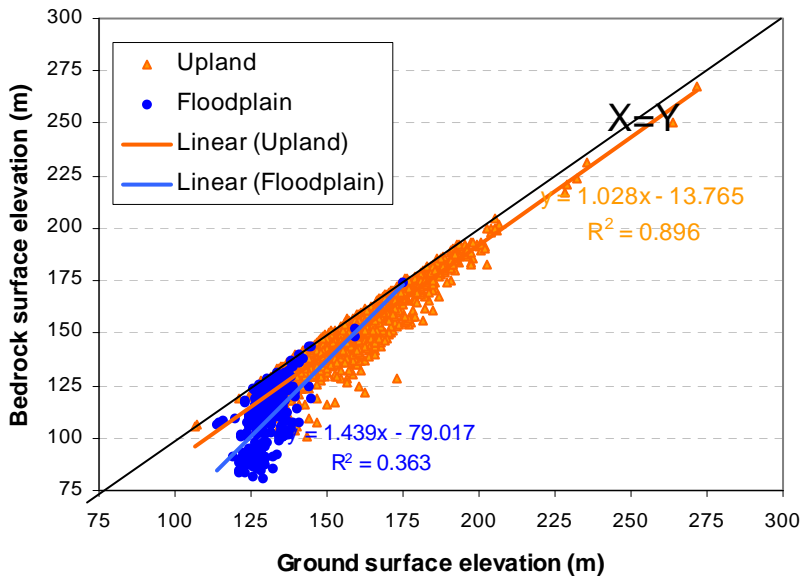


Figure 5.2. A) Graph showing the distribution between depth-to-bedrock and ground surface elevation in flood plains and uplands. The bedrock interface lies well beneath the land surface. B) The lower graph illustrates the relationships between bedrock elevation and ground surface elevation in flood plains and uplands. In the uplands, bedrock elevation appears to be more or less proportional to ground surface elevation.

5.4. METHODS EMPLOYED TO INTERPOLATE DEPTH-TO-BEDROCK

The plots of bedrock and ground surface elevations across the study area presented in Figure 5.2 reveal some interesting trends: 1) bedrock elevation is proportional to the ground elevation in the uplands, but a less distinct correlation in the flood plains, and 2) the depth-to-bedrock thins considerably in hilly upland areas, although this trend was not correlated with ground elevation.

The depth-to-bedrock and bedrock interface elevations between sampled sites were interpolated, and corresponding uncertainties were computed using geostatistics (ordinary kriging and cokriging). The theory of kriging was first introduced by D. R. Krige for evaluating ore deposits and developed by Matheron (1971). Kriging uses the information from data points in close proximity to the areas to be estimated by incorporating the autocorrelation structure of the data. The primary advantages of the kriging method are its abilities to interpolate an actual value at a known data point, and to provide kriged estimates, with their corresponding uncertainties, at unmeasured sites (Dunlap and Spinazola, 1980; Isaaks and Srivastava, 1989; Journel and Hujibregts, 1978).

5.4.1. Kriging Map of Depth to Bedrock. Based on the analysis of depth to Bedrock data, the study area was subdivided into uplands and flood plains. Boreholes that terminated above the bedrock interface were useful in determining the minimum depth to bedrock, which would be above the interpolated bedrock surface.

Ordinary kriging was employed with the spherical model provided by ArcGIS 9.1 software. Two interpolation maps of the depth-to-bedrock surface were initially generated: 1) one using 5,104 borings logs and seismic reflection profiles that pierced the bedrock basement (Figure.5.3A and 5.4A), and, 2) a minimum depth-to-bedrock map interpolated from 8,260 boring logs and seismic reflection profiles, which included borings that did not pierce bedrock interface (Figure. 5.3B and 5.4B).

The resulting depth-to-bedrock map was refined by discarding minimum depth interpolation values that were shallower than the depths predicted by the depth-to-bedrock map and by including minimum depth interpolations that were deeper than those elevations predicted by the depth-to-bedrock map (Figure. 5.3C and Figure. 5.4C). The bedrock outcrops exposed along the river bluffs were then added to final map in order to

portray the data more realistically for the bedrock topography map. Figure 5.4D shows the map of kriging standard error.

The corresponding bedrock elevations were generated by subtracting the kriged depths-to-bedrock values (shown in Figure 5.4C) from the ground elevations, which were derived from the DEMs with a 10 m square grid spacing (Figure. 5.4E).

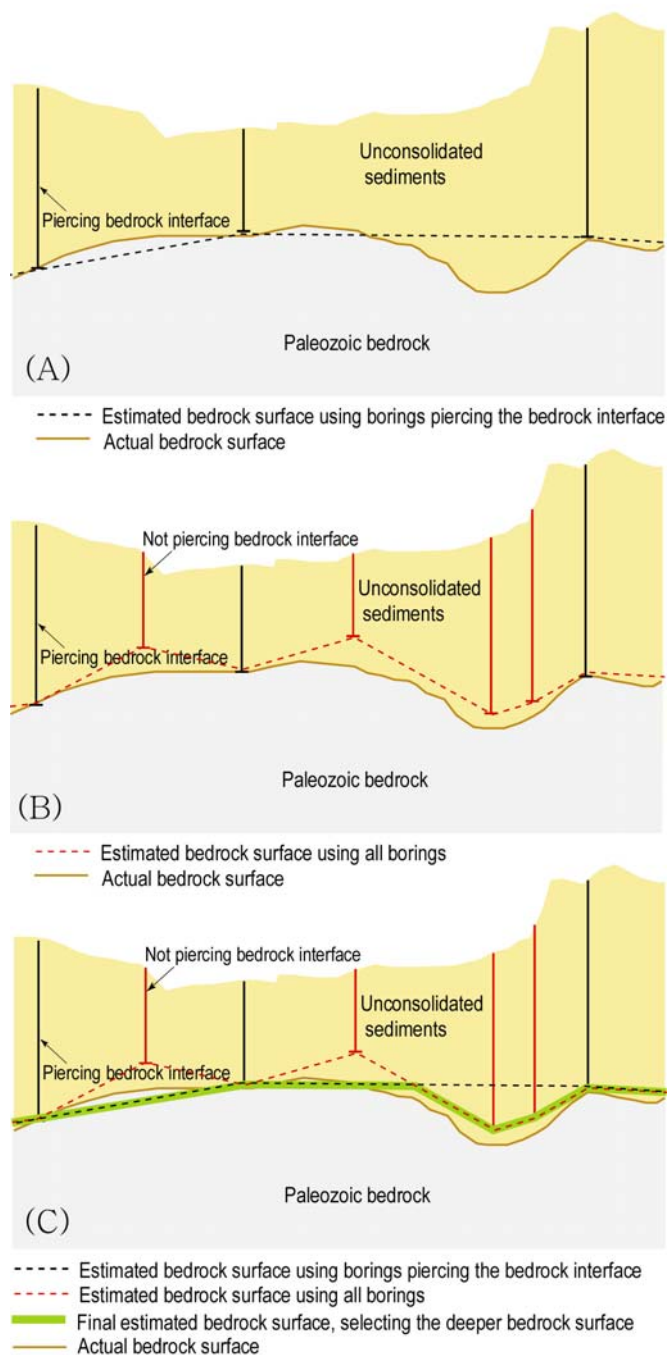
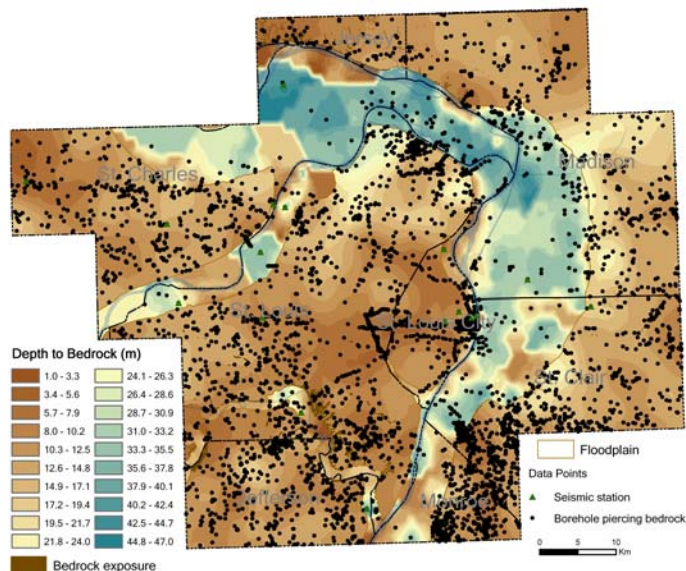


Figure 5.3. Schematic diagrams illustrating the proposed technique for estimating the surficial material thickness, employing kriging. A) Approximating the bedrock surface using borings that pierce the bedrock interface. B) Approximating the minimum bedrock surface, using all borings, including those that do not pierce the bedrock interface. C) Of these two approximations, the model then selects the deeper of the two predicted bedrock surfaces. This deeper surface appears to be a more accurate.

(A)



(B)

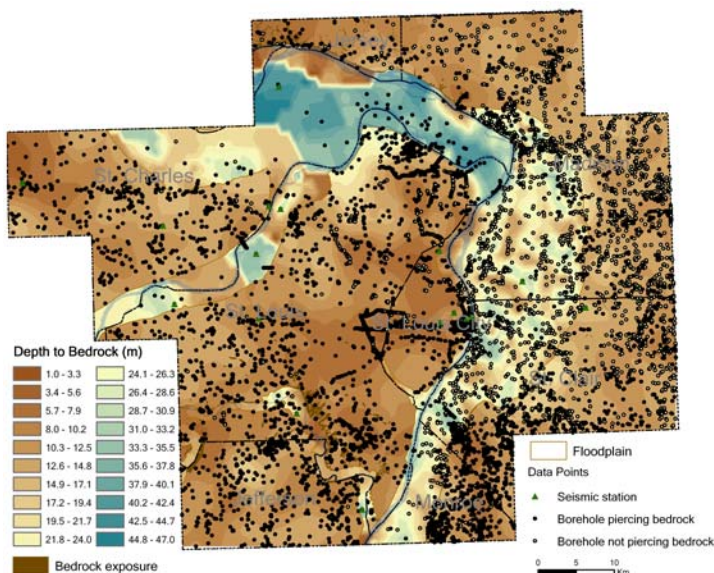
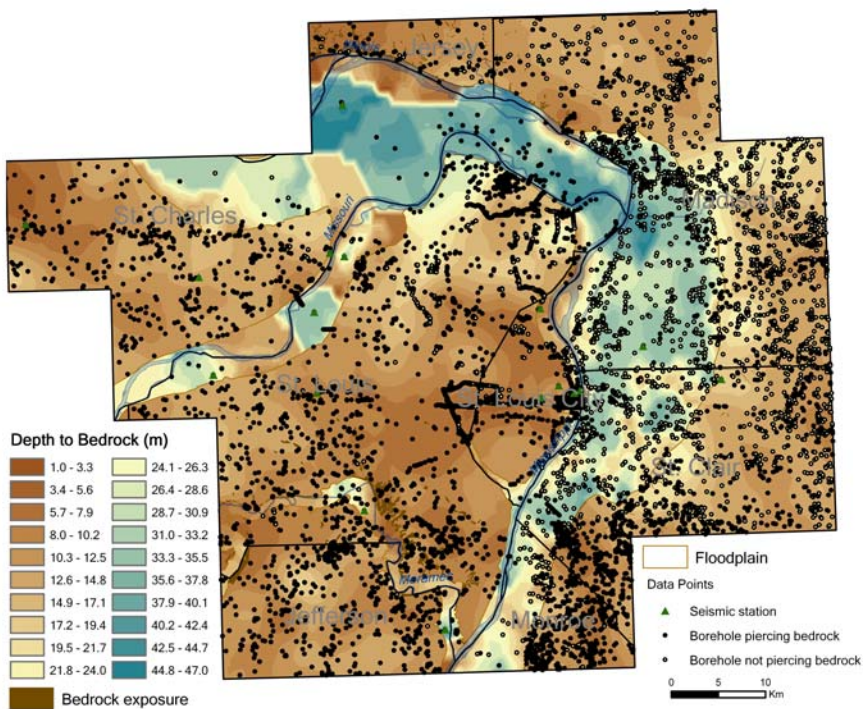


Figure 5.4. Depth-to-bedrock maps predicted by kriging and corresponding standard error maps, showing sample distributions. A) The interpolated bedrock surface using borings piercing the bedrock interface. B) The kriged bedrock surface using all borings, including those that do not pierce the bedrock interface. C) Proposed model then selects the deeper of the two predicted bedrock surfaces. D) Map of kriging standard error. E) Corresponding bedrock elevations, generated by subtracting the kriged final depth-to-bedrock map from ground surface elevations taken from 10m DEMs.

(C)



(D)

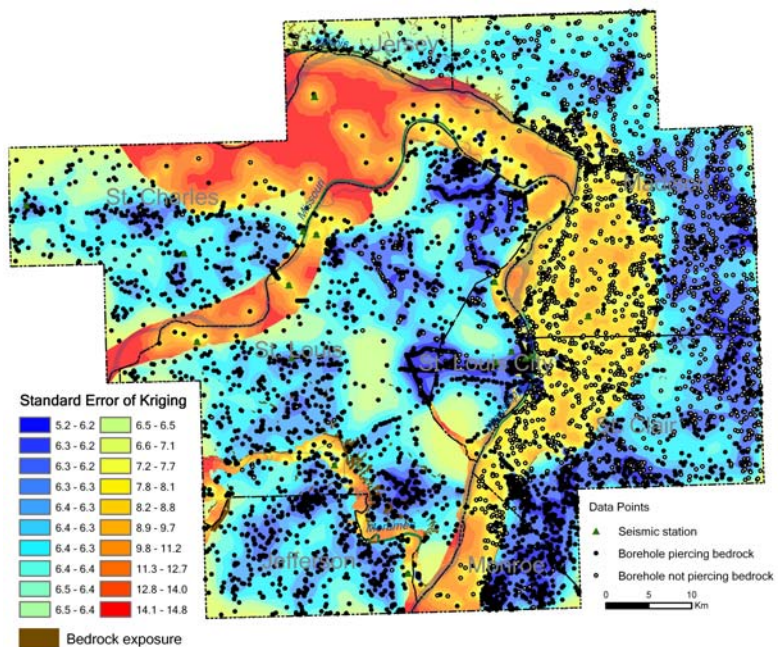


Figure 5.4. Continued

(E)

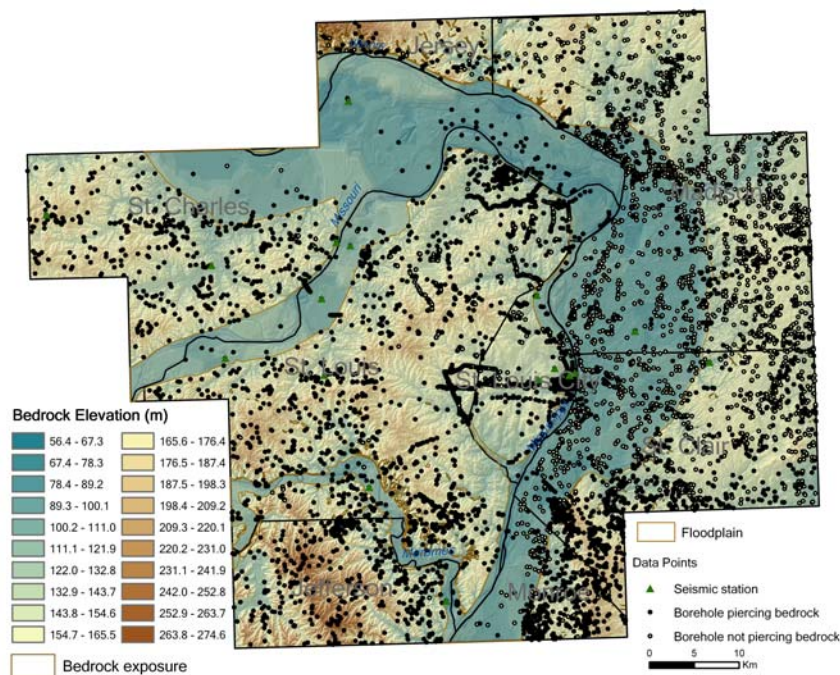


Figure 5.4. Continued

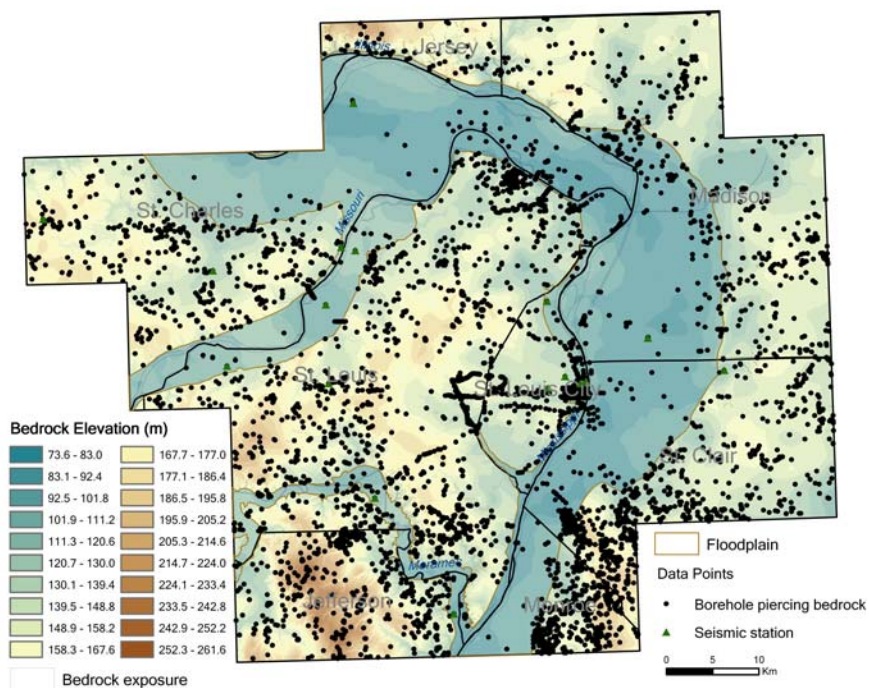
5.4.2. Cokriging Map of Bedrock Elevation. Based on the strong correlation between bedrock and ground surface elevations, cokriging was employed to interpolate bedrock elevations, by exploiting ground surface data, which was acquired from USGS 10m DEMs. Cokriging is a geostatistical technique which utilizes the correlation between a primary variable (bedrock elevation in this analysis) and secondary variable (ground elevation) to improve the estimate. The second variable is more densely and evenly obtained; thus, unsampled values can be estimated at locations where there is no primary variable, only the secondary variable. The estimate is then based on the spatial autocorrelation of both variables.

5,104 data points were extracted from geotechnical borings and seismic reflection profiles to provide elevations of the bedrock interface, as well as ground surface elevations. These data were also selected for the cokriging interpolation of the elevations of the bedrock interface. Ground elevations, consisting of 602 points per a quadrangle

(17,473 points for the whole study area) were extracted from the 30m DEMs using a 500m square grid spacing (with MICRODEM software). These data were input into the cokriging model as a second variable. As in previous kriging models, the study area was subdivided into uplands and flood plains. Cokriging was employed using the spherical model provided by ArcGIS 9.1 software. This interpolated bedrock elevations within each subarea (uplands and flood plains).

The cokriging map and cokriging standard error of the bedrock interface elevations are presented in Figures 5.5A and 5.5B, respectively. The corresponding depth-to-bedrock was generated by subtracting the cokriging map of bedrock elevation from the ground surface elevations, which were derived from 10 m DEMs (Figure 5.5C).

(A)



(B)

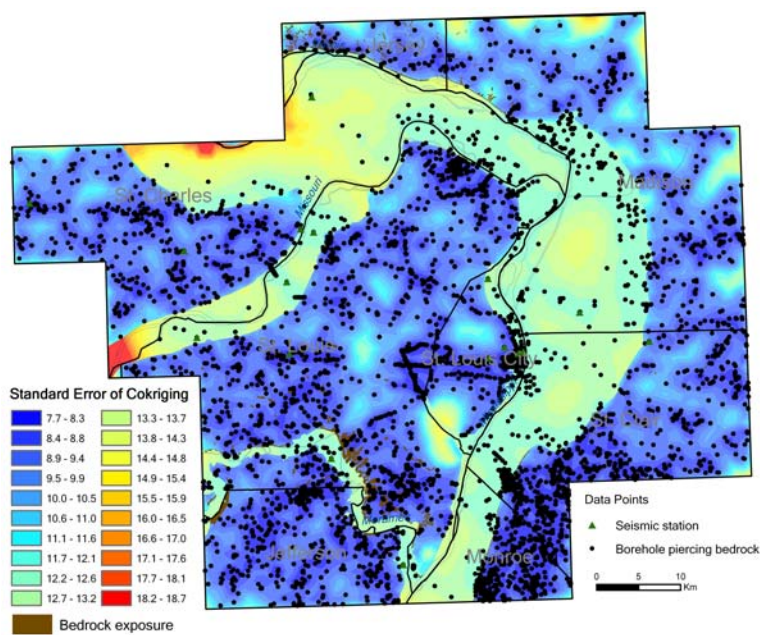


Figure 5.5. Cokriging maps of A) bedrock interface elevations, and B) Standard error. (C) Corresponding depths-to-bedrock, determined by subtracting the cokriged bedrock elevations from 10m DEMs.

(C)

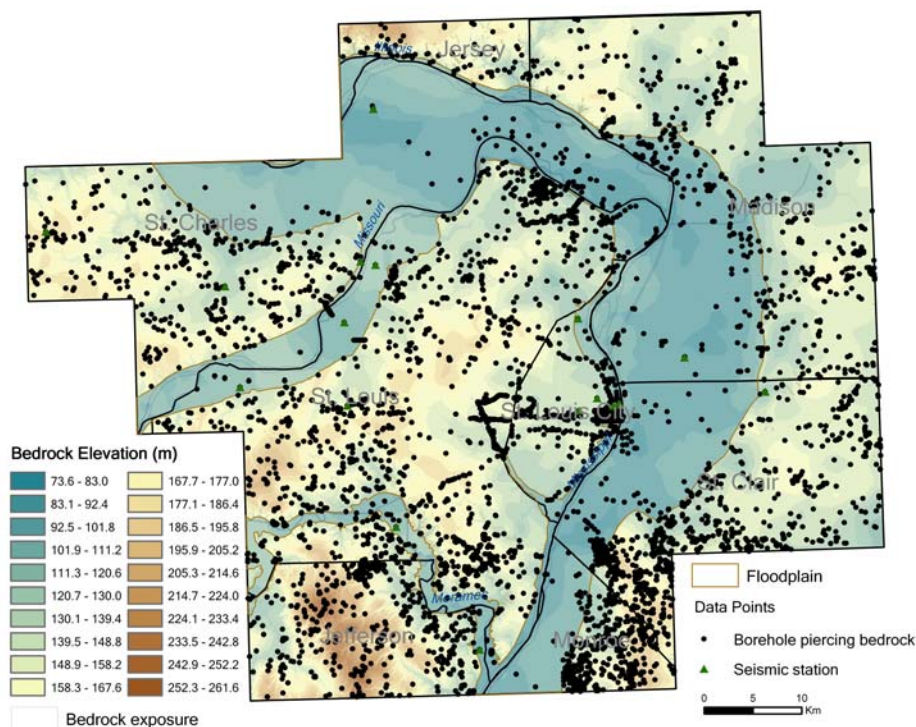


Figure 5.5. Continued

5.5. RESULTS

The depth to bedrock maps were constructed from estimates generated by interpolation of subsurface data using kriging techniques. These same techniques were compared with the nearest factual data to assess those areas where linear interpolations might lead to erroneously high estimates of the bedrock interface, because of dips and valleys in the bedrock interface.

Although sample populations were limited, the depth-to-bedrock estimates are generally less than 12m in Missouri and Illinois, while the elevations of the bedrock interface range between 90m and 269m above sea level in Missouri and from 95m to 234 m above sea level in Illinois, in the loess covered uplands.

After making several comparisons, it was concluded that a few areas still exist where the data did not match the results of the cokriged predictions. Major discrepancies

between the interpolated values and the true values were usually found along ridge lines in Jefferson County, Missouri, and along river bluffs in Jersey County, Illinois, where the depth-to-bedrock values extracted from the nearest adjacent data points would not exceed 10m, although the estimates produced by the cokriging analysis predict a depth of approximately 60m. This cokriging value of 60m is considerably deeper than the actual value, which is known to be close to ~10m in this area. This erroneous estimate may be attributed to smoothly underestimating bedrock elevations at unsampled areas in alluvium valleys, because the data points were many kilometers apart in this area (Figure. 5.5B). In such instances, where there is a real paucity of data, it would appear that cokriging methods can gross overestimate or underestimate the actual values.

The depths to bedrock inferred from the kriging technique were estimated to be 4m to 42m in the uplands and 1m to 47m in flood plains (Figure. 5.4D). These ranges agree well with previously reported data and the data points (0m to 44m and 0m to 48m, respectively; Figure. 5.2A) used in this study. The model for interpolating the depth-to-bedrock map appears to be more reliable than the model for interpolating bedrock elevation. This implies that, for the rugged terrain like St. Louis Metro area, the method for estimating bedrock depth yields a more realistic model to predict the position of the bedrock interface than the method used to predict bedrock elevation.

6. MAPPING LIQUEFACTION POTENTIAL USING GIS-DATABASES

6.1. INTRODUCTION

Liquefaction is a soil failure mechanism that occurs when the pore water pressure produced in cohesionless soils equals or exceeds the effective confining stress acting upon them, causing them to lose shear strength and behave as a fluid. Cohesionless soils such as silt, sand, and gravel are most susceptible to liquefaction hazards. Liquefaction can be triggered by rapid loading, where there is insufficient time for excess pore water pressures to alleviate through natural drainage. Rapid loading situations can develop from sudden movements, such as translation during slope movements, or in response to seismic excitation, which elevates pore water pressures. For these reasons, liquefaction is most commonly associated with earthquakes. Liquefaction can also cause a loss of bearing strength, ground settlement, and horizontal displacements, commonly manifest in lateral spreads, sand boils, sand blows, and sand or clastic dikes.

Liquefaction usually occurs in granular (<15% clay) unconsolidated sediments with low relative density (Youd, 1973). Iwasaki et al. (1982) provided general criteria for triggering of liquefaction, as follows; whenever: 1) cohesionless material of low relative density such as sand and silt is saturated, 2) there is some low permeability material overlaying the affected layer, which retards rapid drainage, 3) the liquefied layer is shallow (<12m below the ground surface, and, 4) the Factor of Safety (FS) of the liquefied layer < 1.0.

Ground failure susceptibility refers to the various mechanisms by which a unconsolidated soil can lose appreciable shear strength in response to seismic shaking, resulting in permanent ground displacements (Youd and Perkins, 1978). Liquefaction susceptibility is influenced by the age (induration) and physical properties of the sediments, the depth of the groundwater table, and the presence and characteristics of an impermeable confining layer(s) (Kramer, 1996; Tuttle et al., 1999; Youd and Perkins, 1978). Liquefaction susceptibility is also independent of the expected seismicity of the region.

The susceptibility of older soil deposits to liquefaction is generally lower than that of younger deposits, because they generally exhibit more cementation or bonding

between their constitutive particles (Obermeier, 1989). For example, Holocene sediments are considered more susceptible than Pleistocene sediments. Even weak cementation can play a significant role in resisting liquefaction. Loose granular fills, such as those placed in dredged hydraulic fills or without compaction, are generally considered most susceptible to liquefaction (Kramer, 1996). Well-graded soils are generally less susceptible to liquefaction than poorly graded soils; the voids between the larger particles being filled by smaller particles in a well-graded soil results in a lower void ratio and increased relative density, both of which make it less vulnerable to sudden changes in pore pressure under undrained conditions (Kramer, 1996).

When pore water pressure increases during shaking, liquefied sand often migrates upward through existing fractures, to the ground surface. The sites most prone to sand blows are those that are capped by relatively impermeable fine-grained sediments. Obermeier (1989) observed earthquake-induced sand blows in vicinity of the New Madrid Seismic Zone and concluded that sand blows can develop wherever the cover stratum is less than 6 to 7m thick during severe ground shaking. But, he also concluded that the cover stratum texture exerts little influence on sand blow development if insufficient silt or clay exists to cause the covering material to have a hydraulic conductivity (permeability with respect to water) significantly less than the substratum.

6.1.1. Previous Studies of Regional Liquefaction Potential Mapping. Regional liquefaction potential has been mapped by qualitatively or quantitatively characterizing surficial geology commonly recognized to be most susceptible to liquefaction (Baise et al., 2006; Wills and Hitchcock, 1999; Youd and Perkins, 1978). These qualitative assessments are based solely on Quaternary geology or, in some cases, on the calculated factor of safety. Several methods have been proposed for regional mapping of soil liquefaction potential, where insufficient data exists to assess either the liquefaction potential index or the dynamic factor of safety. Geologic units are identified by their age and depositional environment and then characterized in terms of their susceptibility, assuming that unconsolidated cohesionless soils are most vulnerable.

Kuribayashi and Tatsuoka (1975) investigated several hundred liquefaction sites that had been affected by 44 historic earthquakes in Japan. They mapped the percent of liquefied area of each recognized geomorphic landform. Iwasaki et al. (1982) developed

the microzonation method using Kuribayashi and Tatsuoka's classification scheme and then outlined the channels of active and abandoned/filled river beds and reclaimed lands, which are most prone to liquefaction.

Hitchcock et al. (1999) classified liquefaction susceptibility in the Simi Valley, Ventura County, California on the basis of three factors: 1) the total thickness of loose sandy deposits within 12m of the ground surface, 2) the depth to groundwater, and 3) the estimated threshold peak ground acceleration (PGA) values required to initiate liquefaction, based on the evaluation of corrected standard penetration test (SPT) blow counts, where available. Geologic criteria used in the absence of subsurface data include the age and texture of deposits, mapping of surficial (unconsolidated) geologic units, historical liquefaction features within the same area, and, the estimated depth to groundwater. Hitchcock et al. (1999) assumed that the relative ages of unconsolidated deposits are useful for estimating liquefaction susceptibility when reliable borehole data is unavailable, because surficial deposits develop increased cohesion with age, cementation, burial, and confinement, which make them less likely to liquefy.

Holzer et al. (2006) grouped 202 cone penetration test-based (CPT) liquefaction potential index (LPI) values in surficial geologic units along the margins of San Francisco Bay, California. Cumulative frequency distributions of the LPI of surficial geologic units were then analyzed. It was assumed that surface manifestations of liquefaction occur where $LPI \geq 5$. The percentage of LPIs higher than 5 for each geologic unit indicates that the approximate percentage of these units that can be expected to exhibit surface manifestations of liquefaction. Based on the LPI distribution in recognized surficial geologic units, Holzer et al. (2006) predicted that 73% of the artificial fill and 3% of Holocene alluvial fan deposits could be expected to show surface manifestations of liquefaction during an M 7.1 earthquake with the PGA of 0.50g.

Computing the SPT-based probability proposed by Cetin et al. (2004), Baise et al. (2006) calculated the probability of the liquefaction potential for each penetration interval in each subsurface boring assuming a M 6.5 (moment magnitude) earthquake with a PGA of 0.24g. They also explored the percentage of intervals with high (>65%) and low (<35%) liquefaction probability within each surficial geologic unit. If the data in each geologic unit exhibits a recognizable pattern of occurrence (spatial relationship), an

ordinary kriging technique could be applied to predict the liquefaction probability values at unsampled locations in Cambridge, Massachusetts.

6.1.2. Statement of Problems. When quantifying liquefaction potential, existing methods rely on the assumption that sediments from different depositional environments and ages will generally exhibit unique distributions of the liquefaction potential. These methods also assume that a single surficial geologic unit is spatially homogenous and more or less possesses the same liquefaction potential. These methods also assumed that the depth to groundwater is also homogeneous within a recognized geologic unit.

Depth to groundwater plays a pivotal role in liquefaction evaluation because saturation is necessary to trigger liquefaction. The effective vertical stress is also required to calculate the factor of safety (FS) against liquefaction using the simplified procedure for liquefaction potential (Seed and Idriss, 1971). Groundwater fluctuations are also important in assessing long-term liquefaction hazards (Hitchcock et al., 1999; Kramer, 1996).

Absent better data groundwater elevation is often assumed to be a subdued replica of ground elevation (King, 1899; Domenico and Schwartz, 1998). The depth to groundwater is generally deepest beneath ridgelines in hilly areas (Daniels et al., 1984; Peck and Payne, 2003), and is more or less equal to the land surface in perennial channels (Daniels et al., 1984; Peck and Payne, 2003). These common attributes of the permanent groundwater table allow approximations of the depth-to-groundwater to be estimated where the surficial materials are relatively homogeneous. The depth-to-groundwater can be expected to vary considerably, in proportion to the ground surface. In hilly terrain, like the loess covered uplands west of St. Louis, the water table will come closest to the surface along steeply incised valley bottoms and along the few alluvial filled channels that pass through the area (Meramec River, Mill Creek, etc.).

Data to assess liquefaction potential using the simplified procedure of Seed and Idriss (1971) can vary considerably, even within mapped surficial units, due to variations in depth to groundwater as well as the physical properties of near surface soils, which are subject to subareal weathering and/or may be locally disturbed, by grading, natural slope creep, or past slope instability. The approximate methods described above generally ignore variation in the depth to groundwater within surficial geologic units, and thereby,

would be inappropriate to apply to an area of dissected topography, like the hills west of St. Louis.

6.1.3. Purpose of this Study. The purpose of this study was to apply liquefaction potential mapping in the St. Louis Metro area in Missouri and Illinois. The Liquefaction Potential Index (LPI) proposed by Iwasaki et al. (1978 and 1982) was estimated from 564 boring logs in the study area. The locations of LPI assessments were grouped into surficial geologic units (loess, till, alluvium, and other materials). LPI was then characterized by its relationship to depth to groundwater within each surficial geologic unit using ArcGIS. The resultant maps identify the severity of liquefaction that can be expected in the St. Louis Metro area, based on three scenario earthquakes. This study will provide urban planners, building inspection departments, and engineers with a relative sense for which portions of the STL area are most susceptible to liquefaction hazards.

6.2. BACKGROUND

6.2.1. Liquefaction Potential Index (LPI). The liquefaction potential index (LPI) was originally proposed by Iwasaki et al. (1978 and 1982). Iwasaki et al. (1982) validated his LPI values by comparing them to physical evidence of historic liquefaction at 63 liquefied sites and 22 non-liquefied sites impacted by six earthquakes that struck Japan between 1891 and 1978. This method has since been applied to evaluate liquefaction potential in North America (Holzer et al., 2006; Luna, 1995; Luna and Frost, 1998; Toprak and Holzer, 2003). Liquefaction often causes crippling structural damage in the upper 20m. A weighting function gives more value to the layers closest to the ground surface, and decreases linearly to zero, at a depth of 20m.

The Liquefaction Potential Index defined by Iwasaki et al. (1978 and 1982) can be expressed as follows:

$$LPI = \int_0^{20} F(z) \cdot w(z) dz$$

where z = depth (0~20m), dz = the differential increment of depth, $F(z)$ = severity; and $w(z)$ = weight function (= $10-0.5z$).

Iwasaki et al. (1978 and 1982) found that severe liquefaction and minor liquefaction are likely to occur whenever the LPI > 15 and the LPI < 5, respectively. The LPI is inversely proportional to the FS and the depth of the saturated layer. The higher the index, the greater the potential for liquefaction. The categories of liquefaction severity were modified by Luna and Frost (1998), and Sonmez (2003), and they are summarized in Table 6.1.

6.2.2. Liquefaction Potential Based on Corrected SPT (N_1)₆₀ Values. LPI values are fundamentally derived from the simplified procedure to estimate the factor of safety (FS) of each soil layer. The FS against liquefaction is expressed as the ratio of the cyclic resistance ratio (CRR) to the cyclic stress ratio (CSR) for the liquefaction potential (Seed and Idriss, 1971). A SPT-based simplified procedure to evaluate liquefaction was initially proposed by Seed and Idriss (1971), and this procedure was recently updated by Youd et al. (2001).

6.2.2.1 CSR (Cyclic Stress Ratio). The simplified procedure to evaluate stresses causing liquefaction (CSR) is expressed as follows, taken from Seed and Idriss (1971):

$$CSR(Cyclic\ Stress\ Ratio) = 0.65 \left(\frac{a_{max}}{g} \right) \left(\frac{\sigma}{\sigma'} \right) r_d$$

where a_{max} = the peak horizontal acceleration, g = the gravity, σ = the overburden stress, σ' = the effective overburden stress, r_d = the stress reduction coefficient, and $(N_1)_{60}$ = the corrected SPT blow count.

Table 6.1. Historic liquefaction severity assessed from the liquefaction potential index (LPI; Iwasaki et al., 1982).

LPI	Iwasaki et al (1978)	Luna and Frost (1998)	Sonmez (2003)	This study
0	Not likable	Little to None	Little to none	None
$0 < LPI \leq 2$		Minor	Low	Little to none
$2 < LPI \leq 5$			Moderate	
$5 < LPI \leq 15$		Moderate	High	Moderate
$15 < LPI \leq 100$	Severe	Major	Very high	Severe

6.2.2.2 CRR (Cyclic Resistance Ratio). Criteria for the evaluation of liquefaction resistance, CRR, based on the corrected SPT blow count values $(N_1)_{60}$ were developed by Seed et al. (1985), who studied 125 liquefaction case histories in North and South America, Japan, and China. Sites containing sandy soils that were subjected to known earthquake liquefaction case histories were categorized as liquefied or non-liquefied on the basis of the presence or absence of surficial liquefaction features. By plotting CSR versus SPT $(N_1)_{60}$ pairs for liquefied and non-liquefied zones, a curving threshold boundary between liquefied and non-liquefied zones defines the CRR value.

The factor of safety (FS) against liquefaction is defined as the ratio of liquefaction resistance to seismic demand ($FS = CRR/CSR$). Generally, the FS within any soil unit is always more than 1.0 when the unit lies above the groundwater table. An FS of 1.0 or less, where CSR equals or exceeds the CRR, indicates the presence of potentially liquefiable soil. The FS for moment magnitude (M) 7.5 earthquake is expressed as follows:

$$FS \text{ (Factor of Safety)} = \left(\frac{CRR_{7.5}}{CSR} \right) MSF$$

where $CRR_{7.5}$ = Cyclic Resistance Ratio for M 7.5, CSR = Cyclic Stress Ratio, and MSF = magnitude scaling factor (Seed and Idriss, 1982).

6.2.2.3 Advantage of the LPI Method. The LPI method embraces the concept of a factor of safety (FS) against liquefaction. The FS with depth can be calculated and used to determine the liquefaction potential at any particular depth of interest, realizing that severe liquefaction is more likely to occur at sites or within soil horizons where the saturated layer has a low FS (<1.0) and the groundwater table is shallow. The liquefaction potential is described by evaluating the variation of FS with depth within discrete, identifiable soil horizons identified in a single geotechnical boring. Therefore, it is difficult to judge the liquefaction potential for an entire soil column, where a mixture of liquefiable and non-liquefiable soils are stacked one upon another.

The LPI reflects the calculated safety factors for each stratigraphic horizon, accounting for the depth and thickness of each saturated layer, integrating these factors along soil columns up to 20m deep. The simplified procedure is used to predict the liquefaction potential of a single stratigraphic layer. Thus, estimations by the LPI Method are more representative of the actual conditions of occurrence during earthquakes (Holzer et al., 2006), where discrete horizons can be expected to lose strength and fail at different thresholds of acceleration, frequency, and duration (number of equivalent cycles of loading). Additionally, once the LPI interval is classified based on evidence of historic liquefaction, the index reflects the increasing severity of the liquefaction hazard, which is useful to predict liquefaction damage (Iwasaki et al., 1978 and 1982; Luna and Frost, 1998; Sonmez, 2003).

6.3. STUDY AREA

6.3.1. The St. Louis Metropolitan Area (STL). The study area encompasses 29 7.5-minute USGS quadrangles in the St. Louis Metropolitan area of Missouri and Illinois, which covers a land area of 4,432 km². This area will be referred to in this study as *STL*. The topographic altitude in STL generally ranges from 116m to 288m above sea level. STL includes the confluence regions of the Mississippi River-Missouri, Mississippi-Illinois, and Mississippi-Meramec rivers. STL is traversed by a low-lying alluvial floodplain along these four major rivers, which are bordered by dissected loess covered uplands on either side. The floodplains are generally flat with a slope less than 2%, while

the slopes more than 5% are found in the southwest STL and along the bluffs of the river valleys (Lutzen and Rockaway, 1987).

The floodplains are made up of extensive Holocene and Pleistocene alluvial deposits. Several thin flood beds, thicker lacustrine or alluvial deposits in eastern STL, Illinois were loaded and deposited adjacent to major river valleys during the last two glaciations (pre- Illinoian and Illinoian; Grimley et al., 2001).

In upland areas, extensive Peoria and Roxana loess, which was derived from the floodplain of the rivers during the Pleistocene (glacial) time, covers the Paleozoic bedrock. The 15m ~ 20m thick loess is found along the bluffs of the Mississippi and Missouri rivers, while loess is seldom found on the hillsides in southwestern St. Louis County due to removal by surface water (Fehrenbacher et al., 1986; Goodfield, 1965).

6.3.2. New Madrid and Wabash Valley Seismic Zones. STL is located near known seismic sources, the New Madrid Seismic Zone (NMSZ) and the Wabash Valley Seismic Zone (WVSZ), which have produced prehistoric and historic liquefaction features in the study area.

By examining relationships between Holocene surficial deformation and seismicity, Russ (1982) found that earthquake of body wave magnitude (m_b) ≥ 6.2 (equivalent to $M \geq 6.4$; Tuttle and Schweig, 1995) have occurred at least three times in the past 2000 years caused surface deformation such as faulting, folding, and liquefaction in the vicinity of NMSZ. He suggested that $m_b 6.2$ is the approximate threshold of liquefaction in the NMSZ.

Large intraplate earthquakes occurred on the New Madrid Seismic Zone (NMSZ) on Dec. 16, 1811, Jan. 23, 1812, and Feb. 7, 1812. The February 1812 shock was the largest of the earthquake series. The location of the February 1812 earthquake in the NMSZ was about 230 km south of the St. Louis City. Converting Modified Mercalli intensity (MMI) from the February 1812 event into a corresponding magnitude, Hough et al. (2000) obtained $M 7.4\sim 7.5$, and Bakun and Hopper (2004) determined $M 7.0\sim 8.1$ at a 95% confidence level. Atkinson and Beresnev (2002) simulated ground motions at the St. Louis for $M 7.5$ or $M 8.0$ earthquake, and they concluded that $M 7.5$ or $M 8.0$ are possible scenarios for the observed MMI of 7 to 8 at St. Louis, which was induced from the 1811 and 1812 New Madrid earthquakes.

The 1811 and 1812 sequences caused liquefaction more than 240 km from their inferred epicenter (Street and Nutti, 1984; Johnston and Schweig, 1996). Large earthquake-induced liquefactions across the NMSZ were interpreted to have formed in 900 +/- 100 A.D., and 1450 +/- 150 A.D. by radiocarbon dating of organics and artifacts (Tuttle, 2001; Tuttle et al., 2002). Cramer (2001) analyzed recurrence intervals for prehistoric and historic New Madrid earthquakes and employed MonteCarlo sampling of 1000 recurrence intervals. He suggested that recurrence intervals for 900 A.D., 1450 A.D., and 1811-1812 sized events at New Madrid range from 267 to 725 years at a 68% confidence level and from 160 to 1196 years at a 95% confidence level. Employing a logic tree derived from historic seismic events, the U.S. Geological Survey currently defines NMSZ as a M7.5 seismic hazard region with a 500-year recurrence interval (Frankel et al., 2002).

The Wabash Valley Seismic Zone (WVSZ) in southeastern Illinois and southwestern Indiana is about 240 km east of the St. Louis City. The Vincennes Earthquake, which was the largest earthquake in Vincennes, Wabash Valley, Indiana is interpreted to have occurred about 6100 +/- 200 years BP, based on radiocarbon dating of associated archaeological artifacts as well as flood plain stratigraphy. The Vincennes Earthquake is believed to have produced M 7.5, which was determined using back-calculated ground motion characteristic from paleoliquefaction sites (Green et al., 2005).

6.3.3. Liquefaction Features in STL. Along the lower Meramec River and along Cahokia and Piasa creeks, Tuttle (2005) and Tuttle et al. (1999) examined and dated paleoliquefaction features (e.g., sand blows and clastic dikes) and estimated the age of these events, using ¹⁴C dating. Two main sites of sand blows and dikes were evaluated along the Meramec River, about 9 and 15 river km northwest of its confluence with the Mississippi River (Figure. 1.3). Radiocarbon (¹⁴C) dating of charcoal above the dike indicated that the dike formed after 4340 B.C. with some uncertainty, and was reactivated during the 1811-1812 New Madrid earthquake sequence. The formation of sand dikes in the banks along Cahokia and Piasa Creeks (tributaries to the Mississippi River) were interpreted by radiocarbon dating to have developed since Middle Holocene time, or since 160 B.C. along Cahokia Creek and during Late Holocene time in Piasa Creek.

6.3.4. Previous Liquefaction Potential Mapping in the STL. A seismic hazard map of STL was compiled by Hoffman (1995). He mapped the liquefaction potential based on the presence of thick sands with a high groundwater table. These areas were defined as alluvium along rivers and creeks, terrace deposits, and valleys sloping less than 2% where surficial material was of unknown origin. Alluvium in southeastern St. Charles County was assumed to be more variable or unknown (because of the perennially high groundwater table in that area). However, this mapping did not evaluate the differences in relative liquefaction susceptibility that exist due to differences in the depositional environment, texture, and age of surficial units.

Pearce and Baldwin (2005) assessed the relative liquefaction susceptibility of Quaternary deposits in five 7.5-minute quadrangles (Columbia Bottom, Wood River, Granite City, Monks Mound, and Cahokia) in the St. Louis area. They analyzed the liquefaction susceptibility of surficial deposits on the basis of the following criteria: 1) qualitative geologic criteria, such as texture, density, and age of unconsolidated sediments, depositional environment, and depth to groundwater [this qualitative assessment is recommended by Youd and Perkins (1987)] and Hitchcock et al. (1999) in areas where reliable subsurface data is lacking), and 2) quantitative analyses based on the simplified SPT procedure where borehole data is available. Pearce and Baldwin (2005) used M 7.5 with a peak ground acceleration (PGA) of 0.10g, 0.20g, and 0.30g as their scenario earthquakes. The results of the integrated analyses suggested that the Holocene alluvial units were most susceptible to liquefaction. Late Pleistocene and Peoria loess exhibited low to very low susceptibility. Artificial fill deposits, which are highly variable and complex, were conservatively assessed as having a very high susceptibility.

6.4. DATA

To develop seismically-induced liquefaction hazard maps in STL, the physical properties of surficial soils were acquired from geotechnical data, surficial geologic mapping, and the depth to the groundwater table. These data were collected and evaluated.

6.4.1. Geotechnical Boring Data. In this study, the logs of 450 boreholes were collected from the Missouri Division of Geology and Land Survey (MoDGLS) for the Missouri side of STL and 114 borings from the Illinois State Geological Survey (ISGS) for the Illinois side of STL, shown in Figure 6.1.

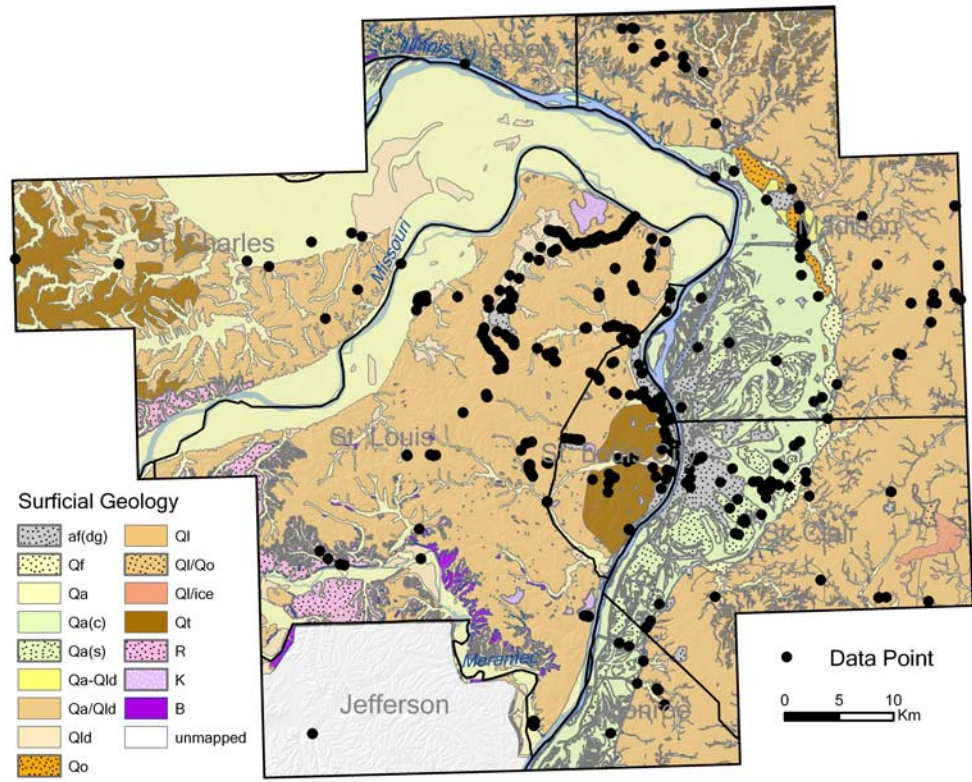


Figure 6.1. Locations of geotechnical borings used to calculate the liquefaction potential index (LPI).

These geotechnical data were compiled from borehole logs made for bridge and highway construction by the Missouri and Illinois Department of Transportation (MoDOT and IDOT) and other private geotechnical agencies (Palmer et al. 2006). These data provided the collar location coordinates, ground surface elevation, depth to groundwater, and a stratigraphic profile of each boring site. The soils sampled at each

depth interval included the following physical properties: 1) Unified Soil Classification System, 2) sample bulk density (dry and wet) (only for Missouri), 3) SPT-N blow count values, and 4) depth to groundwater at time of drilling. These borehole data were used to calculate FS and LPI values.

6.4.2. Quaternary Geologic Map. Quaternary geologic maps used in this study originated from three sources: 1) St. Charles County (Allen and Ward, 1977), 2) St. Louis City and County (Goodfield, 1965), and 3) ISGS 1:24000 scale maps. Schultz (1997) compiled data from St. Charles and St. Louis Counties into a St. Louis 30'x 60' quadrangle, which proved useful in this study. Quaternary geologic maps were also conjoined to form a GIS shapefile that described the surficial materials map of STL.

Because the geologic classification schemes employed by the Missouri and Illinois geological surveys differs across the state boundary, map units had be correlated for internal consistency. Table 6.2 presents the correlations and descriptions of mapped stratigraphic units recognized in the study area. These proposed stratigraphic correlations are based on similar interpretations of depositional environments of each correlated unit. This study used Grimley's suggestion (2007, commun.) to unify and simplify a stratigraphic unit for the liquefaction susceptibility analyses (Figure 6.1; Table 6.2). Geologic units bereft of borehole logs are defined as 'no data,' while bedrock exposures are simply noted as 'bedrock.'

Table 6.2. Surficial geologic units and map symbols used in this study.

This Study (STL)		Missouri	Illinois	Time Scale
Grimley(2007)	Genetic Unit	Schultz (1993)	ISGS	
af(dg)	Artificial fill	af	dg	Holocene
R	Residuum	R		
Qa	Alluvium	Qa	c	
Qa(c)	Alluvium(clayey facies)		c(c)	
Qa(s)	Alluvium(sandy facies)		c(s)	
Qf	Alluvial fan		c(f)	
Qa/Qld	Alluvium over lake deposits		c/e	Holocene/Pleistocene(Wisconsinan)
Qa-Qld	Alluvium or lake deposits		c(c)-e	
Ql	Loess	Qp(Peyton)	py	
Ql	Loess	Ql	pr	Pleistocene(Wisconsinan)
Qo	Outwash		h	
Qld	Lake deposits	Qtd	e	
Ql	Loess		pr/pb	Pleistocene(Wisconsinan/Illinoian)
Ql/ice	Loess over ice-contact deposits		pr/pl-h	
Ql/Qo	Loess over outwash		pr/pl	
Ql	Loess		tr	Pleistocene(Illinoian)
Qt	Till	Qt	g	
K	Karst	K		Paleozoic
B	Bedrock	B	R	

6.4.3. Depth to Groundwater. The predictive map of groundwater elevation was prepared by using cokriging with 1,069 well logs and 2,569 data points along major rivers and perennial water courses (described in Chapter 4). The corresponding depth to groundwater was determined by subtracting the cokriged groundwater elevations from the ground surface elevations, which were derived from 10 m DEMs (Figure. 6.2).

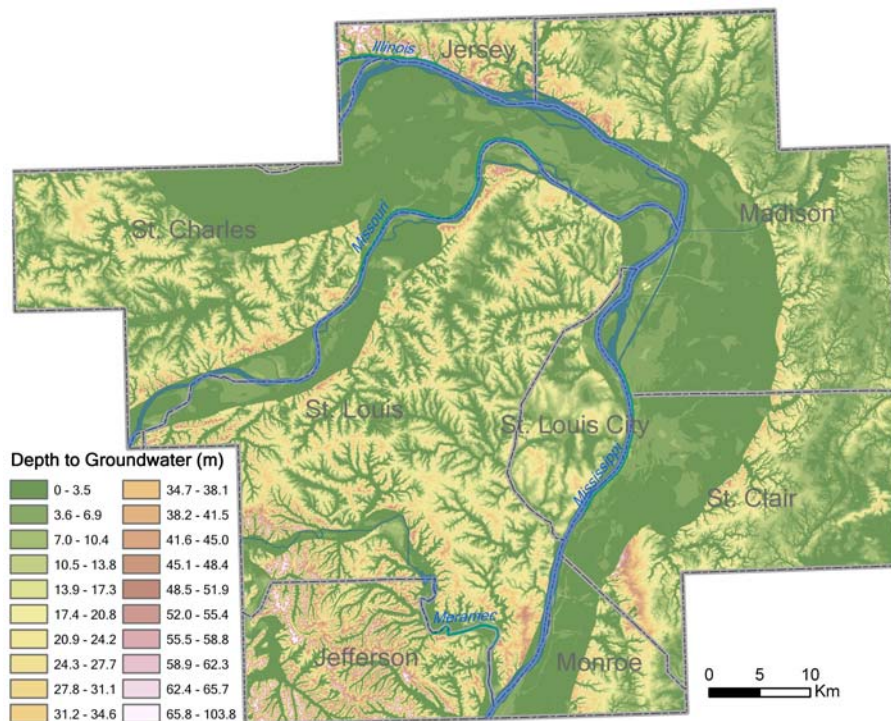


Figure 6.2. Map illustrating predicted depths to groundwater in the St. Louis Metro area. The depths were estimated by subtracting the cokriged groundwater elevations from the 10m DEM surface elevations.

6.5. RESULTS

6.5.1. Factor of Safety Calculations. A quantitative FS for the liquefaction susceptibility of the unconsolidated soil cap beneath the STL area was analyzed using the simplified procedure of Seed and Idriss (1971), using SPT N-values taken from geotechnical boring logs. The SPT N-value is an indicator of the relative density of soil, which correlates with observed resistance to liquefaction. More consolidated sediments with higher blow counts (i.e. greater density and cohesion) are generally less susceptible to liquefaction. A quantitative estimate of CRR, which is a function of the soil geotechnical properties, was calculated using a clean-sand base curve by Rauch's equation for M 7.5 quakes, given as follows:

$$CRR_{7.5} = \frac{1}{34 - (N_1)_{60}} + \frac{(N_1)_{60}}{135} + \frac{50}{[10(N_1)_{60} + 45]^2} - \frac{1}{200}$$

where, $(N_1)_{60}$ = the SPT blow count normalized to an overburden pressure of approximately 100 kpa and a hammer energy ratio, or hammer efficiency, of 60%.

$$(N_1)_{60} = NC_N C_E$$

where N is the raw SPT N-value, and $C_E = ER/60\%$ is the correction to account for rod energy (ER = the actual energy ratio of the drill rig used in percent), and C_N = the correction for effective overburden stress which is based on the following equation (Liao and Whitman, 1986; Rogers 2006):

$$C_N = \frac{100kPa}{\sqrt{\sigma'_v}} \leq 2$$

where σ'_v = the vertical effective stress.

6.5.2. Unit Weight of Soil. The overburden stress below the ground surface can be calculated as follows:

$$\sigma_v = \sum \gamma_i h_i$$

where σ_v = the overburden stress at a point in the soil, γ_i = the unit weight of soil stratum i , and h_i = the thickness of soil stratum i .

The effective overburden stress can be estimated as follows:

$$\begin{aligned} \sigma'_v &= \sigma_v - u \\ u &= \gamma_w z_w \end{aligned}$$

where σ'_v = the effective overburden stress, u = the pore water pressure at a given depth in the soil column, γ_w = the unit weight of water (9.81 kN/m³), and z_w = the depth of that point below the groundwater table.

The boring log data from ISGS (and some of that from MoDGLS) did not include the unit weights (dry and wet) of the sampled soils at each depth interval. These values are used

to calculate the effective overburden stress in the soil column. The average soil unit weights (dry and wet) from other MoDGLS boring logs and typical values for these materials (taken from Coduto, 1994) were used to calculate the overburden stress in the soil stratum (APPENDIX B).

6.5.3. Estimated Earthquake Magnitude and PGA. Three scenario earthquakes were selected for this assessment. A M 7.5 quake emanating from the New Madrid Seismic Zone (NMSZ) was chosen as the scenario event for the liquefaction analysis. The M 7.5 magnitude is that proposed by the 2002 National Seismic Hazard Map (Frankel et al., 2002). A scenario earthquake map in the New Madrid and Wabash Valley Seismic Zones by Toro and Silva (2001) indicate that PGAs of 0.10g and 0.30g can be used for soil, for a 10% and 2% probability of exceedance (PE) in 50 years, respectively. These are the same values of magnitude and peak ground acceleration used by Pearce and Baldwin (2005) for their scenario earthquakes in St. Louis. The magnitude (M) and peak ground acceleration (PGA) for the STL area were used to compute the FS required for calculation of the LPI. Computations of the FS in soil profiles were obtained for a M 7.5 with PGAs of 0.10g, 0.20g, and 0.30g.

6.5.4. LPI Computation. LPIs of individual borings were computed by integrating the FS with depth and the depth as well as thickness of the soil layer within the soil column described in each borehole log, using the above-cited equations. Some geotechnical borings were excluded from the LPI computations, if any of the following conditions were met: 1) the boring log did not penetrate the permanent groundwater table, 2) the position of the groundwater table was not noted on the log, or 3) the groundwater table was in the Paleozoic bedrock (well below the unconsolidated soils). Where bedrock was encountered at depths less than 20m, calculations were only performed on the soil units above the bedrock. This study used a discredited form by Luna and Frost (1998) to find the LPI, given as:

$$LPI = \sum_{i=1}^{NL} (10 - 0.5z_i) F_i H_i$$

$$F_i = 1 - FS_i \quad \text{for } FS_i \leq 1.0$$

$$F_i = 0 \quad \text{for } FS_i > 1.0$$

where H_i = the thickness of the discredited layer, NL = the number of discredited number, F_i = severity for layer i , FS_i = factor of safety for layer i , and z = the depth (m). This study used the LPI categories established by Iwasaki et al (1978 and 1982) and Luna and Frost (1998; Table 6.1) to assess liquefaction severity.

6.6. DISCUSSION

The liquefaction potential index (LPI) was calculated for each borehole. Each data point represents a one-dimensional analysis at the sampled sites (borehole location) to assess liquefaction potential. The locations of liquefaction potential index (LPI) test holes were grouped by surficial geologic unit. LPI calculations within the mapped surficial units exhibited considerable variability of results (Table 6.3; Figure 6.3). It was difficult to assess a specific value for liquefaction severity due to the heterogeneous nature of the mapped surficial units, reflected in the wide array of LPI values. To understand why the liquefaction severities vary so much within similar surficial geologic units, this study proposed a method of combining susceptibility of the respective surficial geologic units, LPI values, and depth to groundwater (DTW) values using a statistical computation.

Table 6.3. Liquefaction Potential Index (LPI) values and corresponding depths to groundwater within mapped surficial geologic units.

Geologic Symbol	Depth to groundwater (m)	LPI values for a M7.5 with 0.10, 0.20 and 0.30 PGAs		
	Range (Mean +/- Std)	0.10 PGA Range (Mean +/- Std)	0.20 PGA Range (Mean +/- Std)	0.30 PGA Range (Mean +/- Std)
af(dg)	10.6~11.3 (5.3 +/- 2.6)	0~34.4 (2.2 +/- 6.5)	0~64.8 (11.9 +/- 14)	0~75 (19 +/- 16.7)
Qa	0~19.5 (5.4 +/- 3.1)	0~25 (2.5 +/- 4.7)	0~58.8 (14.2 +/- 12.4)	0~71.1 (20.3 +/- 15)
Qa(c)	1.6~8.2 (4 +/- 1.7)	0~21.4 (3.1 +/- 5.5)	0~48.2 (20.8 +/- 14)	4.9~58.1 (33.2 +/- 14)
Qa(s)	2.7~7 (4.7 +/- 1.4)	0~4.1 (0.9 +/- 1.5)	4.7~35.3 (19.3 +/- 10.5)	13.7~46.7 (13.7 +/- 10.9)
Qf	0.7~6.4 (4.1 +/- 2)	0~24.1 (3.9 +/- 8.9)	0.9~56.7 (18.4 +/- 19)	5.5~69.7 (28.6 +/- 22.2)
Qo	1.1~85 (4.7 +/- 3.2)	0 (0)	0~5.4 (1.4 +/- 2.3)	0~22.9 (9.6 +/- 12)
Ql	0~36.9 (5.5 +/- 4.1)	0~27.6 (1.4 +/- 3.8)	0~57.8 (8.6 +/- 10.9)	0~67.9 (13.3 +/- 14.1)
Qld	0~12.2 (4.8 +/- 2.8)	0~27.6 (3.3 +/- 6.1)	0~56.6 (15.8 +/- 14.1)	0~66.3 (21.9 +/- 16.9)
Qt	0~11.4 (4.9 +/- 2.7)	0~3.9 (0.4 +/- 1.1)	0~28.3 (9.6 +/- 9.3)	0~46.4 (16 +/- 14.3)
K	1.7~10.1 (5.4 +/- 2.5)	0~20.3 (3.3 +/- 7)	1.8~49.8 (15.2 +/- 6.3)	4.1~60.2 (23.6 +/- 17.9)

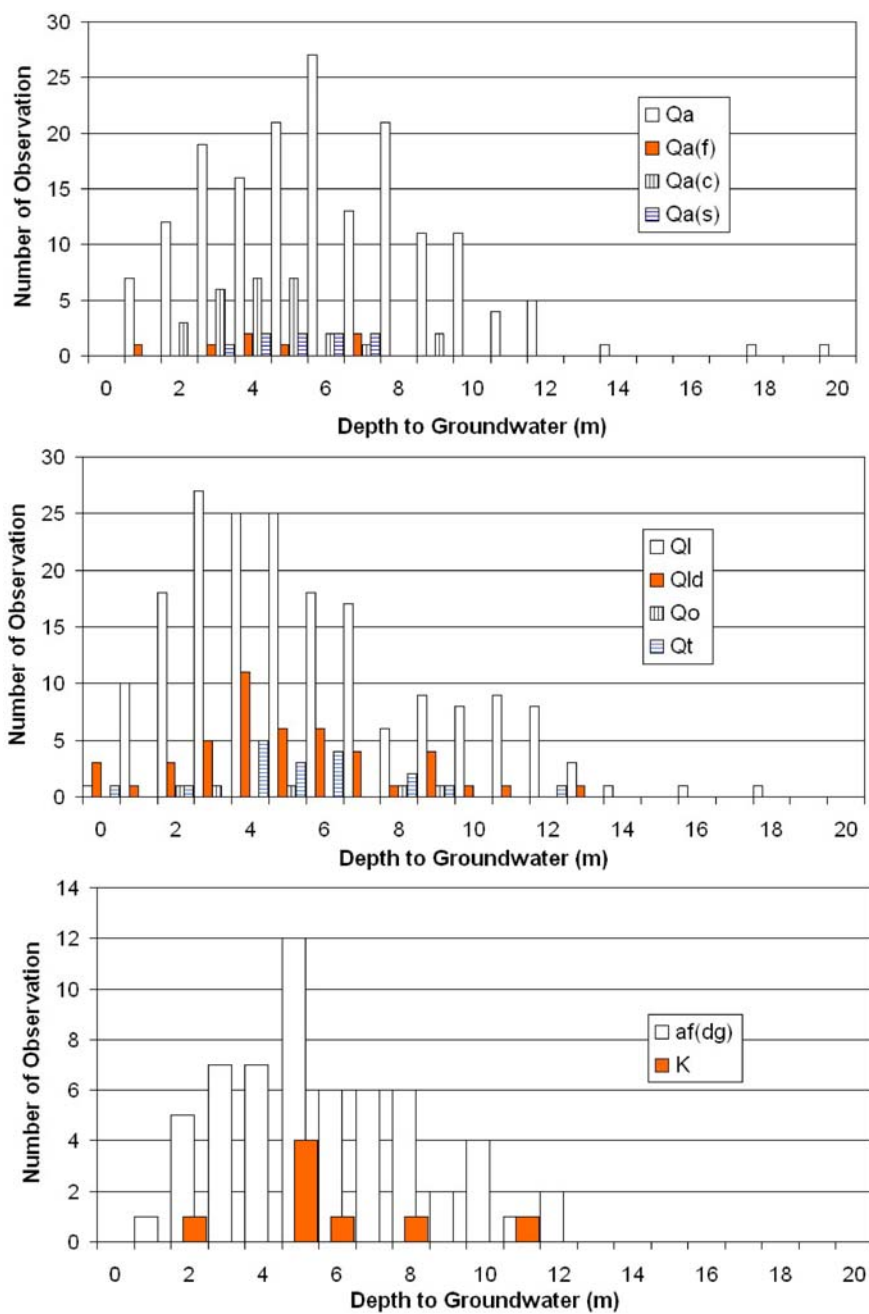


Figure 6.3. The distribution of depths to groundwater in mapped surficial geologic units.

This study sought to establish a fundamental relationship between LPI values, depth to groundwater, and surficial geologic units. This was desirable so that predictions could be made over a large unsampled area. Some fundamental assumptions employed in this study included the following criteria:

1) Each mapped surficial geologic unit was assumed to be spatially homogeneous and thus, likely to possess similar physical properties, such as: thickness, unit weight, and SPT N-value of soil.

2) Depth-to-groundwater (DTW) values vary linearly within a mapped surficial geologic units.

These assumptions have uncertainties associated with the thickness and physical properties of the mapped surficial units, and other factors (e.g., sedimentation process, age of deposit, grain-size distribution, and proximity of a free face), as well as DTW, values are important factors that tend to control liquefaction susceptibility.

The proposed procedure for interpolating LPI in terms of DTW and assessing liquefaction severity consists of the following steps:

1) establishing the fundamental relationship between LPI and DTW,

2) grouping LPIs into corresponding surficial geologic units and setting up each statistical equation (linear regression) between LPI and DTW for those units, in a given earthquake scenario,

3) converting the existing cokriging map of DTW into a LPI map, and applying each equation obtained from step 2),

4) compiling LPI maps into a single LPI map, and

5) assessing regional liquefaction severity by evaluating LPI values in three scenario earthquakes of M7.5 with 0.10g, 0.20g, and 0.30g PGA, according to the categories proposed by Iwasaki et al (1978 and 1982). A detailed explanation of each step is provided below.

Step 1) Liquefaction only occurs in saturated soils, so the depth to groundwater (either free or perched) controls liquefaction susceptibility. Liquefaction susceptibility decreases with increasing groundwater depth. The effects of liquefaction are most commonly observed at sites where groundwater is within a few meters of the ground surface).

The typical geotechnical boring collected subsurface sampling at depth intervals of 0.76m (2.5ft), with their respective SPT blow counts (N_1). (N_1)₆₀ values were calculated for these sampling intervals, the depth-to-groundwater was noted, and each sampling horizon was then evaluated for its respective LPI, using the procedures outlined above. This involved about 30 calculations for each 20m deep borehole, as show in Figure 6.4. The Factor of Safety (FS) and the square root of the liquefaction potential index ($LPI^{1/2}$) were plotted against depth-to-groundwater (DTW) to see if a fundamental relationship emerged. These relationships could be useful in predicting the LPI in unsampled locations within the same mapped surficial geologic units. An example of the fundamental relationships between FS to DTW and $LPI^{1/2}$ to DTW are presented in Figure 6.4. Once these relationships are established, the DTW can be used to estimate the FS and $LPI^{1/2}$. The fundamental relationships showed in Figure 6.4 indicate that the FS of the soil layer at a particular depth is linearly proportional to increasing DTW (deeper groundwater).

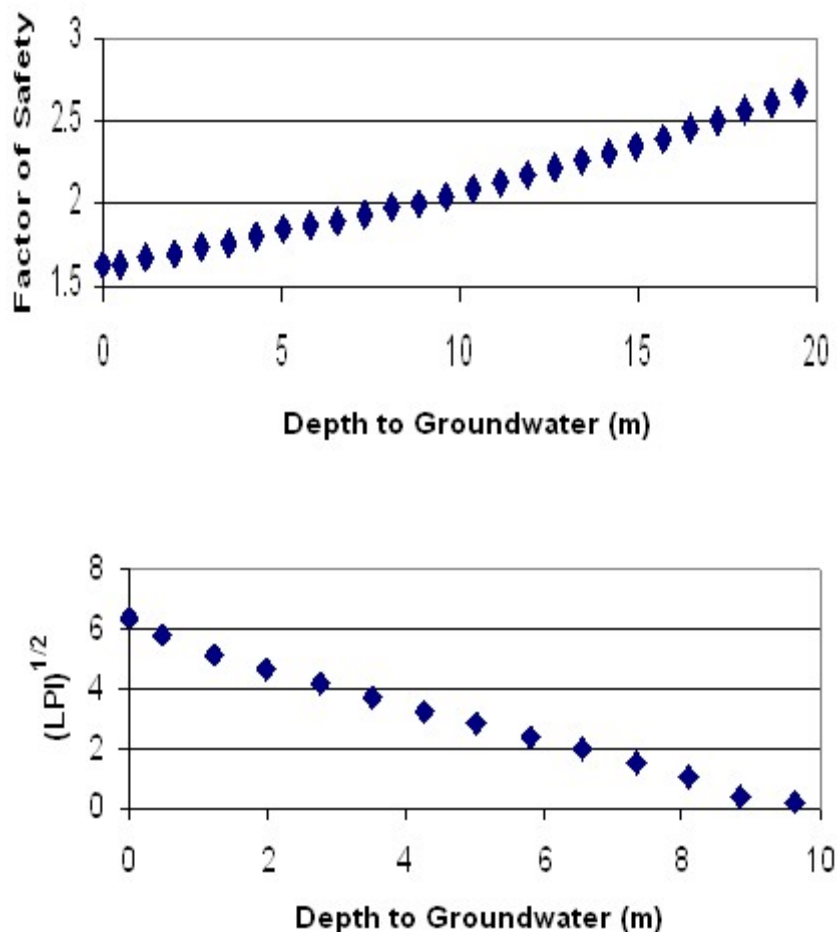


Figure 6.4. Fundamental relationships derived from the equations for factor of safety (FS) against liquefaction and liquefaction potential index (LPI). A) Data plotted on the upper graph suggests that FS is proportional to groundwater depth. B) LPI data plotted on the lower graph suggests that $(LPI)^{1/2}$ is inversely proportional to the depth of the groundwater table. These relationships are useful in predicting the LPI in unsampled locations within the same mapped surficial geologic units.

LPI appears to be inversely proportional to the FS and the depth of the groundwater table (zone of saturation). Increasing DTW increases the FS of all soil layers below the water table, and decreases the LPI value for the whole soil column (from the ground surface to 20m deep). Although it is difficult to obtain a precise linear correlation, these graphs show that the DTW has a fairly linear relationship with the factor of safety and the square root of the LPI (Figure. 6.4B).

The fundamental equation derived from the relationship between LPI and DTW shown on the preceding graphs can be described as;

$$(LPI)^{1/2} = a \cdot DTW + b$$

where LPI = liquefaction potential index, DTW = depth to groundwater, a = slope, and b = intercept.

Step 2) LPI locations were grouped into their respective surficial geologic units. LPIs and corresponding DTW values were then plotted for each mapped unit in the scenario M7.5 quake with 0.10g, 0.20g, and 0.30g PGA. Data outliers were removed for clarity and a better fit. The plots allowed an equation of linear regression to describe the expected behavior of each geologic unit. These were obtained from these plots for each earthquake scenario (Figure. 6.5; Table 6.4). Using these equations, the LPI values are estimated for assumed DTW.

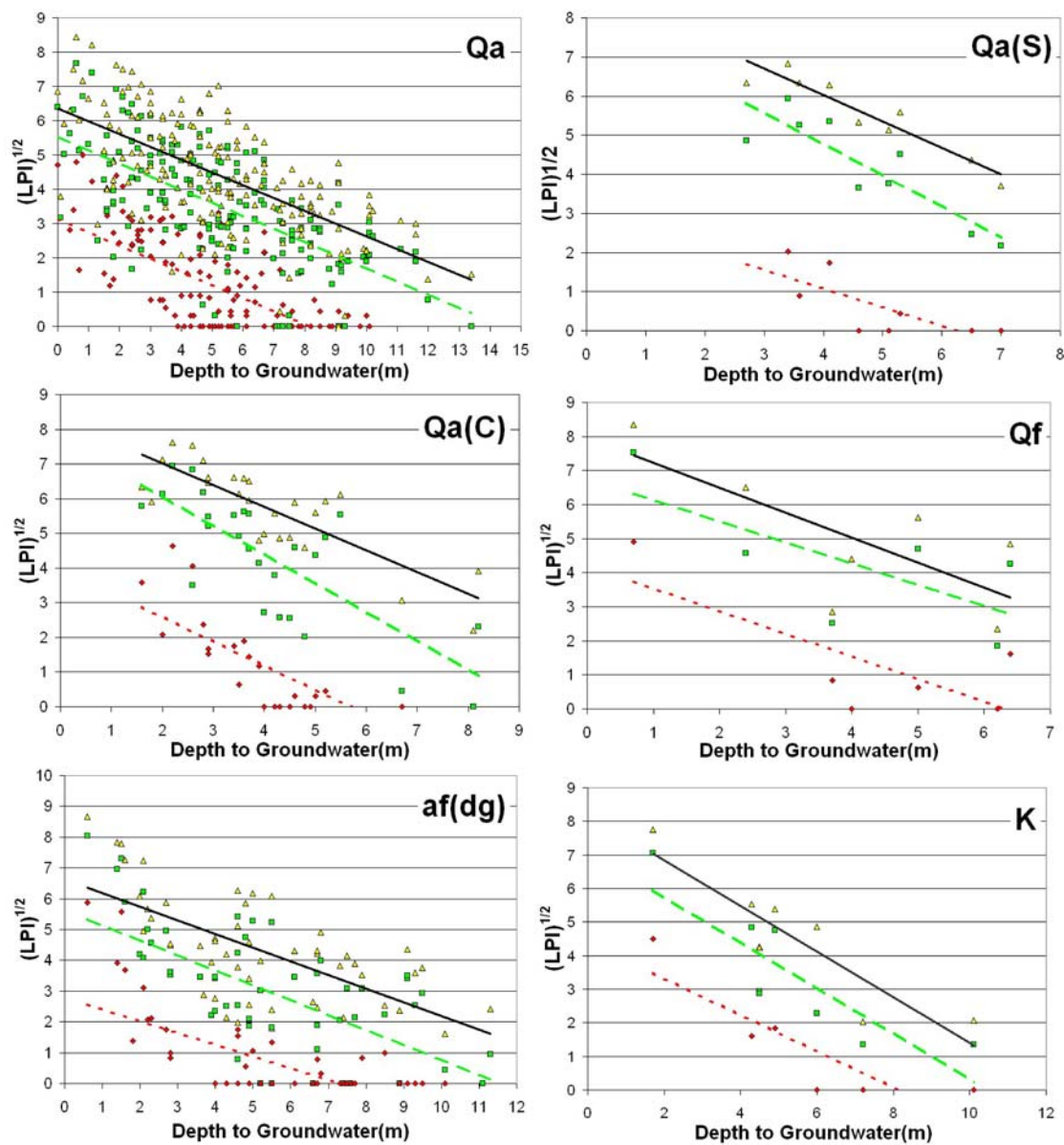


Figure 6.5. Plots showing liquefaction potential index (LPI) versus depth to groundwater and the best fits for each earthquake scenario.

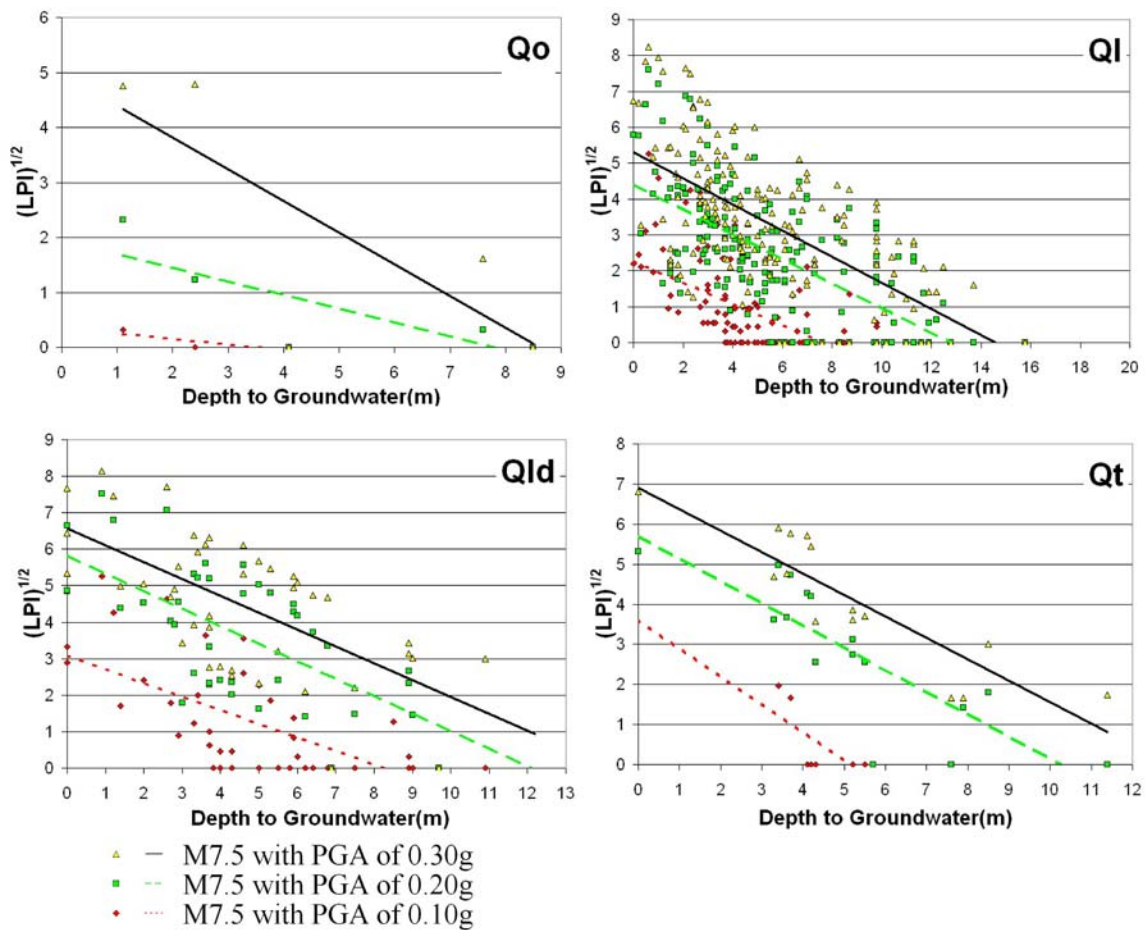


Figure 6.5. Continued

Table 6.4. Regression of liquefaction potential index (LPI) versus depth to groundwater (DTW) of mapped surficial geologic units.

Geologic Unit	count	0.10g PGA				0.20g PGA				0.30g PGA			
		Slope	Intercept	R ²	DTW	Slope	Intercept	R ²	DTW	Slope	Intercept	R ²	DTW
af(dg)	59	-0.38	2.81	0.43	0.00	-0.49	5.64	0.40	3.63	-0.44	6.63	0.45	6.21
Qa	195	-0.38	3.15	0.50	0.00	-0.38	5.54	0.42	4.34	-0.37	6.35	0.42	6.64
Qa(c)	28	-0.70	4.01	0.56	0.19	-0.84	7.74	0.58	4.63	-0.63	8.28	0.68	7.02
Qa(s)	9	-0.48	3.01	0.56	-1.81	-0.81	8.01	0.78	5.13	-0.68	8.73	0.88	7.18
Qf	7	-0.67	4.22	0.57	0.52	-0.62	6.77	0.49	4.65	-0.73	7.96	0.52	5.58
Qo	5	-0.10	0.36	0.68	-35.10	-0.25	1.96	0.65	0.00	-0.58	4.96	0.59	1.89
Ql	188	-0.30	2.28	0.35	-5.37	-0.34	4.42	0.40	1.59	-0.36	5.30	0.40	3.92
Qld	47	-0.37	3.09	0.43	-2.10	-0.48	5.84	0.42	4.07	-0.46	6.57	0.41	5.85
Qt	18	-0.70	3.61	0.51	-0.37	-0.56	5.72	0.69	3.31	-0.53	6.89	0.78	5.67
K	8	-0.49	3.85	0.58	-0.04	-0.68	7.11	0.72	4.74	-0.68	8.19	0.79	6.36
Qa/Qld	n.a												
Qa-Qld	n.a												
Ql/ice	n.a												
Ql/Qo	n.a												
R	n.a												
B	n.a												

For example, the LPI value of sandy alluvium is expected to be about 15.7, 3.7, and 0 when the DTW is 5m, 7.5m, and 10m, respectively, for the scenario M7.5 with 0.20g PGA. The threshold DTW required to initiate severe liquefaction (LPI>15) was also computed based on these equations. Given the same conditions of DTW and scenario earthquake (i.g., DTW =5m, and M7.5 with 0.20g PGA), Holocene sandy alluvium has the highest LPI value (=15.8), whereas Pleistocene glacial deposits, such as outwash (=0.7), and till (= 8.6), sediments, and Pleistocene loess deposits (=7.3) have the lowest LPI values. These results indicate that sandy alluvium consisting of relatively unconsolidated sediments, tend to exhibit lower SPT-N values and/or lower bulk density

than other deposits. On the other hand, Pleistocene glacial deposits and Pleistocene loess deposits are composed of less liquefiable layers, because these deposits are older and more consolidated (having a higher SPT-N value and/or higher density) than Holocene alluvium deposits.

6.6.1. Resultant Map of Liquefaction Potential. Steps 3) and 4) A cokriged DTW map for a single geologic unit was clipped and converted into an LPI map, by applying each equation obtained above. Converted LPI maps were compiled into a single LPI map for the study area, employing ArcGIS.

Step 5) The regional liquefaction severities determined from the LPI values were evaluated based on the categories proposed by Iwasaki et al (1978 and 1982). The resultant maps in the scenario M7.5 with 0.10g, 0.20g, and 0.30g PGA are shown in Figures 6.6. The zones exhibiting severe liquefaction (LPI >15) are most likely to occur are summarized below.

At M7.5 with a PGA of 0.10g: 1) alluvial fan deposits where the spring zone lies along the lower edge of the fan with a DTW shallower than 0.5m, and, 2) the confluence region of Mississippi and Illinois rivers (Figure. 6.6A)

At M7.5 with a PGA of 0.20g: 1) alluvial fan deposits where spring zones lie along the lower edge of the fan with the DTW shallower than 4.7m, 2) alluvium along major rivers and streams, where the DTW is shallower than 4.4m, and, 3) clayey alluvium (Cahokia) and sandy alluvium (Cahokia) forming oxbows where the DTW is less than 4.6m and 5.1m, respectively (Figure. 6.6B),

At M7.5 with a PGA of 0.30g: most alluvial valleys along major rivers and stream channels, except clayey alluvium and areas underlain by artificial fill, where DTW is deeper than 7m and 6.3m, respectively (Figure. 6.6C). The high fines content of units, such as clayey alluvium, or alluvial fans, makes it relatively resistant to liquefaction, or even interspersed lenses of coarser grained textures, due to its depositional environment. Because of the high fines content (cohesion), clayey alluvium or alluvial fan deposits will exhibit less liquefaction potential than predicted using FS and LPI calculations.

Additionally, the liquefaction potential of artificial fill is the most difficult to assess because of their highly variable composition, thickness, and underlying surficial geologic units. Youd and Perkins (1978) qualitatively assessed uncompacted fills as

having high liquefaction susceptibility, although this decreases markedly if compacted as engineered fill, on worldwide earthquake reports.

(A)

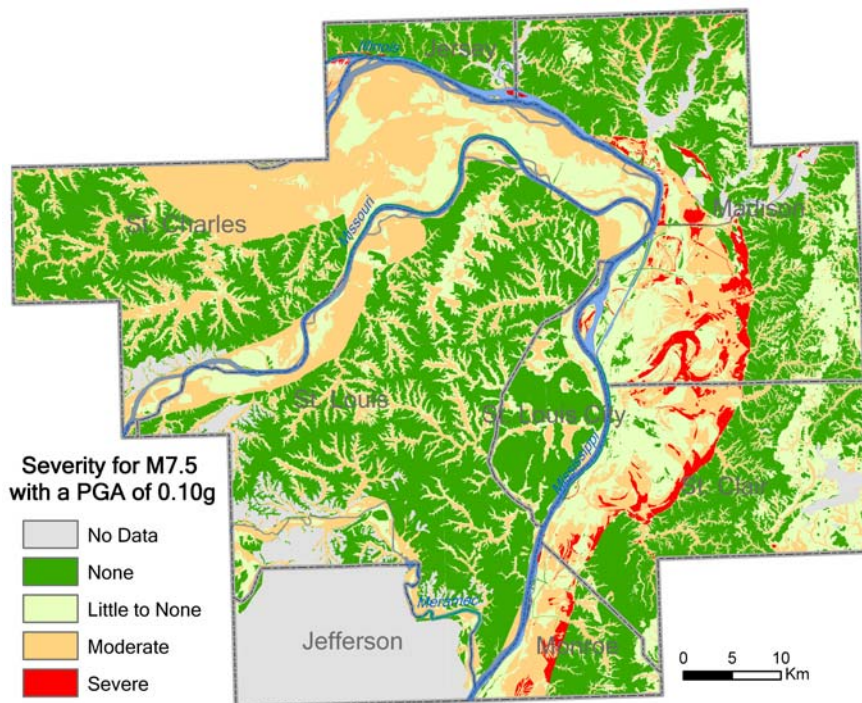
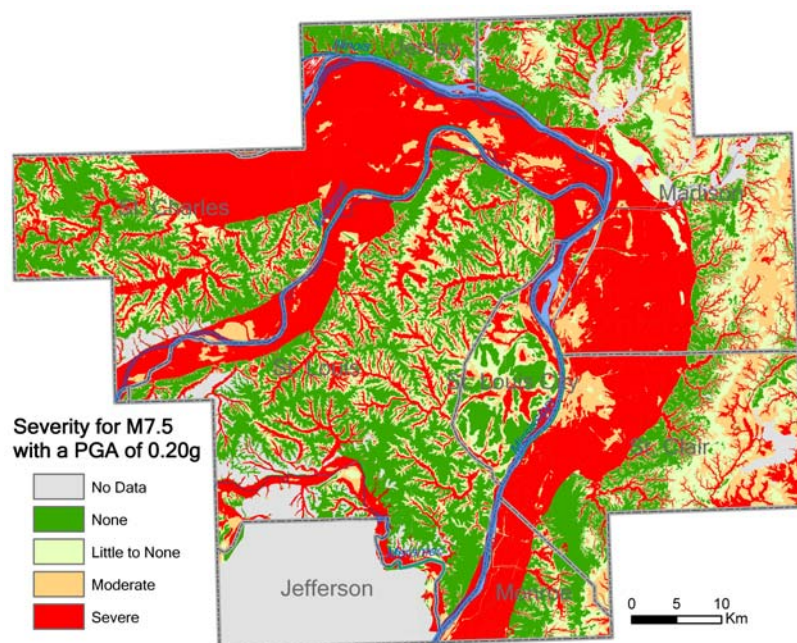


Figure 6.6. Liquefaction potential maps inferred from LPI. A) Liquefaction potential for earthquake scenario for a moment magnitude (M)7.5 with 0.10 peak ground acceleration (PGA). B) Liquefaction potential for earthquake scenario for a M7.5 with 0.20 PGA. C) Liquefaction potential for earthquake scenario for a M7.5 with 0.30 PGA.

(B)



(C)

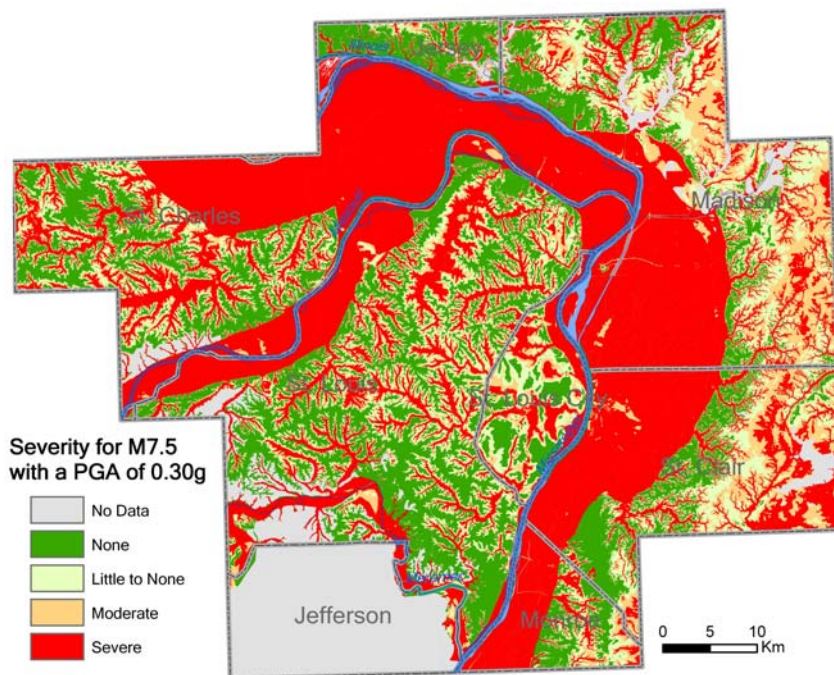


Figure 6.6. Continued

6.6.2. Uncertainty. The proposed method of estimating liquefaction potential implies that the estimation of LPI values depends solely on the depth-to-groundwater interpolated from well log data using cokriging techniques, and, therefore, is sensitive to small changes in the groundwater level. This uncertainty can be quantified by deriving the cokriging errors for each location on the ground water surface and are generally greatest in areas of sparse data. The uncertainty in using DTW to estimate LPI is contoured with equal interval from high to low in Figure 6.7. The most crucial aspect of the proposed method is the construction of the fundamental relationship plots illustrating the statistical trends for the entire data set, meaning that it may estimate LPI values differently from true values at sampled sites. This method implies that LPI values and the corresponding potential for liquefaction severity at the sites with the same conditions of geologic setting and DTW would be the same. It can be concluded, therefore, that this method might be inadequate for evaluating local anomalies.

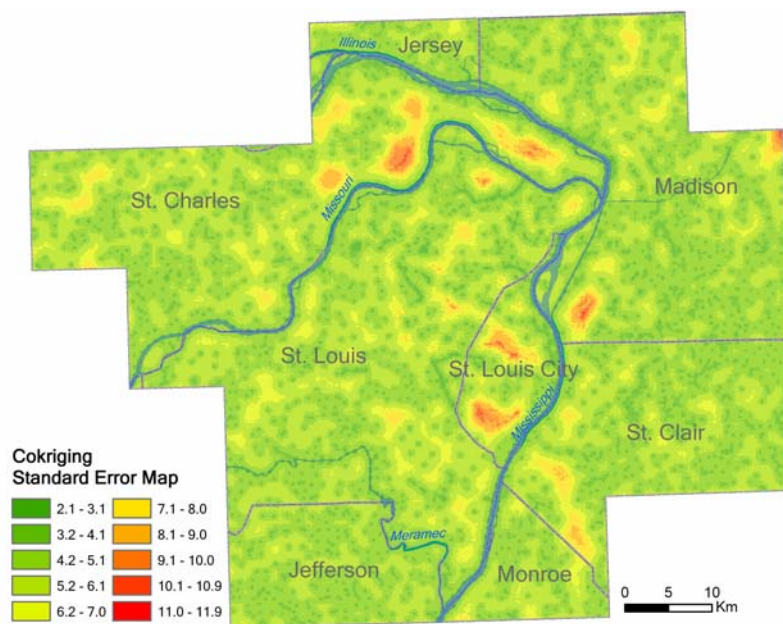


Figure 6.7. Map illustrating the standard error of liquefaction potential, based on cokriged depth to groundwater table. The region with the larger error value of cokriging produces less reliable values for liquefaction potential because the regional LPIs were computed based on the cokriged depth to groundwater map.

7. CONCLUSIONS

The purpose of this study was to construct seven data layers in a Virtual Geotechnical Database (VGDB) in a Geographic Information Systems for the St. Louis metropolitan area of Missouri and Illinois, encompassing a land area of 4,432 km². This process involved combining vast quantities of dissimilar geologic, hydrologic, geophysical, and topographic data from a number of public agencies and private sector sources that was stored in dissimilar analog and electronic formats. All of these data were then georeferenced and entered into the VGDB. The study also manipulated data in the VGDB to construct liquefaction potential maps of the St Louis Metropolitan area for three earthquake scenarios.

The data sources included 17 publications addressing surficial geologic mapping, which were adjusted, manipulated, georeferenced and compiled into a single composite map in a GIS format. In order to correlate and conjoin so much dissimilar data, many difficult problems had to be solved using innovative techniques developed by the author, as well as other scientists working on similar problems in other parts of the USA. These included developing practical techniques for joining maps of dissimilar age and scales, with different stratigraphic nomenclature across the Missouri-Illinois border in the St. Louis Metropolitan area. For instance, the State of Missouri has traditionally employed depositional environment mapping at scales above 1:62,500, whereas the State of Illinois has used formational mapping of geologic units at a much larger scale of 1:24,000.

Five sources of data were compiled as input for constructing a seamless map predicting the thickness of wind blown loess that mantles the elevated uplands ringing the St. Louis Metro area. The respective thicknesses of three mapped loessal units were combined into one map unit for this product. These included the Peoria and Roxana Silts and the older Loveland Loess. In St. Charles and Jefferson Counties in Missouri loess deposits were mapped at a much smaller scale (1:2,500,000) as compared to the rest of the St. Louis Metro area, where loess was mapped at scales ranging from 1:24,000 to 1:100,000. These disparities in scale lead to increased uncertainties in the predicted thicknesses in areas like St. Charles and Jefferson Counties.

Five bedrock geology maps prepared by the Missouri and Illinois state geological surveys and the U.S Geological Survey were analyzed and integrated into a seamless bedrock geologic map in a GIS format that public agencies, researchers, and private sector businesses can manipulate. Numerous problems with edge-matching between dissimilar maps (and scales of mapping) had to be solved. A number of innovative approaches were attempted before settling on a technique that overlaid USGS 1:24,000 DRGs on the 1:100,000 DLG base map, which allowed geologic contacts to be shifted slightly on the larger scale (24K) map, so they would have smooth connections with those shown on the smaller scale (100K) map.

7,211 borehole records were collected from the Missouri and Illinois geological surveys for their respective portions of the study area, east and west of the Mississippi River. These data were digitized or converted to a compatible georeferenced format and input into the St. Louis Metro area VGDB. Some of these boring logs were discarded because they contained insufficient metadata, such as borehole location and/or elevation, or same locations as more recent and more reliable borings logs, which were input into the VGDB. The subsurface data in the VGDB were used for interpolating the groundwater table and depths to bedrock, and calculating the liquefaction potential index.

The unconsolidated surficial sediments blanketing the St. Louis study area were classified according to the NEHRP soil profile types, grouping 117 shear wave velocity (V_s) data with the corresponding surficial geologic units and determining the arithmetic mean V_s^{30} value for each map unit. The results indicate that most of the surficial deposits in St. Charles County exhibited higher V_s^{30} values than those in other parts of the St. Louis study area. This was an expected result insofar as St. Charles County is a distinctly different geomorphic province, north of the lower Missouri River. Characteristic V_s profiles were constructed for the dominant surficial geologic units, wherever sufficient V_s data was collected. These characteristic profiles are crucial to modeling seismic site response and liquefaction potential over any broad area, in excess of a few square kilometers.

Groundwater levels were interpolated using three methods: the least squares approach (power regression model), ordinary kriging, and cokriging. The least squares approach is the simplest method, which averages the observed relationship between the

elevations of the permanent groundwater table and the ground surface. The results garnered from cross validation of the kriging and cokriging predictions indicate that cokriging provided the least error between the measured and estimated values, as opposed to ordinary kriging.

The study area was divided into its respective geomorphic provinces because data collected in these areas tends to converge much better than data taken from across the entire study area. These local provinces included alluvial filled flood plains and loess and till covered uplands, east and west of the Mississippi River. Subsurface data recording depths to bedrock were soon observed to exhibit noticeable patterns, limited to each of these provinces. The map showing estimated depths-to-bedrock predicted by kriging and a companion map showing elevations of the bedrock-soil cap interface was prepared using cokriging techniques. A comparison was made between the actual and interpolated depth-to-bedrock values in the elevated uplands and river bluffs. The map produced using cokriging underestimates the elevations of the buried bedrock interface, whereas the depths-to-bedrock estimated by kriging appear to be more reliable (when compared to the actual borehole data). This result implies that, for the more rugged terrain, like the loess covered uplands, the method for estimating bedrock depth provides a better prediction of the bedrock interface than the methods used to predict bedrock elevation.

Values of the liquefaction potential index (LPI) were calculated for 564 geotechnical boreholes across the St. Louis Metropolitan area. The LPI values and the corresponding depths-to-groundwater (DTW) varied considerably within the mapped surficial geologic (stratigraphic) units. It is assumed in this study that depth-to-groundwater values exert the strongest influence on the calculated LPI values, given the body of available subsurface data. After establishing the relationship between LPI and DTW within mapped surficial geologic units, LPI values could be estimated in unsampled areas from the predicted DTW values. The liquefaction severities assessed from the estimated LPI values suggest that the alluvial filled valleys (where the DTW is shallow and the soils have low SPT values), are most susceptible to severe liquefaction in the scenario earthquakes of M7.5 with PGA values between 0.10 to 0.30g.

APPENDIX A. SHEAR WAVE VELOCITY

Table A. The mean values of shear wave velocity (V_s^{30}) in the upper 30m and the measuring agencies.

ID	Quadrangle (1:24,000 scale)	State	Vs30 (m/s)	Site Class	Measuring Agency	Provider
Artificial fill						
1	Cahokia	Missouri	295	D	UMR	D. Hoffman
13	Granite City	Missouri	239	D	UMR	D. Hoffman
14	Cahokia	Missouri	396	C	UMR	D. Hoffman
30	Clayton	Missouri	293	D	UMR	D. Hoffman
33	Florissant	Missouri	179	E	UMR	D. Hoffman
53	Monks Mound	Illinois	159	E	UMR	D. Hoffman
55	Granite City	Illinois	231	D	UMR	D. Hoffman
58	Granite City	Illinois	275	D	UMR	D. Hoffman
74	Monks Mound	Illinois	232	D	UMR	D. Hoffman
75	Cahokia	Illinois	246	D	UMR	D. Hoffman
76	Cahokia	Illinois	232	D	UMR	D. Hoffman
80	Cahokia	Illinois	243	D	UMR	D. Hoffman
82	Clayton	Illinois	240	D	UMR	D. Hoffman
125	Granite City	Missouri	620	C	USGS	R. Williams
	Average		277	D		
Alluvium in upland in St.Charles County						
86	Wentzville	Missouri	436	C	UMR	D. Hoffman
88	Wentzville	Missouri	n.a		UMR	D. Hoffman
90	Wentzville	Missouri	454	C	UMR	D. Hoffman
107	Wentzville	Missouri	409	C	UMR	D. Hoffman
	Average		433	C		
Alluvium in upland in St. Louis County & City						
6	Granite City	Missouri	327	D	UMR	D. Hoffman
8	Granite City	Missouri	258	D	UMR	D. Hoffman
9	Granite City	Missouri	302	D	UMR	D. Hoffman
21	Webster Groves	Missouri	240	D	UMR	D. Hoffman
22	Webster Groves	Missouri	456	C	UMR	D. Hoffman
24	Webster Groves	Missouri	330	D	UMR	D. Hoffman
	Average		319	D		
Alluvium along major rivers						

Table A. (Continued)

12	Granite City	Missouri	235	D	UMR	D. Hoffman
68	Columbia Bottom	Missouri	221	D	UMR	D. Hoffman
69	Columbia Bottom	Missouri	209	D	UMR	D. Hoffman
70	Columbia Bottom	Missouri	192	D	UMR	D. Hoffman
71	Columbia Bottom	Missouri	259	D	UMR	D. Hoffman
72	Columbia Bottom	Missouri	254	D	UMR	D. Hoffman
115	Grafton	Missouri	200	D	USGS	R. Williams
118	St. Charles	Missouri	250	D	USGS	R. Williams
120	Weldon Spring	Missouri	235	D	USGS	R. Williams
121	Chesterfield	Missouri	225	D	USGS	R. Williams
	Average		228	D		
Cahokia fan						
46	Monks Mound	Illinois	254	D	UMR	D. Hoffman
78	Cahokia	Illinois	137	E	UMR	D. Hoffman
	Average		195	D to E		
Cahokia clayey facies						
47	Monks Mound	Illinois	194	D	UMR	D. Hoffman
52	Monks Mound	Illinois	200	D	UMR	D. Hoffman
56	Granite City	Illinois	255	D	UMR	D. Hoffman
57	Granite City	Illinois	209	D	UMR	D. Hoffman
59	Granite City	Illinois	233	D	UMR	D. Hoffman
60	Granite City	Illinois	234	D	UMR	D. Hoffman
73	Columbia Bottom	Illinois	228	D	UMR	D. Hoffman
83	Granite City	Illinois	236	D	UMR	D. Hoffman
84	Cahokia	Illinois	221	D	UMR	D. Hoffman
111	Monk Mound	Illinois	304	D	ISGS	R. Bauer
119	Monk Mound	Illinois	210	D	USGS	R. Williams
	Average		228	D		
Cahokia sandy facies						
48	Monks Mound	Illinois	213	D	UMR	D. Hoffman
49	Monks Mound	Illinois	197	D	UMR	D. Hoffman
50	Monks Mound	Illinois	199	D	UMR	D. Hoffman
51	Monks Mound	Illinois	224	D	UMR	D. Hoffman
54	Monks Mound	Illinois	219	D	UMR	D. Hoffman

Table A. (Continued)

61	Granite City	Illinois	262	D	UMR	D. Hoffman
79	Cahokia	Illinois	221	D	UMR	D. Hoffman
109	Monk Mound	Illinois	n.a		ISGS	R. Bauer
110	Monk Mound	Illinois	n.a		ISGS	R. Bauer
	Average		226	D		
Terrace or lake deposits in St. Louis County & City						
2	Granite City	Missouri	615	C	UMR	D. Hoffman
3	Granite City	Missouri	350	D	UMR	D. Hoffman
36	Clayton	Missouri	n.a		UMR	D. Hoffman
67	Columbia Bottom	Missouri	347	D	UMR	D. Hoffman
114	Oak Ville	Missouri	200	D	USGS	R. Williams
116	Kirk Wood	Missouri	290	D	USGS	R. Williams
	Average		360	C to D		
Loess in St. Charles County						
87	Wentzville	Missouri	601	C	UMR	D. Hoffman
95	Wentzville	Missouri	631	C	UMR	D. Hoffman
96	Wentzville	Missouri	n.a		UMR	D. Hoffman
97	Wentzville	Missouri	n.a		UMR	D. Hoffman
98	Wentzville	Missouri	410	C	UMR	D. Hoffman
99	Wentzville	Missouri	n.a		UMR	D. Hoffman
108	Wentzville	Missouri	1123	B	UMR	D. Hoffman
128	O' Fallon	Missouri	785	B	USGS	R. Williams
129	St. Charles	Missouri	740	C	USGS	R. Williams
	Average		715	C		
Loess in St. Louis County & City						
5	Clayton	Missouri	416	C	UMR	D. Hoffman
10	Granite City	Missouri	295	D	UMR	D. Hoffman
11	Granite City	Missouri	182	D	UMR	D. Hoffman
19	Webster Groves	Missouri	521	C	UMR	D. Hoffman
20	Webster Groves	Missouri	334	D	UMR	D. Hoffman
23	Webster Groves	Missouri	498	C	UMR	D. Hoffman
28	Webster Groves	Missouri	390	C	UMR	D. Hoffman
29	Clayton	Missouri	419	C	UMR	D. Hoffman
31	Clayton	Missouri	363	C	UMR	D. Hoffman

Table A. (Continued)

32	Clayton	Missouri	406	C	UMR	D. Hoffman
34	Clayton	Missouri	321	D	UMR	D. Hoffman
35	Clayton	Missouri	346	D	UMR	D. Hoffman
37	Clayton	Missouri	470	C	UMR	D. Hoffman
38	Clayton	Missouri	335	D	UMR	D. Hoffman
39	Clayton	Missouri	368	C	UMR	D. Hoffman
40	Clayton	Missouri	315	D	UMR	D. Hoffman
41	Clayton	Missouri	285	D	UMR	D. Hoffman
42	Clayton	Missouri	n.a		UMR	D. Hoffman
62	Columbia Bottom	Missouri	275	D	UMR	D. Hoffman
63	Columbia Bottom	Missouri	307	D	UMR	D. Hoffman
64	Columbia Bottom	Missouri	259	D	UMR	D. Hoffman
65	Columbia Bottom	Missouri	244	D	UMR	D. Hoffman
66	Columbia Bottom	Missouri	298	D	UMR	D. Hoffman
124	Granite City	Missouri	460	C	USGS	R. Williams
127	Chesterfield	Missouri	720	C	USGS	R. Williams
	Average		368	C to D		
Loess in Illinois						
44	Monks Mound	Illinois	249	D	UMR	D. Hoffman
45	Monks Mound	Illinois	201	D	UMR	D. Hoffman
77	Cahokia	Illinois	271	D	UMR	D. Hoffman
81	Cahokia	Illinois	386	C	UMR	D. Hoffman
117	Monk Mound	Illinois	245	D	USGS	R. Williams
	Average		270	D		
Till in St. Charles County						
85	Wentzville	Missouri	397	C	UMR	D. Hoffman
89	Wentzville	Missouri	384	C	UMR	D. Hoffman
91	Wentzville	Missouri	840	B	UMR	D. Hoffman
92	Wentzville	Missouri	406	C	UMR	D. Hoffman
93	Wentzville	Missouri	555	C	UMR	D. Hoffman
94	Wentzville	Missouri	n.a		UMR	D. Hoffman
100	Wentzville	Missouri	603	C	UMR	D. Hoffman
101	Wentzville	Missouri	387	C	UMR	D. Hoffman
102	Wentzville	Missouri	448	C	UMR	D. Hoffman

Table A. (Continued)

103	Wentzville	Missouri	411	C	UMR	D. Hoffman
104	Wentzville	Missouri	440	C	UMR	D. Hoffman
105	Wentzville	Missouri	293	D	UMR	D. Hoffman
106	Wentzville	Missouri	449	C	UMR	D. Hoffman
130	Wentzville	Missouri	595	C	USGS	R. Williams
	Average		448	C		
Till in St. Louis City						
4	Granite City	Missouri	278	D	UMR	D. Hoffman
7	Granite City	Missouri	249	D	UMR	D. Hoffman
16	Cahokia	Missouri	n.a		UMR	D. Hoffman
17	Webster Groves	Missouri	218	D	UMR	D. Hoffman
18	Webster Groves	Missouri	n.a		UMR	D. Hoffman
43	Granite City	Missouri	306	D	UMR	D. Hoffman
122	Granite City	Missouri	430	C	USGS	R. Williams
126	Granite City	Missouri	560	C	USGS	R. Williams
	Average		340	C to D		
Karst						
15	Cahokia	Missouri	506	C	UMR	D. Hoffman
25	Webster Groves	Missouri	449	C	UMR	D. Hoffman
26	Webster Groves	Missouri	534	C	UMR	D. Hoffman
27	Webster Groves	Missouri	534	C	UMR	D. Hoffman
123	Granite City	Missouri	410	C	USGS	R. Williams
	Average		487	C		

APPENDIX B. AVERAGE SOIL UNIT WEIGHTS

Table B. The average soil unit weights used to compute the overburden stress of the soil stratum.

Soil Type (USCS)	Sample #	Unit Weight (KN/m ³)							
		Range		Mean		Median		Standard deviation	
		γ_d	γ	γ_d	γ	γ_d	γ	γ_d	γ
CH	(80)	10.21~20.11	16.24~27.35	15.06	19.48	15.12	19.23	1.89	1.98
CL	(379)	11.47~21.49	13.55~25.81	16.14	20.01	15.71	19.48	1.82	2.26
CL-CH	(1)			17.28	20.56				
CL-ML	(15)	13.51~19.48	16.23~24.52	15.08	18.18	14.63	17.97	1.40	2.17
MH	(2)		16.51~16.62	11.31	16.57	11.31	16.57		0.08
ML	(51)	12.25~22.20	16.18~25.37	16.61	20.65	16.18	19.32	2.47	3.02
ML-CL	(3)	15.40~16.35	19.71~21.02	15.72	20.14	15.40	19.71	0.55	0.76
ML-SM	(1)			13.83	17.28				
SC-CL	(1)			15.71	22.63				
SM	(1)			13.98	20.13				
Fill	(11)	14.14~17.75	18.06~21.66	15.68	19.37	15.71	19.51	0.98	0.99
GP		17.5~20.5	19.5~22.0	19.0	20.75				
GW		17.5~22.0	19.5~23.5	19.75	21.5				
GM		16.0~20.5	19.5~22.0	18.25	20.75				
GC		16.0~20.5	19.5~22.0	18.25	20.75				
SP		15.0~19.5	19.0~21.0	17.25	20.0				
SW		15.0~21.0	19.0~23.0	18.0	21.0				

γ_d : Dry unit weight, γ : Wet unit weight

BIBLIOGRAPHY

- Allen, W.H.Jr., and Ward, R.A., 1977, Soil, *in* Howe, W. B., and Fellows, L.D., ed., The resources of St. Charles County, Missouri land, water, and minerals: Rolla, Missouri Geological Survey, Department of Natural Resources, p. 108-145.
- Andres, A.S., and Martin, M.J., 2005, Estimation of the water table for the Inland Bays watershed: Newark, Delaware, University of Delaware, Delaware Geological Survey Report of Investigations, No. 68, 20 p.
- Atkinson, G.M., and Beresnev, I.A., 2002, Ground motions at Memphis and St. Louis from M 7.5-8.0 earthquakes in the New Madrid seismic zone: Bulletin of the Seismological Society of America, v. 92, no. 3, p. 1015-1024.
- Baise, L.G., Higgins, R.B., and Brankman, C.M., 2006, Liquefaction hazard mapping - Statistical and spatial characterization of susceptible units: Journal of Geotechnical and Geoenvironmental Engineering, v. 132, no. 6, p. 705-715.
- Bakun, W.H., and Hopper, M.G., 2004, Magnitudes and locations of the 1811-1812 New Madrid, Missouri, and the 1886 Charleston, South Carolina, earthquakes: Bulletin of the Seismological Society of America, v. 94, no. 1, p. 64-75.
- Bauer, R.A., Kiefer, J., and Hester, N., 2001, Soil amplification maps for estimating earthquake ground motions in the Central US: Engineering Geology, v. 62, no. 1-3, p. 7-17.
- Bergstrom, R.E., and Walker, T.R., 1956, Ground-water geology of the East St. Louis area, Illinois: Illinois State Geological Survey Report of Investigations 191, 44 p.
- Borcherdt, R.D., 1994, Estimates of site-dependent response spectra for design (methodology and justification): Earthquake Spectra, v. 10, p. 617-654.
- Borcherdt, R.D., and Gibbs, J.F., 1976, Effects of local geological conditions in the San Francisco Bay region on ground motions and the intensities of the 1906 earthquake: Bulletin of the Seismological Society of America, v. 66, p. 467-500.
- Borcherdt, R., Wentworth, C.M., Janssen, A., Fumal, T., and Gibbs, J., 1991, Methodology for predictive GIS mapping of special study zones for strong ground shaking in the San Francisco Bay region, CA, *in* Fourth International Conference on Seismic zonation Stanford, California, USA, p. 545-552.
- Brill, K.J., 1986, Geologic map of the Kirkwood 7.5' quadrangle Jefferson and St. Louis Counties, Missouri: Missouri Department of Natural Resources, Geological Survey and Resource Assessment Division, scale 1:24,000.

- , 1987, Geologic map of the Webster Groves 7.5' quadrangle St. Louis County, Missouri: Missouri Department of Natural Resources, Geological Survey and Resource Assessment Division, scale 1:24,000.
- , 1988, Geologic map of the Manchester 7.5' quadrangle Jefferson and St. Louis Counties, Missouri: Missouri Department of Natural Resources, Geological Survey and Resource Assessment Division, scale 1:24,000.
- BSSC, 2003, NEHRP recommended provisions for seismic regulations for new buildings and other structures part I: Provisions (FEMA 450): Washington, D.C., Building Seismic Safety Council, Federal Emergency Management Agency.
- Cannon, S.H., Gartner, J.E., Rupert, M.G., and Michael, J.A., 2004, Emergency assessment of debris-flow hazards from basins burned by the Padua fire of 2003, Southern California: U.S. Geological Survey Open-File Report 2004-1085.
- Carrara, A., Cardinali, M., Guzzetti, F., and Reichenbach, P., 1995, Multivariate regression analysis for landslide hazard zonation, geographical information systems in assessing natural hazards, *in* Carrara, A., and Guzzetti, F., eds., *Geographical Information Systems in Assessing Natural Hazards*: Dordrecht, Netherlands, Kluwer Academic, p. 135-175.
- Cetin, K.O., Seed, R.B., Der Kiureghian, A., Tokimatsu, K., Harder, L.F., Kayen, R.E., and Moss, R.E.S., 2004, Standard penetration test-based probabilistic and deterministic assessment of seismic soil liquefaction potential: *Journal of Geotechnical and Geoenvironmental Engineering*, v. 130, no. 12, p. 1314-1340.
- Coduto, D.P., 1994, *Foundation design: Principles and practices*: Englewood Cliffs, New Jersey, Prentice-Hall 720 p.
- Cramer, C.H., 2001, A seismic hazard uncertainty analysis for the New Madrid seismic zone: *Engineering Geology*, v. 62, no. 1-3, p. 251-266.
- Dai, F.C., and Lee, C.F., 2002, Landslide characteristics and slope instability modeling using GIS, Lantau Island, Hong Kong: *Geomorphology*, v. 42, no. 3-4, p. 213-228.
- Daniels, R.B., Kleiss, H.J., Buol, S.W., Byrd, H.J., and Phillips, J.A., 1984, *Soil systems in North Carolina*: Raleigh, North Carolina, North Carolina State University, North Carolina Agricultural Research Service Bulletin 467
- Denny, F.B., 2003, *Bedrock geology of Oakville quadrangle, Monroe County, Illinois*: Illinois State Geological Survey, scale 1:24,000.
- Denny, F.B., and Devera, J.A., 2001a, *Bedrock geologic map of Monks Mound quadrangle, Madison and St. Clair Counties, Illinois*: Illinois State Geological Survey, scale 1:24,000.
- , 2001b, *Bedrock geologic map of Wood River quadrangle, Madison County, Illinois*: Illinois State Geological Survey, scale 1:24,000.

- Devera, J.A., 2004, Bedrock geology of Bethalto quadrangle, Madison and Macoupin Counties, Illinois: Illinois State Geological Survey, scale 1:24,000.
- , 2006, Bedrock geology of Chester quadrangle, Randolph County, Illinois: Illinois State Geological Survey, scale 1:24,000.
- , unpublished, Surficial geology of Oakville quadrangle, Monroe County, Illinois and St. Louis County, Missouri: Illinois State Geological Survey, scale 1:24,000.
- Devera, J.A., and Denny, F.B., 2001, Bedrock geologic map of Collinsville quadrangle, Madison and St. Clair Counties, Illinois: Illinois State Geological Survey, scale 1:24,000.
- , 2003, Bedrock geology of Edwardsville quadrangle, Madison County, Illinois: Illinois State Geological Survey, scale 1:24,000.
- Domenico, P.A., and Schwartz, F.W., 1998, Physical and chemical hydrogeology: New York, Wiley, xiii, 506 p.
- Donati, L., and Turrini, M. C., 2002, An objective method to rank, the importance of the factors predisposing to landslides with the GIS methodology: Application to an area of the Apennines, (Valnerina; Perugia, Italy): Engineering Geology, v. 63, no. 3-4, p. 277-289.
- Doyle, B.C., and Rogers, J.D., 2005, Seismically induced lateral spread features in the western New Madrid seismic zone: Environmental & Engineering Geoscience, v. 11, no. 3, p. 251-258.
- Dunlap, L.E., and Spinazola, J.M., 1984, Interpolating water-table altitudes in west-central Kansas using kriging techniques: Denver, Colorado, U.S. Geological Survey Water-Supply Paper 2238 iv, 19 p.
- Fehrenbacher, J.B., Jansen, I.J., and Olson, K.R., 1986, Loess thickness and its effect on soils in Illinois: University of Illinois, Department of Agriculture Bulletin 782, 14 p.
- Frankel, A.D., Petersen, M.D., Mueller, C.S., Haller, K.M., Wheeler, R.L., Leyendecker, E.V., Wesson, R.L., Harmsen, S.C., Cramer, C.H., Perkins, D.M., and Rukstales, K.S., 2002, Documentation for the 2002 update of the national seismic hazard map: U.S. Geological Survey Open-File Report 02-420.
- Frye, J.C., and Willman, H.B, 1960, Classification of the Wisconsinan Stage in the Lake Michigan glacial lobe: Illinois Geological Survey Circular 285, 16 p.
- Fumal, T.E., and Tinsley, J.S., 1985, Mapping shear-wave velocities of near-surface geologic materials, *in* Ziony, J. I., ed., Evaluating Earthquake Hazards in the Los Angeles Region-An Earth-Science Perspective: U.S. Geological Survey Professional Paper 1360, p. 127-149.
- Gambolati, G., and Volpi, G., 1979, A conceptual deterministic analysis of the kriging technique in hydrology: Water Resources Research, v. 15, no. 3, p. 625-629.

- Gao, C., Shiota, J., Kelly, R.I., Brunton, F.R., and van Haaften, S., 2006, Bedrock topography and overburden thickness mapping, southern Ontario, summary of field work and other activities 2006: Ontario Geological Survey Open File Report 6192, p. 34-1 to 34-10.
- Gomberg, J., Waldron, B., Schweig, E., Hwang, H., Webbers, A., VanArsdale, R., Tucker, K., Williams, R., Street, R., Mayne, P., Stephenson, W., Odum, J., Cramer, C., Updike, R., Hutson, S., and Bradley, M., 2003, Lithology and shear-wave velocity in Memphis, Tennessee: Bulletin of the Seismological Society of America, v. 93, no. 3, p. 986-997.
- Goodfield, A.G., 1965, Pleistocene and surficial geology of the City of St. Louis and the adjacent St. Louis County, Missouri [Ph.D thesis]: Urbana-Champaign, University of Illinois, 207 p.
- Green, R.A., Obermeier, S.F., and Olson, S.M., 2005, Engineering geologic and geotechnical analysis of paleoseismic shaking using liquefaction effects: Field examples: Engineering Geology, v. 76, no. 3-4, p. 263-293.
- Grimley, D.A., 1999, Surficial geology of Alton Village quadrangle (Illinois portion), Madison County, Illinois: Illinois State Geological Survey, scale 1:24,000.
- Grimley, D. A., Phillips, A.C., Follmet, L.R., and Wang, H., 2001, Quaternary and environmental geology of the St. Louis Metro East area, *in* Malone, D., ed., Guidebook for Fieldtrips for the Thirty-Fifth Annual Meeting of the North-Central Section of the Geological Society of America, Illinois State Geological Survey Guidebook 33, p. 21-67.
- Grimley, D.A., 2002, Surficial geology of Elsah quadrangle, Jersey and Madison Counties, Illinois: Illinois State Geological Survey, scale 1:24,000.
- , 2005, Surficial geology of Bethalto quadrangle, Madison and Macoupin Counties, Illinois: Illinois State Geological Survey, scale 1:24,000.
- , in review, Surficial geology of Columbia quadrangle, St. Clair and Monroe Counties, Illinois: Illinois State Geological Survey, scale 1:24,000.
- , in review, Surficial geology of O'Fallon quadrangle, St. Clair County, Illinois: Illinois State Geological Survey, scale 1:24,000.
- Grimley, D.A., and Lepley, S. W., 2005, Surficial geology of Wood River quadrangle, Madison County, Illinois: Illinois State Geological Survey, scale 1:24,000.
- Grimley, D.A., and McKay, E. D., 1999, Surficial geology of Grafton quadrangle (Illinois portion), Jersey and Calhoun Counties, Illinois: Illinois State Geological Survey scale, 1:24,000.
- , 2004, Surficial geology of French Village quadrangle, St. Clair County, Illinois: Illinois State Geological Survey, scale 1:24,000.

- Grimley, D. A., and Denny, F.B., 2004, Bedrock topography of French Village quadrangle, St. Clair County, Illinois: Illinois State Geological Survey, scale 1:24,000.
- Grimley, D.A., and Phillips, A. C., 2006, Surficial geology of Madison County, Illinois: Illinois State Geological Survey, scale 1:100,000.
- Grimley, D. A., Phillips, A.C., and Lepley, S.W, in review, Surficial geology of Monks Mound quadrangle, Illinois: Illinois State Geological Survey, scale 1:24,000.
- Harrison, R.W., 1997, Bedrock geologic map of the St. Louis 30' x 60' Quadrangle, Missouri and Illinois: U.S. Geological Survey, Miscellaneous Investigations Series Map I-2533, scale 1:100,000.
- Hasenmueller, W.A., 2006, Modeling the bedrock surface in Indiana with contouring software: Geological Society of America Abstracts with Programs, v. 38, no. 7, p. 166.
- Herzog, B.L., Stiff, B.J., Chenoweth, C.A., Warner, K.L., Sieverling, J. B., and Avery, C., 1995, Buried bedrock surface of Illinois: Illinois State Geological Survey Illinois Map 5, scale 1:500,000.
- Hitchcock, C.S., Loyd, R.C., and Haydon, W.D., 1999, Mapping liquefaction hazards in Simi Valley, Ventura County, California: Environmental & Engineering Geoscience, v. 5, no. 4, p. 441-458.
- Hoeksema, R.J., Clapp, R. B., Thomas, A. L., Hunley, A. E., Farrow, N. D., and Dearstone, K. C., 1989, Cokriging model for estimation of water table elevation: Water Resources Research, v. 25, no. 3, p. 429-438.
- Hoffman, D., 1995, Earthquake hazard map of the St. Louis Missouri metro area: Missouri Department of Natural Resources, Division of Geology & Land Survey, scale 1:100,000.
- Holdstock, D.A., 1998, Basics of geographic information systems (GIS): Journal of Computing in Civil Engineering, v. 12, no. 1, p. 1-4.
- Holzer, T.L., Bennett, M.J., Noce, T.E., Padovani, A.C., and Tinsley, J.C., 2006, Liquefaction hazard mapping with LPI in the Greater Oakland, California, area: Earthquake Spectra, v. 22, no. 3, p. 693-708.
- Hough, S.E., Armbruster, J.G., Seeber, L., and Hough, J.F., 2000, On the Modified Mercalli Intensities and Magnitudes of the 1811-1812 New Madrid, Central United States earthquakes: Journal of Geophysical Research, v. 105, no. B10, p. 23,839-23,864.
- Isaaks, E.H., and Srivastava, R.M., 1989, Applied geostatistics: New York, Oxford University Press, xix, 561 p. p.
- Iwasaki, T., Tokida, K., Tatsuko, F., and Yasuda, S., 1978, A practical method for assessing soil liquefaction potential based on case studies at various site in Japan, *in* 2nd International Conference on Microzonation, San Francisco, p. 885-896.

- Iwasaki, T., Tokida, K., Tatsuoka, F., Watanabe, S., Yasuda, S., and Sato, H., 1982, Microzonation for soil liquefaction potential using simplified methods, *in* Proceedings 3rd International Conference on Microzonation, Seattle, USA, p. 1319-1330.
- Johnston, A., and Schweig, E.S., 1996, The enigma of the New Madrid Earthquakes of 1811-1812: Annual Review of Earth and Planetary Sciences, v. 23, p. 339-384.
- Johnston, K., 2003, Using arcgis geostatistical analyst: Redlands, California, Environmental Systems Research Institute, 316 p.
- Journel, A.G., and Huijbregts, C., 1978, Mining geostatistics: London; New York, Academic Press, x, 600 p.
- Karadeniz, D., 2007, Pilot program to assess seismic hazards of the Granite City, Monks Mound, and Columbia Bottom quadrangles, St. Louis metropolitan area, Missouri and Illinois [Ph.D dissertation]: Rolla, University of Missouri, 268 p.
- Kelkar, M., and Perez, G., 2002, Applied geostatistics for reservoir characterization: Richardson, Texas, Society of Petroleum Engineers, viii, 264 p.
- Kelly, D., 2006, Seismic site classification for structural engineers: Structure Magazine, p. 21-24.
- King, F.H., 1899, Principles and conditions of the movements of groundwater, U.S. Geological Survey 19th Annual Report, p. 59-294.
- Kolata, D.R., 2005, Bedrock geology of Illinois: Illinois State Geological Survey, scale 1:500,000.
- Kramer, S.L., 1996, Geotechnical earthquake engineering: Upper Saddle River, New Jersey, Prentice Hall, xviii, 653 p.
- Kuribayashi, E., and Tatsuoka, F., 1975, Brief review of liquefaction during earthquakes in Japan: Soils and Foundations, v. 15, no. 4, p. 81-92.
- Liao, S.C., and Whitman, R.V., 1986, Overburden correction factors for SPT in sand: Journal of Geotechnical Engineering, v. 112, no. 3, p. 373-377.
- Lo, C.P., and Yeung, A.K.W., 2002, Concepts and techniques of geographic information systems, PH series in geographic information science: Upper Saddle River, New Jersey, Prentice Hall, xii, 492 p.
- Luna, R., 1995, Liquefaction evaluation using a spatial analysis system [Ph.D. thesis]: Atlanta, Georgia Institute of Technology, 309 p.
- Luna, R., and Frost, J.D., 1998, Spatial liquefaction analysis system: Journal of Computing in Civil Engineering, v. 12, no. 1, p. 48-56.

- Lutzen, E., and Rockaway, J. D., Jr., 1971, Engineering geology of St. Louis County, Missouri, Engineering Geology Series, no. 4: Rolla, Missouri, Missouri Department of Natural Resources, Division of Geology and Land Survey.
- Mansoor, N.M., Niemi, T.M., and Misra, A., 2004, A GIS-based assessment of liquefaction potential of the city of Aqaba, Jordan: Environmental & Engineering Geoscience, v. 10, no. 4, p. 297-320.
- Matheron, G., 1971, The theory of regionalized variables and its application: Les Cahiers du Centre de Morphologie Mathematique de Fontainebleau, p. 221.
- McKay, E.D., 1977, Stratigraphy and zonation of Wisconsinan loesses in southwestern Illinois [Ph.D. dissertation]: Urbana-Champaign, University of Illinois, 242 p.
- , 1979, Stratigraphy of Wisconsinan and older loesses in southwestern Illinois, geology of western Illinois, 43rd Annual Tri-State Geological Field Conference: Champaign, Illinois State Geological Survey Guidebook 14, p. 37-67.
- Middendorf, M.A., and Brill, K.G., 2002, Geologic map of the Oakville 7.5' quadrangle Jefferson and St. Louis Counties, Missouri: Missouri Department of Natural Resources, Geological Survey and Resource Assessment Division, scale 1:24,000.
- MoDNR-DGLS, 2006, Missouri environmental geology atlas: Rolla, Missouri Department of Natural Resources (MoDNR)-Division of Geology and Land Survey (DGLS). [CD-ROM].
- , 2007, Missouri environmental geology atlas: Rolla, Missouri Department of Natural Resources (MoDNR)-Division of Geology and Land Survey (DGLS). [CD-ROM].
- Myers, D.E., 1982, Matrix Formulation of Co-kriging: Mathematical Geology, v. 14, no. 3, p. 249-257.
- Nelson, W.J., 1998, Bedrock Geology of the Paducah 1° x 2° CUSMAP Quadrangle, Illinois, Indiana, Kentucky, and Missouri: Washington; Denver, Colorado, U.S. Geological Survey Bulletin, Resource and Topical Investigations 2150 B
- Nyquist, J.E., Doll, W.E., Davis, R.K., and Hopkins, R.A., 1996, Cokriging surface topography and seismic refraction data for bedrock topography: Journal of Environmental and Engineering Geophysics, v. 1, no. 1, p. 67-74.
- Obermeier, S.F., 1989, The New Madrid earthquakes: an engineering-geologic interpretation of relict liquefaction features: U.S. Geological Survey Professional Paper 1336-B.
- O'Hara, C. G., and Reed, T.B., 1995, Depth to the water table in Mississippi USGS Water-Resources Investigations Report, 95-4242.
- Olea, R. A., 1999, Geostatistics for engineers and earth scientists Boston, Kluwer Academic, 303 p.

- Palmer, J., Mesko, T., Cadoret, J., James, K., and Jones, R., 2006, St. Louis, Missouri surficial materials database: Missouri Department of Natural Resources, Division of Geology and Land Survey.
- Palmer, J.R., and Siemens, M.A., 2006, Surficial material geologic map of the Wentzville 7.5' quadrangle, St. Charles County, Missouri: Missouri Department of Natural Resources Division of Geology and Land Survey, scale 1:24,000.
- Park, S. and Elrick, S., 1998, Predictions of shear-wave velocities in Southern California using surface geology: *Bulletin of the Seismological Society of America*, v. 88, p. 677-685.
- Parson, R.L., and Frost, J. D., 2000, Interactive analysis of spatial subsurface data using GIS-based tool: *Journal of Computing in Civil Engineering*, v. 14, no. 4, p. 215-222.
- Pearce, J.T., and Baldwin, J.B., 2005, Liquefaction susceptibility mapping, St. Louis, Missouri and Illinois: U.S. Geological Survey, National Earthquake Hazard Reduction Program Final Technical Report, 46 p.
- Peck, M. F., and Payne, D.F., 2003, Development of an estimated water-table map for coastal Georgia and adjacent parts of Florida and South Carolina, *in* the 2003 Georgia Water Resources Conference, Athens, Georgia.
- Phillips, A.C., 2003, Surficial geology of Edwardsville quadrangle, Madison County, Illinois: Illinois State Geological Survey scale 1:24,000.
- , 2004, Surficial geology of Collinsville quadrangle, Madison and St. Clair Counties, Illinois: Illinois State Geological Survey scale 1:24,000.
- Phillips, A.C., Grimley, D.A., and Lepley, S.W., in review, Surficial geology of Granite City quadrangle, Madison and St. Clair Counties, Illinois: Illinois State Geological Survey scale 1:24,000.
- Rahn, P.H., 1996, *Engineering geology: An environmental approach*: Englewood Cliffs, New Jersey, PTR Prentice Hall, xiii, 657 p.
- Rhind, D., 1989, Why GIS?: *ARC News*, v. 11, no. 3, p. 28-29.
- Rogers, J.D., 2006, Subsurface exploration using the standard penetration test and the cone penetrometer test: *Environmental & Engineering Geoscience*, v. 12, no. 2, p. 161-179.
- Rogers, J.D., and Luna, R., 2004, Impact of geographical information systems on geotechnical engineering, *in* *Proceedings of the 5th International Conference on Case Histories in Geotechnical Engineering*, New York, USA, p. 1-23.
- Rogers, J. D., Karadeniz, D., and Kaibel, C.K., 2007, Seismic response modeling for Missouri River Highway Bridges: *Journal of Earthquake Engineering*: v. 11, no. 3 (May), p. 400-424.

- Romero, S., and Rix, G. J., 2001, Regional variations in near surface shear wave velocity in the Greater Memphis area: *Engineering Geology*, v. 62, no. 1-3, p. 137-158.
- Ruhe, R.V., 1983, Depositional environment of Late Wisconsin loess in the Midcontinental United States, *in* Wright, H.E., Jr ed., *Late Quaternary Environments of the United States Vol. 1: The late Pleistocene*: Minneapolis, University of Minnesota Press, p. 130-138.
- Russ, D. P., 1982, Style and significance of surface deformation in the vicinity of New Madrid, Missouri, *in* McKeown, F. A., and Pakiser, L.C., ed., *Investigations of the New Madrid, Missouri, earthquake region*, U.S. Geological Survey Professional Paper 1236, p. 95-114.
- Satterfield, I.R., 1977, Rock, *in* Howe, W. B., and Fellows, L.D., ed., *The resources of St. Charles County, Missouri land, water, and minerals*: Rolla, Missouri Geological Survey, Department of Natural Resources, p. 146-153.
- Schultz, A.P., 1993 (unpublished), Map showing surficial geology of the St. Louis 30x60 minute quadrangle: U.S. Geological Survey Open-File Report 93-288, scale 1:100,000.
- Seed, H.B., and Idriss, I.M., 1971, Simplified procedure for evaluating soil liquefaction potential: *Journal of the Soil Mechanics and Foundations Division*, v. 97, p. 1249-1273.
- Seed, H.B., Tokimatsu L.F., Harder, L.F., and Chung, R.M, 1985, Influence of SPT procedures in soil liquefaction resistance evaluations: *Journal of Geotechnical Engineering*, v. 111, no. 12, p. 1425-1445.
- Sepulveda, N., 2003, A statistical estimator of the spatial distribution of the water-table altitude: *Ground Water*, v. 41, no. 1, p. 66-71.
- Smith, L.M., and Smith, F.L., 1984, Engineering geology of selected areas, US Army Engineer Division, Lower Mississippi Valley. Report 1. The American Bottom Area, MO-IL. Volume 1: U.S. Army Corps of Engineers, Geotechnical Laboratory, Technical Report GL-84-14.
- Sonmez, H., 2003, Modification of the liquefaction potential index and liquefaction susceptibility mapping for a liquefaction-prone area (Inegol, Turkey): *Environmental Geology*, v. 44, no. 7, p. 862-871.
- Sonmez, H., and Gokceoglu, C., 2005, A liquefaction severity index suggested for engineering practice: *Environmental Geology*, v. 48, no. 1, p. 81-91.
- Stinchcomb, B.L., and Fellows, L.D., 2002, Geologic map of the Maxville 7.5' quadrangle Jefferson and St. Louis Counties, Missouri: Missouri Department of Natural Resources, Geological Survey and Resource Assessment Division, scale 1:24,000.

- Street, R., and Nuttli, O., 1984, The central Mississippi Valley earthquakes of 1811-1812, *in* Proceedings Symposium on the New Madrid Seismic Zone, U.S. Geological Survey Open-File Report 84-770, p. 33-63.
- Su, W.-J., 2001, Engineering problems caused by loess in the St. Louis metro east area, *in* Malone, D., ed., Guidebook for fieldtrips for the thirty-fifth annual meeting of the North-Central section of the Geological Society of America: Champaign, Illinois State Geological Survey Guidebook 33, p. 68-70.
- Thorp, J., and Smith, H.T.U., 1952, Pleistocene eolian deposits of the United States, Alaska, and Part of Canada: Geological Society of America, scale 1:2,500,000.
- Tinsley, J.S., and Fumal, T.E., 1985, Mapping quaternary sedimentary deposits for areal variations in shaking response, *in* Ziony, J. I., ed., Evaluating earthquake hazards in the Los Angeles region: Washington, D.C, U.S. Geological Survey Professional Paper 1360, p. 101-125.
- Toprak, S., and Holzer, T.L., 2003, Liquefaction potential index: Field assessment: Journal of Geotechnical and Geoenvironmental Engineering, v. 129, no. 4, p. 315-322.
- Toro, G.R., and Silva, W.J., 2001, Scenario earthquakes for Saint Louis, MO, and Memphis, TN, and seismic hazard maps for the central United States region including the effect of site conditions: U.S. Geological Survey Final Technical Report.
- Tuttle, M.P., and Schweig, E.S., 1995, Archeological and pedological evidence for large earthquakes in the New Madrid seismic zone, central United States: *Geology*, v. 23, p. 253-256.
- Tuttle, M.P., 2001, The use of liquefaction features in paleoseismology: Lessons learned in the New Madrid seismic zone, central United States: *Journal of Seismology*, v. 5, no. 3, p. 361-380.
- Tuttle, M.P., 2005, Paleoseismological Study in the St. Louis region, U.S. Geological Survey Final Technical Report.
- Tuttle, M.P. C., J., Lafferty, R., Dyer-Williams, K., and Cande, B., 1999, Paleoseismology study northwest of the New Madrid Seismic Zone: U.S. Nuclear Regulatory Commission, NUREG/CR-5730.
- Tuttle, M.P., Schweig, E.S., Sims, J.D., Lafferty, R.H., Wolf, L.W., and Haynes, M.L., 2002, The earthquake potential of the New Madrid seismic zone: *Bulletin of the Seismological Society of America*, v. 92, no. 6, p. 2080-2089.
- USGS, 1997, Geographic information systems: Reston, Virginia, U.S. Geological Survey An Information Brochure.
- Whitfield, J.W., 2002, Geologic map of the House Spring 7.5' quadrangle Jefferson County, Missouri: Missouri Department of Natural Resources, Geological Survey and Resource Assessment Division, scale 1:24,000.

- Williams, R.A., Odum, J.K., Stephenson, W.J., and Herrman R.B., 2007, Shallow P- and S-wave velocities and site resonances in the St. Louis region, Missouri-Illinois: *Earthquake Spectra*, v. 3, p 711-726.
- Williams, T. A., and Williamson, A.K., 1989, Estimating water-table altitudes for regional ground-water flow modeling, U.S. Gulf Coast: *Ground Water*, v. 27, no. 3, p. 333-340.
- Wills, C.J., and Hitchcock, C.S., 1999, Late Quaternary sedimentation and liquefaction hazard in the San Fernando Valley, Los Angeles County, California: *Environmental & Engineering Geoscience*, v. 5, no. 4, p. 419-439.
- Wills, C.J., Petersen, M., Bryant, W.A., Reichle, M., Saucedo, G.J., Tan, S., Taylor, G., and Treiman, J., 2000, A site-condition map for California based on geology and shear-wave velocity: *Bulletin of the Seismological Society of America*, v. 90, p. S187-S208.
- Youd, T.L., 1973, Liquefaction, flow, and associated ground failure: U.S. Geological Survey Circular 688.
- Youd, T.L., and Perkins, D.M, 1978, Mapping liquefaction induced ground failure potential: *Journal of Geotechnical Engineering*, v. 104, p. 433-446.
- Youd, T.L., and Perkins, D.M., 1987, Mapping of liquefaction severity index: *Journal of Geotechnical Engineering*, v. 113, no. 11, p. 1374-1392.
- Youd, T.L., Idriss, I.M., Andrus, R.D., Arango, I., Castro, G., Christian, J.T., Dobry, R., Finn, W.D.L., Harder, L.F., Hynes, M.E., Ishihara, K., Koester, J.P., Liao, S.S.C., Marcuson, W.F., Martin, G.R., Mitchell, J.K., Moriwaki, Y., Power, M.S., Robertson, P.K., Seed, R.B., and Stokoe, K.H., 2001, Liquefaction resistance of soils: Summary report from the 1996 NCEER and 1998 NCEER/NSF workshops on evaluation of liquefaction resistance of soils: *Journal of Geotechnical and Geoenvironmental Engineering*, v. 127, no. 10, p. 817-833.

VITA

Jae-Won Chung was born in Seoul, Korea, on October 18, 1971. He received his B.S. in Geology from the Yonsei University, Seoul, Korea in March 1996. He received M.S. degree in Geology from the Seoul National University, Korea in May 1996 and from Texas A&M University-College Station in December 2003. He received his Ph.D. in Geological Engineering from the University of Missouri-Rolla, Missouri, USA in December 2007.